

REVIEW ARTICLE

Muon spin rotation and relaxation in magnetic materials

P Dalmas de Réotier and A Yaouanc

Commissariat à l'Energie Atomique,
Département de Recherche Fondamentale sur la Matière Condensée,
Service de Physique Statistique, Magnétisme et Supraconductivité,
F-38054 Grenoble cedex 9

November 26, 2024

Abstract. A review of the muon spin rotation and relaxation (μ SR) studies on magnetic materials published from July 1993 is presented. It covers the investigation of magnetic phase diagrams, of spin dynamics and the analysis of the magnetic properties of superconductors. We have chosen to focus on selected experimental works in these different topics. In addition, a list of published works is provided.

PACS numbers: 76.75.+1, 68.35.Rh, 67.57.Lm, 74.60.Ec

Contents

1	Introduction	2
2	μ SR: Muon Spin Rotation, Relaxation	2
2.1	The transverse depolarization function	7
2.2	The longitudinal depolarization function	8
2.3	The magnetic field at the muon site	10
3	Magnetic phase diagrams	11
3.1	Magnetic ordering in organic compounds	12
3.2	Magnetic ordering in spin chains and ladders	14
3.3	Diamagnetic domains in beryllium	16
3.4	Localized and itinerant f electrons in heavy fermion materials	18
4	Spin dynamics in magnets	21
4.1	Critical and low temperature spin dynamics in ferromagnets	21
4.2	The correlation-function in spin-glasses	25
5	Probing the magnetic properties of superconductors	27
5.1	The symmetry of the superconducting order-parameter in $\text{YBa}_2\text{Cu}_3\text{O}_{6.95}$	28
5.2	The vortex state in highly anisotropic high T_c superconductors	31
5.3	Anisotropy of the magnetic response in UPt_3	32
6	Summary and perspectives	36
7	List of works published from July 1993	37
Appendix A	The magnetic field at the muon site	44
Appendix B	The magnetic field in the laboratory and crystal reference frames	44
Appendix C	The Fourier components of the magnetic field	44

Appendix A	The field distribution at the muon site	46
Appendix B	Muon spin relaxation in a longitudinal field	48
Appendix C	Longitudinal relaxation rate and correlation-functions	49
Appendix D	The μ SR response function for hard superconductors	50

1. Introduction

The breadth, format and style of this article is intended to provide an accessible and stimulating review of recent investigations of the physical properties of magnetic materials by the μ SR experimental technique. μ SR is an acronym for Muon Spin Rotation, Relaxation or Resonance. We shall only deal with the first two of these techniques, i.e. the two most commonly used in studies of magnetic materials. Measurements can be carried out with positive and negative muons. Since almost all the investigations were performed using the positive muon, we shall only discuss these. By no means have we attempted to write a comprehensive review. At the risk of being invidious, we discuss in three sections selected recent works which display the possibilities of the technique. To achieve a balanced picture, we list the works published from July 1993. The material published before July 1993, including that presented at the μ SR conference held in early 1993 on the island of Maui, Hawaii, has already been nicely reviewed (Schenck and Gygax 1995).

The organisation of this article is as follows. In section 2 we introduce the basic concepts of μ SR. In section 3 we discuss magnetic phase diagram studies. Section 4 presents two examples of the investigation of spin dynamics in magnets. The next section (section 5) deals with the very successful studies of the magnetic properties of superconductors. In section 6 we summarize the present status of μ SR and mention the scheduled technical developments at the μ SR facilities. In the last section (section 7) we give a list of published works. This review is completed by four appendices, the material of which is partly original.

2. μ SR: Muon Spin Rotation, Relaxation

Since the μ SR technique has been described in many reports (Seeger 1978, Chappert and Grynszpan 1984, Schenck 1985, Chappert and Yaouanc 1986, Cox 1987, Karlsson 1995, Schenck and Gygax 1995, Schatz and Weidinger 1995), we will only sketch it briefly. More information is provided in the appendices.

Currently, μ SR experiments can be performed at three facilities located at i) TRIUMF (4004 Wesbrook Mall, Vancouver BC, Canada V6T 2A3), ii) the Paul Scherrer Institut (PSI μ SR Facility, CH-5232 Villigen PSI, Switzerland) and iii) the Rutherford Appleton Laboratory (ISIS Facility, Chilton, Didcot, Oxon OX11 0QX, United Kingdom). In addition, measurements are carried out at the Meson Science Laboratory of the Faculty of Science of the University of Tokyo (Bunkyo-ku, Tokyo 113, Japan) and the Phasotron of the Joint Institute for Nuclear Research (Dubna, Head Post Office, P.O. Box 79, Moscow, Russia). The muon beams at the ISIS Facility and Meson Science Laboratory being pulsed beams are well adapted to study weak magnetic signals: this capability results from the virtual absence of background related to contamination of the beam with particles other than muons. However, their relatively low time-resolution means they are unsuitable for investigating systems exhibiting fast relaxation processes or appreciable local fields (larger than ~ 50 mT) at the muon site. The latter limitations do not apply to the beams at the other

institutions since they are quasi-continuous. In fact, the muon beams at the different institutions are complementary.

The μ SR technique uses the positive muon as a probe. The muon may form a bound state with an electron, called muonium, an exotic isotope of hydrogen. However muonium has never been observed in metals and the probability of its formation in oxides is small. We shall therefore consider only free muons.

In the μ SR technique polarized muons are implanted into a sample where their polarization evolves in the local magnetic field until they decay (the muon lifetime is $2.2 \mu\text{s}$). Because of its positive charge, the muon localizes at an interstitial site. Due to the absence of quadrupolar electric moment (spin $1/2$) the muon does not couple to electric field gradients. The decay positron is emitted preferentially along the muon spin direction; by collecting several million positrons, one can reconstruct the time dependence of the muon spin-depolarization function which, in turn, reflects the spatial and temporal distribution of magnetic fields at the muon site. Because of their large kinetic energy ($\approx 30 \text{ MeV}$), the positrons easily go through the sample. Fortunately they are weakly absorbed by cryostat or furnace walls so that complex sample-environment equipment may be used.

Two types of experimental geometries are generally used, see figure 1. In the longitudinal geometry an external magnetic field \mathbf{B}_{ext} is applied along the initial muon beam polarization direction \mathbf{S}_μ and positron detectors are set parallel and antiparallel to \mathbf{S}_μ . We then refer to the forward and backward direction, respectively. In the transverse geometry \mathbf{B}_{ext} is perpendicular to \mathbf{S}_μ and the positrons are detected perpendicular to \mathbf{B}_{ext} . The zero-field measurements are performed with the longitudinal geometry.

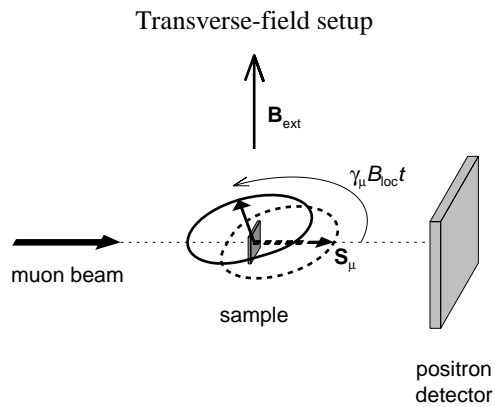
The μ SR technique is a local-probe hyperfine-method as are nuclear magnetic resonance (NMR), perturbed angular correlations (PAC) and Mössbauer spectroscopy. Therefore the basic physical concepts developed for the latter techniques can be transferred to μ SR. One of its unique characteristics is its ability to detect very small magnetic moments. This is understood as follows.

We first recall that a magnetic moment precesses around a local magnetic field \mathbf{B}_{loc} at a pulsation frequency ω proportional to B_{loc} : this is the Larmor precession. For the muon $\omega_\mu = 2\pi\nu_\mu = \gamma_\mu B_{\text{loc}}$ where ν_μ is the precession frequency and γ_μ is the muon gyromagnetic ratio ($\gamma_\mu = 851.6 \text{ Mrad s}^{-1}\text{T}^{-1}$). Therefore, in a constant field, the moment rotates by an angle $\gamma_\mu B_{\text{loc}} t$ in the elapsed time t . Since an angle of 0.5 radian is measurable ($\cos 0.5 \simeq 0.88$) and a μ SR measurement can be routinely carried out up to $t = 15 \mu\text{s}$, a local field as small as 0.04 mT can be detected. It might be produced by a nuclear magnetic moment which is $\sim 10^3$ times smaller than an electronic magnetic moment.

While the μ SR technique can detect very small magnetic fields, very high fields can not be measured: with a conventional spectrometer of a continuous muon source the maximum field is $\sim 3 \text{ T}$. Recent measurements at 6.5 T have been performed by Riseman *et al* 1995.

The muon spin depolarization function is written as $aP_\alpha(t)$. It is also called the asymmetry. a is the initial asymmetry (at $t = 0$) and $P_\alpha(t)$ the normalized depolarization function which will be referred to as the depolarization function. The Cartesian label α denotes the direction along which the muon polarization is measured, i.e. it can be X , Y or Z . The value of a depends on the experimental geometry; typically $a = 0.25$. We use an orthonormal laboratory reference frame. \mathbf{B}_{ext} is taken along the Z axis and \mathbf{S}_μ parallel to Z or X in the longitudinal and transverse set-

Dalmas de Reotier and Yaouanc: Fig. 1a



Dalmas de Reotier and Yaouanc: Fig. 1b

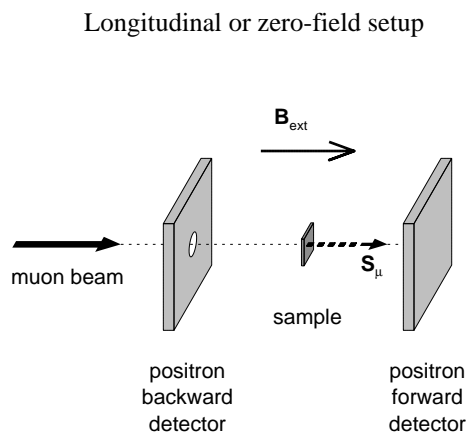


Figure 1. Principle of the two types of experimental geometries: the transverse and longitudinal set-ups are cartooned in the upper and lower panel, respectively. In order to produce drawings which are easy to understand, the muon beam momentum and the initial muon beam polarization have been taken parallel. In reality, these two vectors are antiparallel. The arrows originating from the sample sketch the muon spin direction: the dashed one at $t = 0$ and the solid one at t . The dashed and solid line cardioids drawn for the transverse field setup panel represent the probability of positron emission in a given direction relative to the muon spin position at the instant of the decay.

up, respectively. Whereas in a longitudinal set-up, only $P_Z(t)$ is of interest, in the transverse set-up, $P_X(t)$ and $P_Y(t)$ can be measured. Since these two functions always contain the same information, we only consider $P_X(t)$.

$P_\alpha(t)$ monitors the properties of the magnetic field at the muon site. If all the muon spins precess in the same static magnetic field, oriented at an angle θ from \mathbf{S}_μ , the Larmor equation yields

$$P_\alpha(t) = \cos^2 \theta + \sin^2 \theta \cos(\omega_\mu t). \quad (1)$$

This is the result on which the entire μ SR technique is based.

We consider a magnet in zero external magnetic field. Then $P_Z(t)$ is of interest. \mathbf{B}_{loc} is usually not zero below the magnetic phase transition. For a magnet in polycrystalline form, the spatial average of (1) has to be performed. If the sample is not textured, we obtain

$$P_Z(t) = \frac{1}{3} + \frac{2}{3} \cos(\omega_\mu t). \quad (2)$$

The oscillating component reflects the magnetic order in the sample. This single component exists even in a polycrystalline sample because we suppose there is only one type of muon localization sites and for these sites \mathbf{B}_{loc} is the same. If the magnet is disordered, i.e., if its correlation length is small, \mathbf{B}_{loc} can take a large number of values. Then the oscillation can be strongly damped and even disappear. If the muon spins precess too quickly relative to the time resolution of the spectrometer, the oscillation will not be observed and the resulting muon spin-polarization will be averaged out to 0. Then, at a magnetic phase transition, if no wiggles are observed in the muon signal, one expects a drop in the effective initial asymmetry from a in the paramagnetic state to $a/3$ in the ordered state. In figure 2 we present examples for two samples.

Whereas for GdNi_5 we do observe the expected behaviour, for UPt_2Si_2 the change at T_N is smoother than expected and the ratio of the effective initial asymmetry in the paramagnetic and ordered state is smaller. We then conclude that the distribution of T_N values is relatively large in the UPt_2Si_2 sample. In addition, this sample has a strong texture. The distribution is the signature of crystalline disorder: probably some Pt and Si atoms interchange their atomic positions. Complementary measurements at ISIS on a single crystal sample of UPt_2Si_2 with \mathbf{S}_μ perpendicular to \mathbf{B}_{loc} (and therefore to the c axis) show that the effective initial asymmetry decreases to zero around T_N in a temperature interval as large as ~ 5 K (Gubbens *et al* 1996). This result supports the conclusion deduced from the polycrystalline sample measurements. Note that the measurement of the effective initial asymmetry offers a stringent test of the sample quality.

Figure 2 shows that the maximum initial asymmetry is smaller than expected. The difference is accounted for by the contribution from the background, i.e. muons which have not been stopped in the sample, but for instance in the sample holder. We write $aP_Z(t) = a_s P_Z^s(t) + a_{\text{bg}} P_Z^{\text{bg}}(t)$ where the first and the second term describes the contribution from the sample and the background, respectively. a_s is plotted in figure 2. Usually the sample holder is a silver plate, $P_Z^{\text{bg}}(t)$ is then taken as time independent ($P_Z^{\text{bg}}(t) = 1$) because silver has no electronic moment and very small nuclear moments. On the other hand, if one analyses an extremely weakly damped μ SR signal, the damping due to the silver nuclear moments should be taken into account.

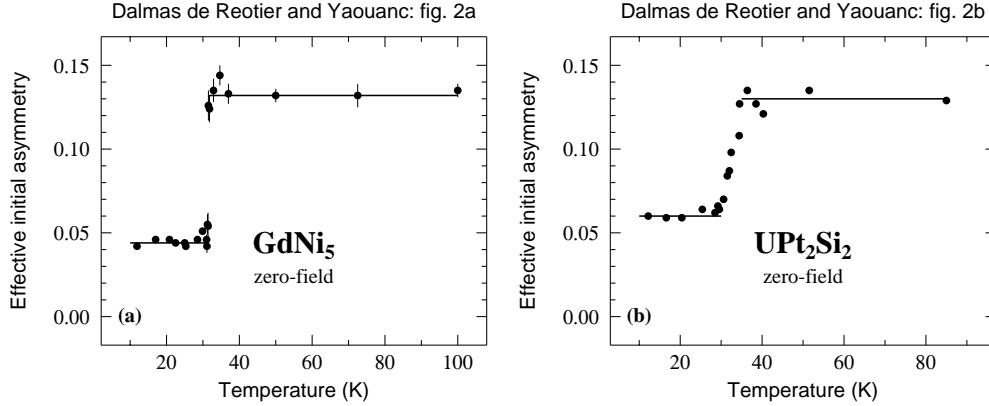


Figure 2. Temperature dependence of the effective initial asymmetry after background subtraction measured in two polycrystalline samples at the ISIS Facility (Dalmas de Réotier *et al* 1990 and Gubbens *et al* 1996). Whereas this asymmetry drops at T_C in a very small temperature range (~ 0.1 K) in the ferromagnet GdNi_5 (a), it changes gradually near T_N (within ~ 5 K) in the antiferromagnet UPt_2Si_2 (b). The solids lines are guide to the eyes.

The depolarization of the muon spins is caused either by a static distribution of local fields (dephasing of the muon spins) or by fluctuating fields (relaxation of the muon spins). The general framework needed to describe the combination of the two mechanisms will be first given. In section 2.1 and section 2.2, respectively, the resulting $P_Z(t)$ and $P_X(t)$ will be presented. The relaxation induced by a purely dynamical process described in section 2.2.

When measuring $P_\alpha(t)$, an ensemble average is made. Usually the muons do not all experience the same local field, i.e. there is a field distribution at the muon site, $D(\mathbf{B}_{\text{loc}})$. The time evolution of the muon magnetic moment experiencing a field \mathbf{B}_{loc} can be computed by solving the Larmor equation in classical mechanics (or the Heisenberg equation in quantum mechanics). We define $\hat{S}_{\mu,\alpha}(t, \mathbf{B}_{\text{loc}})$, the projection along the α axis of the unit vector parallel to the muon moment. The depolarization function is simply written

$$P_\alpha(t) = \int \hat{S}_{\mu,\alpha}(t, \mathbf{B}_{\text{loc}}) D(\mathbf{B}_{\text{loc}}) d\mathbf{B}_{\text{loc}} \quad (3)$$

If the field distribution is sharp, $D(\mathbf{B}_{\text{loc}})$ is a Dirac delta function and we recover (1). Different origins for $D(\mathbf{B}_{\text{loc}})$ exist depending on the physical case. For a magnet the distribution is due to the nuclear and electronic magnetic moments. For a superconductor in the mixed phase, the nuclear magnetic moments and the flux quanta induce the distribution. First, for simplicity, we suppose that this distribution is static, isotropic and Gaussian centered at 0. Therefore the distribution is written as $D(\mathbf{B}_{\text{loc}}) \equiv D(B_{\text{loc}}^X, B_{\text{loc}}^Y, B_{\text{loc}}^Z)$ where

$$D(\mathbf{B}_{\text{loc}}) = \left(\frac{\gamma_\mu}{\sqrt{2\pi}\Delta} \right)^3 \exp \left[-\frac{(\gamma_\mu B_{\text{loc}}^X)^2}{2\Delta^2} \right] \exp \left[-\frac{(\gamma_\mu B_{\text{loc}}^Y)^2}{2\Delta^2} \right] \\ \times \exp \left[-\frac{\gamma_\mu^2 (B_{\text{ext}} - B_{\text{loc}}^Z)^2}{2\Delta^2} \right]. \quad (4)$$

Δ^2/γ_μ^2 is the variance of the components of the field distribution. Δ can be expressed in terms of the interaction between the muon spin and the spins of the compound and the characteristics of the latter spins (see Schenck 1985 for details). In contrast to NMR where the field at the probe of dipolar origin is negligible (except in the case of NMR on protons), the dipolar interaction dominates in the μ SR case. This can have important consequences as shown for example in section 4.1.

Below, we shall present the depolarization function for the two possible experimental geometries, and discuss the meaning of the magnetic field at the muon site.

2.1. The transverse depolarization function

Up to the end of the eighties most of the experiments were performed with the transverse geometry (or in zero external field for the case of magnetically ordered materials), mainly because the spectra are then less sensitive to the quality of the muon beam, e.g., contamination with other particles, than when recorded with the longitudinal geometry. Today the transverse geometry is mainly used for the investigation of the microscopic field distributions arising from either the vortex state in superconductors or magnetic domains in metals. In addition, a very active field of investigation is the measurement of the local susceptibility at the muon site. This type of experiment yields information on the symmetry at the muon site and on the hyperfine coupling-constant.

The field distribution leads to a dephasing of the muon spins responsible for the depolarization. If B_{ext} is sufficiently large relative to Δ/γ_μ , i.e. if $B_{\text{ext}} \geq 5(\Delta/\gamma_\mu)$ (Dalmas de Réotier and Yaouanc 1992), $P_X(t)$ probes only the field distribution along \mathbf{B}_{ext} , i.e. along the Z axis. Then, using (3) and (4), the following simple result is found:

$$P_X(t) = \exp\left(-\frac{\Delta^2 t^2}{2}\right) \cos(\omega_\mu t). \quad (5)$$

If the argument of the Gaussian term is small, i.e. if $t\Delta$ is small, the envelope of $P_X(t)$ is well approximated by the parabolic form $(1 - \Delta^2 t^2/2)$.

Usually the field distribution is not static. A useful first approximation is to account for the dynamics with a single fluctuation rate, ν , and to use the stochastic theory of dynamical processes. Kehr *et al* 1978 have used the strong collision model which supposes that B_{loc} takes a given value for a time $1/\nu$ followed by a new value not related to the previous one, i.e. they consider a Markov process. They have shown that the following analytical formula is a fair approximation:

$$P_X(t) = \exp\left\{-\frac{\Delta^2}{\nu^2} [\exp(-\nu t) - 1 + \nu t]\right\} \cos(\omega_\mu t). \quad (6)$$

This formula, called the Abragam formula (in fact it was first derived by Anderson 1954 as a model for the NMR line shape), interpolates between the static case, (5), and the fast fluctuation limit, the so-called motional-narrowing limit, for which the envelope is an exponential function:

$$P_X(t) = \exp(-\lambda_X t) \cos(\omega_\mu t), \quad \lambda_X = \Delta^2/\nu. \quad (7)$$

Although the Gaussian field distribution model with the dynamics described as a Markov process provides only a rough picture of the physics involved, it is useful since

it clearly shows the physical origin of the measured damped oscillation. The limits of this model for the depolarization induced by nuclear magnetic moments is discussed by Dalmas de Réotier *et al* 1992, Yaouanc and Dalmas de Réotier 1994 and Cameron and Sholl 1994. In a magnet, the functional form of $D(\mathbf{B}_{\text{loc}})$ reflects its magnetic structure. This is discussed in Appendix A. In a type II superconductor, $D(\mathbf{B}_{\text{loc}})$ is usually not Gaussian. In fact its shape is characteristic of the vortex state as shown in section 5. Additional information is provided in Appendix D.

2.2. The longitudinal depolarization function

Nowadays, the longitudinal geometry is popular for the study of magnets since it is well suited for the characterization of a magnetic phase transition. The fact that the measurements can be performed in purely zero-field is a definitive advantage of the μSR method.

In zero-field, an analytical formula is found for $P_Z(t)$ if the distribution is isotropic and Gaussian. Using (3) and (4) one derives

$$P_Z(t) = \frac{1}{3} + \frac{2}{3}(1 - \Delta^2 t^2) \exp(-\frac{1}{2}\Delta^2 t^2). \quad (8)$$

This is the well-known Kubo-Toyabe function which is plotted in figure 3. $P_Z(t)$ exhibits a dip at $t = \sqrt{3}/\Delta$. If $t\Delta$ is sufficiently large, it saturates to $1/3$. If $t\Delta$ is small, $P_Z(t)$ is well approximated by the parabolic form $P_Z(t) = 1 - \Delta^2 t^2$. Relative to the transverse case, the initial depolarization is stronger in zero-field by a factor of two since for the latter geometry the two components of \mathbf{B}_{loc} perpendicular in the Z axis participate to the depolarization. Equation (8) is strictly valid for an isotropic field distribution at the muon site. Szeto 1987, Dalmas de Réotier 1990 and Solt 1995 have computed $P_Z(t)$ for different types of anisotropic field distributions. As expected, the value of $P_Z(t)$ for $t\Delta$ large reflects the type of anisotropy. Equation (8) is derived with the hypothesis that the average field at the muon site is zero. An extension for a finite average field inside a polycrystalline sample has been given by Kornilov and Pomjakushin 1991.

As for the transverse geometry, the dynamics can be accounted for approximately by the strong-collision model (Hayano *et al* 1979). Examples are shown in figure 3. Interestingly, at large t , the functional form of $P_Z(t)$ depends strongly on ν when the distribution is quasi-static, and the Kubo-Toyabe function can still be used but with the $1/3$ factor multiplied by $\exp(-2\nu t/3)$. Therefore, slow dynamical processes can be characterized by zero-field measurements. If ν/Δ is sufficiently large, $P_Z(t)$ is well approximated by the analytical formula (Dalmas de Réotier and Yaouanc 1992)

$$P_Z(t) = \exp\left\{-\frac{2\Delta^2}{\nu^2}[\exp(-\nu t) - 1 + \nu t]\right\}. \quad (9)$$

This approximation is compared in figure 3 to the exact numerical solution for $\nu/\Delta = 3$. This analytical formula is the envelope of the transverse depolarization function (see (6)), except for the substitution $\Delta^2 \rightarrow 2\Delta^2$. The factor 2 reflects again the fact that the depolarization is induced by the two components of \mathbf{B}_{loc} perpendicular to the Z axis. Further analysis of $P_Z(t)$ in a low field for time-dependent random magnetic fields is given by Shibata and Shimoo 1995. In the motional narrowing limit, i.e. when the dynamics is fast, $\nu \ll 1/t$, $P_Z(t)$ is an exponential function

$$P_Z = \exp(-\lambda_Z t), \quad \lambda_Z = 2\Delta^2/\nu. \quad (10)$$

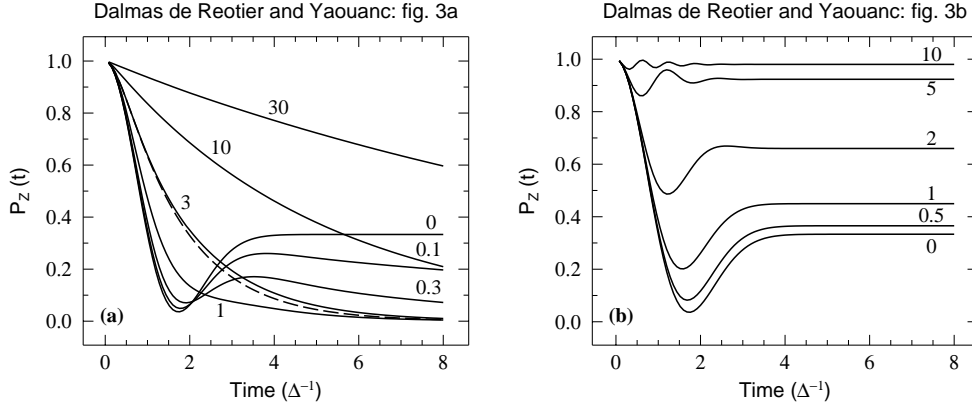


Figure 3. (a) Fluctuation-rate dependence of the zero-field depolarization function derived for a isotropic Gaussian field distribution and a Markov dynamical process. (b) Magnetic field dependence of the longitudinal depolarization function derived for a static isotropic Gaussian field distribution. The values of the fluctuation rate and magnetic field are respectively given in units of Δ and $\Delta/\gamma\mu$. The dashed line in the (a) panel is the prediction of the modified Abragam formula ((9)) for $\nu/\Delta = 3$. The Kubo-Toyabe function (Eq. 8) corresponds to the curves marked with 0 in both panels.

In order to fully characterize a quasi-static process, it is important to perform longitudinal field measurements. Figure 3 presents the field dependence of $P_Z(t)$ for a static field distribution: $P_Z(t)$ is strongly field dependent. Obviously, the strong collision model can be applied to this depolarization functions to account for dynamics. Recently Uemura *et al* 1994 have pointed out that the following scaling property holds:

$$P_Z(\Delta, B_{\text{ext}}, \nu, ft) = P_Z(f\Delta, fB_{\text{ext}}, f\nu, t). \quad (11)$$

Physically, f can be the fraction ($f < 1$) of the time during which the muon experiences a non-zero magnetic field, i.e. in the time fraction $(1 - f)$, this field is zero. Spin liquid systems could be an example of such a model (Uemura *et al* 1994, Bonville *et al* 1997). Note that fitting a spectrum with a regular dynamical Kubo-Toyabe function with a longitudinal field then yields reduced effective $f\Delta$, fB_{ext} and $f\nu$ values.

The field distribution at the muon site in disordered systems is Gaussian only when the spin concentration is large. Walstedt and Walker 1974 have shown that the distribution is Lorentzian for a disordered dilute spin system. Kubo 1981 has computed $P_Z(t)$ for such a distribution. In the motional narrowing limit $P_Z(t)$ is then a square root stretched exponential function. $P_Z(t)$ for disordered systems has been discussed recently by Berzin *et al* 1993, Borgs *et al* 1995 and Crook and Cywinski 1997.

Even if the Gaussian approximation is fair, as it is usually the case for the depolarization due to nuclear spins, the Kubo-Toyabe formula and its extension to dynamical processes does not provide a sufficiently good model to analyse high statistics spectra. The interaction between the muon spin and the lattice spins has to be taken into account, at least in nuclear systems (Celio 1986, Dalmas de Réotier and Yaouanc 1992, Keren 1994, Yaouanc and Dalmas de Réotier 1995).

For a purely fast dynamical process, the relaxation of the muon spin leads to an exponential depolarization function characterized by a relaxation rate λ_Z ; see

Appendix B. This process is very similar to the NMR spin-lattice relaxation, and consists of an exchange of energy between the lattice spins and the two muon Zeeman levels. In that case, the name of relaxation function for $P_Z(t)$ seems more appropriate. We point out that $P_Z(t)$ is an exponential function only if no spatial average is necessary. Therefore, in general, $P_Z(t)$ is not an exponential function for a polycrystalline sample (see Bonville *et al* 1996). In Appendix C we discuss the meaning of λ_Z in terms of the spin correlation-functions of the magnet.

2.3. The magnetic field at the muon site

A detailed discussion of the field at the muon site, \mathbf{B}_{loc} , is given by Schenck and Gygax 1995.

In general \mathbf{B}_{loc} , is the sum of seven terms:

$$\mathbf{B}_{\text{loc}} = \mathbf{B}_{\text{con}} + \mathbf{B}_{\text{trans}} + \mathbf{B}'_{\text{dip}} + \mathbf{B}_{\text{L}} + \mathbf{B}_{\text{dem}} + \mathbf{B}_{\text{dia}} + \mathbf{B}_{\text{ext}}. \quad (12)$$

\mathbf{B}_{con} is the contact hyperfine-field resulting from the spin density at the muon site which is induced by the polarization of the conduction electrons. Therefore it only exists in metals. $\mathbf{B}_{\text{trans}}$ is the transferred hyperfine field. In metals this field is due to the indirect Rudermann-Kittel-Kasuya-Yosida (RKKY) interaction. The next three terms in (12) reflect the muon spin interaction with the localized lattice spins through the dipolar interaction. This interaction gives rise to a dipolar field which is expressed as a lattice sum over the sample. This sum is split into two parts by separating the volume of the sample into a sphere around the muon (the Lorentz sphere) and the rest. \mathbf{B}'_{dip} is given by a lattice sum restricted to the Lorentz sphere; see Appendix A. Summing over the rest yields the Lorentz and the demagnetization fields, $\mathbf{B}_{\text{L}} (= (\mu_0/3)\mathbf{M}_{\text{sat}})$ and $\mathbf{B}_{\text{dem}} (= -\mu_0\mathbf{N}\mathbf{M}_{\text{bulk}})$, respectively. \mathbf{M}_{sat} and \mathbf{M}_{bulk} are respectively the saturation and bulk magnetizations, μ_0 the permeability of free space and \mathbf{N} the demagnetization factor tensor which depends only on the sample shape. The trace of \mathbf{N} is 1. For a sphere $\mathbf{B}_{\text{dem}} = -\mu_0\mathbf{M}_{\text{bulk}}/3$. For an infinite plane, in practice for a disk with extremely small thickness relative to radius, $\mathbf{B}_{\text{dem}} = 0$ if \mathbf{B}_{ext} is applied perpendicular to the disk axis and $\mathbf{B}_{\text{dem}} = -\mu_0\mathbf{M}_{\text{bulk}}$ if \mathbf{B}_{ext} is parallel to the disk axis. \mathbf{B}_{dia} in (12) is the diamagnetic field which is important only for superconductors. In usual magnets, it can be neglected.

In a magnetized ferromagnet all the terms of (12), except \mathbf{B}_{dia} , are to be taken into account. In a ferromagnet which is not macroscopically magnetized, $\mathbf{B}_{\text{dem}} = 0$ because $\mathbf{M}_{\text{bulk}} = 0$. For an antiferromagnet in zero field, \mathbf{B}_{L} and \mathbf{B}_{dem} are necessarily zero. In a metal, \mathbf{B}_{con} and $\mathbf{B}_{\text{trans}}$ are normally independent of the crystal direction. \mathbf{B}'_{dip} depends strongly on the symmetry at the muon site; for examples, see Seeger 1978.

For a paramagnet or a superconductor in an external field, a shift of the muon frequency is usually observed, i.e. \mathbf{B}_{loc} is different from \mathbf{B}_{ext} . The induced field ($\mathbf{B}_{\text{loc}} - \mathbf{B}_{\text{ext}}$) is not necessarily parallel to \mathbf{B}_{ext} . However, in general, $|\mathbf{B}_{\text{loc}} - \mathbf{B}_{\text{ext}}| \ll |\mathbf{B}_{\text{ext}}|$. Therefore it is useful to characterize the observed shift by the projection of ($\mathbf{B}_{\text{loc}} - \mathbf{B}_{\text{ext}}$) onto \mathbf{B}_{ext} :

$$K^{\text{exp}} = \frac{\mathbf{B}_{\text{ext}} \cdot (\mathbf{B}_{\text{loc}} - \mathbf{B}_{\text{ext}})}{B_{\text{ext}}^2}. \quad (13)$$

Since K^{exp} is not intrinsic to the compound (it depends on the sample shape), one

defines a new ratio, K , traditionally called the Knight shift:

$$K = \frac{\mathbf{B}_{\text{ext}} \cdot (\mathbf{B}_{\text{con}} + \mathbf{B}_{\text{trans}} + \mathbf{B}'_{\text{dip}})}{B_{\text{ext}}^2}. \quad (14)$$

The two ratios can be related using (12):

$$K = K^{\text{exp}} - \left(\frac{1}{3} - n\right) \chi_p - (1 - n) \chi_d, \quad (15)$$

where χ_p is the paramagnetic susceptibility, χ_d the diamagnetic susceptibility produced by persistent currents in the mixed state of a superconductor and n the appropriate component of N (Heffner *et al* 1989). Obviously $\chi_d = 0$ if the compound is not superconducting at the temperature of the measurement. At first sight, one may be surprised that χ_p and χ_d are not multiplied by the same factor. This is understood if one remembers that \mathbf{B}_{L} responsible for the $1/3$ factor originates from the dipole moments in the Lorentz sphere. This concept is unsuitable for the superconducting electrons. The factor 1 in $(1 - n)$ originates from \mathbf{B}_{dia} , i.e. it does not concern the paramagnetic properties of the compound.

The concept of Knight shift is useful because one expects this quantity to be field independent. In particular, in superconductors, its thermal behaviour when crossing the superconducting temperature yields direct information on the parity of the superconducting order parameter. However, recent measurements on UBe_{13} and $\text{UBe}_{12.91}B_{0.09}$ indicate that the Knight shift concept is not valid for these compounds since $[B_{\text{loc}}(T) - B_{\text{loc}}(T_c)]$ is field independent (Luke *et al* 1991, Heffner *et al* 1997), i.e. $B_{\text{loc}}(T)$ does not scale with B_{ext} .

Since K depends linearly on the components of the susceptibility tensor, for a given \mathbf{B}_{ext} direction, it is presented as a function of the corresponding susceptibility, the temperature being an implicit parameter. From such plots (the Clogston-Jaccarino plots) the value of the components of the dipolar tensor and of the hyperfine coupling constant can be determined (Schenck and Gygax 1995).

The study of the angular dependence of the local field at the muon site measured in transverse field on a single crystal in the paramagnetic phase gives the opportunity of determining the muon site. In figure 4 such an angular dependence is shown for the cubic system CeB_6 (space group $Pm\bar{3}m$). The presence of two different fields (as seen in the Fourier transform of the measured signal) indicates the existence of two magnetically inequivalent sites for the muon. From the analysis of this angular dependence and the value of the component of the dipolar field deduced from the Clogston-Jaccarino plot, Amato *et al* 1997 infer that the muon occupies the d site $(0, 0, 1/2)$. In recent years this type of procedure has been used to determine the muon site in many intermetallic compounds. The results show that it is not possible to predict reliably the muon site localization. For a given crystal structure, this site depends on the chemical formula of the compound. It may even depend on the temperature. Because of its electric charge, the muon may distort locally the crystal lattice and induce an electric field gradient on its neighbor atoms.

3. Magnetic phase diagrams

The μSR technique has been popular in the condensed matter community for its success in detecting magnetic phase transitions in compounds with small magnetic

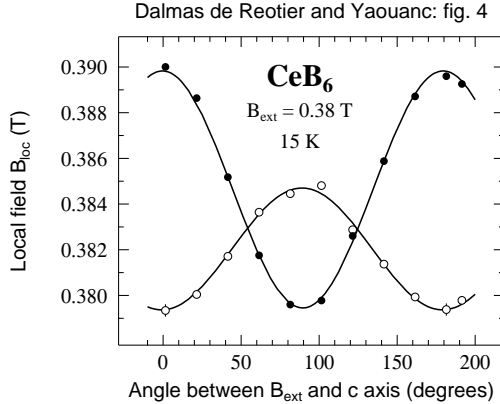


Figure 4. Angular dependence of the two local fields observed in CeB_6 . \mathbf{B}_{ext} was rotated around the $[1, 1, 0]$ axis. The two signals have an amplitude ratio 2:1 corresponding on one hand to the $(1/2, 0, 0)$ and $(0, 1/2, 0)$ sites (open symbols) and on the other hand to the $(0, 0, 1/2)$ site (solid symbols). The solid lines are fit to the data (adapted from Amato *et al* 1997).

moments. In this section we examine four such examples. In section 3.1 and section 3.2 we discuss recent results obtained for the organic and low dimensional magnets, respectively. Whereas for the organic compounds oscillating μSR signals are detected, pointing to the existence of relatively well ordered magnetic structures, in the 3-leg spin ladders one only observes wide field distributions, a fingerprint of disorder. In section 3.3 we show that the μSR technique can be used to detect magnetic domains in a diamagnetic metal such as beryllium. The appearance of the domains is directly connected to the de Haas-van Alphen effect. Finally we present in section 3.4 new results obtained for some heavy fermion metals in which two f electron components exist.

3.1. Magnetic ordering in organic compounds

The search for purely organic molecular ferromagnets which contain only light elements (carbon, nitrogen, hydrogen and oxygen) is a subject of strong current interest. The first such material to be found, the β crystal phase of *para*-nitrophenyl nitronyl nitroxide (*p*-NPNN, $\text{C}_{13}\text{H}_{16}\text{N}_3\text{O}_4$), was reported to have a Curie temperature $T_C \sim 0.6$ K (Tamura *et al* 1991). The unpaired spin is associated with the nitronyl nitroxide group (N-O group). The role of the rest of the molecule is to ensure the appropriate overlap of the correct orbitals on neighbouring molecules to produce 3D ferromagnetism. A whole series of materials which incorporate this N-O group has been synthesized.

The first direct observation of spontaneous magnetic order in *p*-NPNN was done using the μSR technique (Le *et al* 1993b). It has been subsequently confirmed by zero-field neutron diffraction (Zheludev *et al* 1994). In figure 5a we present three zero-field μSR spectra. The mere observation of an oscillating signal at low temperature, i.e. of a spontaneous internal magnetic field B_{loc} , is a clear signature of the existence of static magnetic correlations. Since a long-lived oscillation is detected rather than an increase in damping, *p*-NPNN orders with a well defined magnetic structure. Measurements on crystals indicate that \mathbf{B}_{loc} is nearly parallel to the b crystal axis which is the easy

axis (Le *et al* 1993b). The shape of the spectra changes drastically between 650 mK and 700 mK as seen in figure 5a: the magnetic phase transition occurs between these temperatures. In figure 5b we present the temperature dependence of B_{loc} . The solid line is a fit with $B_{\text{loc}}(T) \propto [1 - (T/T_C)^\alpha]^\beta$. This compact formula allows us to discuss the spin wave ($T \ll T_C$) and the critical regimes: for $T \ll T_C$, $[B_{\text{loc}}(0) - B_{\text{loc}}(T)] \propto T^\alpha$ and $B_{\text{loc}}(T) \propto (T - T_C)^\beta$ near T_C . $B_{\text{loc}}(T)$ is well described in the whole ferromagnetic state by the compact formula with $\alpha = 1.7$ (4) and $\beta = 0.36$ (5) (Le *et al* 1993b and Blundell *et al* 1995). These results are consistent with that of a 3D Heisenberg magnet. The weak magnetic anisotropy is accounted for by the dipolar interaction between the unpaired electron spins (Le *et al* 1993b). The small $B_{\text{loc}}(T = 0\text{K})$ value found in the organic magnets is a strong indication that the magnetic moment carried by the unpaired electrons is small since it would be surprising that the dipolar field at the muon site accidentally cancels almost perfectly in all these compounds. An analysis of the behaviour of the oscillations in an applied longitudinal field, in terms of the magnetization process and demagnetising field, is given by Blundell *et al* 1995.

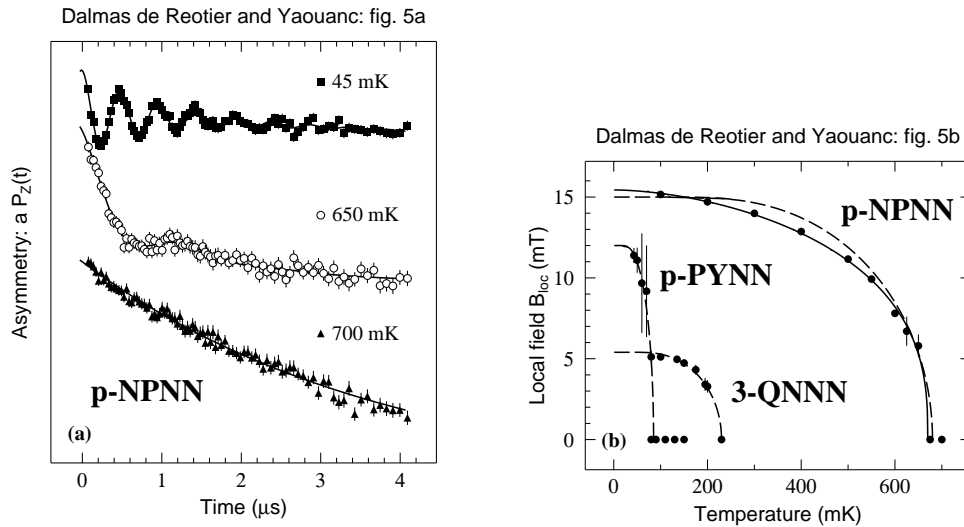


Figure 5. (a): some zero-field spectra recorded for *p*-NPNN (adapted from Blundell *et al* 1995). The solid lines are fits. (b): temperature dependence of the local magnetic field at the muon, B_{loc} , in *p*-NPNN, *p*-PYNN and 3-QNNN (adapted from Blundell *et al* 1994 and 1995). The solid line is a fit with $B_{\text{loc}}(T) \propto [1 - (T/T_C)^\alpha]^\beta$. The dashed lines are fits with the molecular field model with spin $S = 1/2$.

The transition temperature and the nature of the magnetic ground state of the molecular crystals based on the nitronyl nitroxide radical depend strongly on their crystal structure. This is nicely seen in figure 5b: $T_C \approx 90$ mK for *p*-PYNN, $T_C \approx 230$ mK for 3-QNNN and $T_C \approx 670$ mK for *p*-NPNN. Other examples and a detailed discussion are given by Blundell *et al* 1997b.

It is well known that neutron scattering can provide extensive information on magnets, in particular on the magnetic structure and on the excitations. But in compounds with small magnetic moments such as the organic magnets, the μSR technique is a sensitive and useful probe: it easily yields the value of the critical temperature and information on the thermal behaviour of the order parameter. In

addition, it should be possible to investigate the excitations at a very small energy transfer (see section 4.1 for an example for a conventional ferromagnet).

3.2. Magnetic ordering in spin chains and ladders

Hoping to gain insight into the mechanism of superconductivity, some experimentalists and theoreticians have recently turned their attention to systems as simple as one dimensional chains and ladders of copper and oxygen atoms with the aim to eventually apply their findings to the high T_c superconductors where Cu-O planes play an important role. The μ SR technique has been used to determine the magnetic properties of the ground state of some of these systems.

The ground state properties of a linear chain of antiferromagnetically coupled spins have been intensively studied because of the pronounced quantum effects. Both integer and half integer spin chain systems have a singlet ground state (Mermin and Wagner 1966, Haldane 1983a and 1983b). Because the spin excitations are gapless at momentum $q = 0$ and π for half integer spin chains (des Cloizeaux and Pearson 1962), a magnetic ordering can be expected when interchain interactions are taken into account. However, for integer spin chains which have a so-called Haldane energy gap (Haldane 1983a and 1983b), no ordering should occur. The key parameters for half integer spin chains are the magnitude of the ratio T_N/J (J is the intra-chain coupling constant) and the ordered magnetic moment at $T = 0$ K, $M(T = 0)$. J is estimated from magnetic susceptibility and infrared light absorption measurements. The Néel temperature is easily determined by zero-field μ SR in such systems characterized by small magnetic moments. Neutron diffraction is the most direct method to measure $M(T = 0)$. Although the μ SR technique cannot yield a precise $M(T = 0)$ value for a given compound, it is well suited to measure accurately the relative size of moments for iso-structural materials. Therefore a combined neutron diffraction and μ SR study is expected to yield reliable results. Kojima *et al* 1997 have done such a study for the quasi one-dimensional antiferromagnets Sr_2CuO_3 and Ca_2CuO_3 . Plotting $M(T = 0)$ versus T_N/J and comparing with different models, they find that the chain mean field approach best explains the experimental results. This approach takes more quantum effects into account than the two different spin-wave approximations available. Probably, this is the reason why it provides a better description since the moment reduction is dominated by quantum spin fluctuations.

As mentioned, the spin ladder systems have been studied because it is thought that an understanding of their magnetic properties is a prerequisite for a proper description of the magnetic properties of infinite CuO layer systems. A 3-leg ladder structure is displayed in figure 6. The oxides $\text{Sr}_{n-1}\text{Cu}_{n+1}\text{O}_{2n}$ are realizations of such ladders. Indeed, one observes that the geometry of the ladder structure and of the CuO square lattice layer are related. A nice review of the physics of these systems is given by Goss Levi 1996. Note that the physics of the spin ladder systems and of the Haldane spin chains are closely related (Strong 1997).

A key prediction is that only ladders with even numbers of legs have a singlet ground state separated from the triplet state by a large spin gap (Rice *et al* 1993). However, the odd-leg systems are expected to reach a magnetically ordered ground state in the presence of interladder interactions. Kojima *et al* 1995a have performed zero-field and longitudinal field μ SR measurements to test these theoretical predictions.

In figure 7 spectra recorded on the 3-leg system are presented. The strong

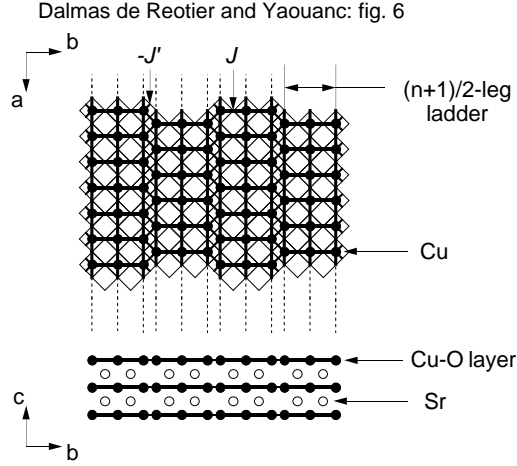


Figure 6. The 3-leg ladder structure (from Kojima *et al* 1995a). Oxygen ions locate at each corner of the squares. The ferromagnetic interladder interaction J' is much smaller than the antiferromagnetic intraladder interaction J .

depolarization of the zero-field spectra at low temperature shows that the ground state is magnetic. Since no wiggles are detected (in contrast to the observations for the organic magnets; see section 3.1), the disorder in the compound is important or the number of muon localization sites with different local fields is large. Comparing the spectra recorded at 50 K and 60 K, we infer that a 3D magnetic phase transition occurs between these temperatures. The longitudinal field measurements confirm the interpretation of the zero-field spectra, i.e. the ground state of the 3-leg system with interladder interactions is a conventional static ordered state rather than a spin liquid system since $f \simeq 1$ (see (11)).

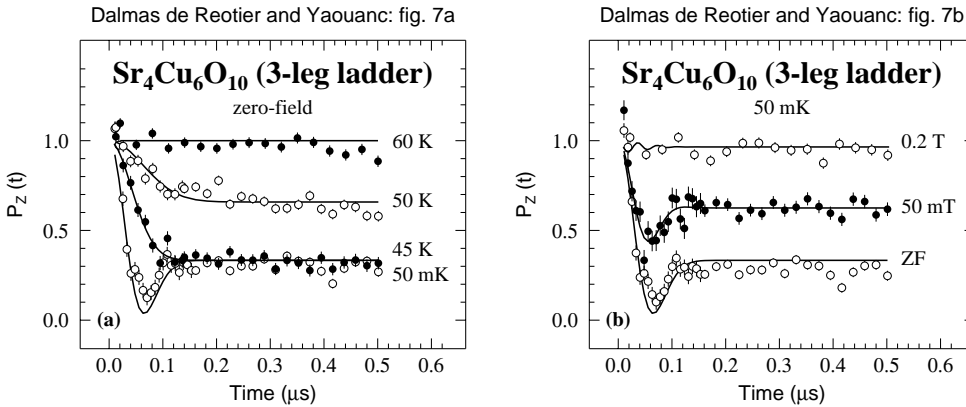


Figure 7. Some spectra recorded on $\text{Sr}_4\text{Cu}_6\text{O}_{10}$ which has a 3-leg spin ladder structure. The solid lines are fits (adapted from Kojima *et al* 1995a).

The magnetic behavior of the 2-leg and 3-leg ladder systems differ remarkably as seen in figure 8. The depolarization functions are described with a square-root exponential function, appropriate for dilute fluctuating moments (see section 2.2).

Therefore no static magnetic ordering is detected. The depolarization originates from dilute unpaired spins which may be associated with defects in the sample.

In conclusion, the work of Kojima *et al* 1995a confirms the theoretical predictions (Rice *et al* 1993) that a 3-leg system becomes magnetic at low temperature but not a 2-leg system.

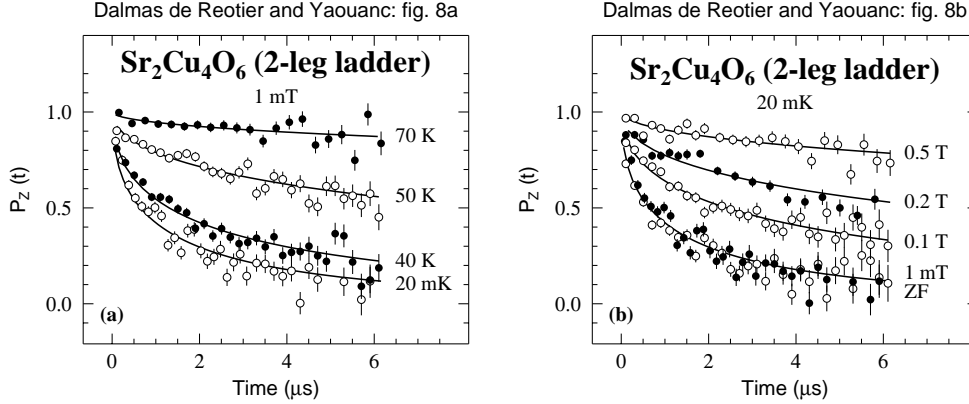


Figure 8. Some spectra recorded on $\text{Sr}_2\text{Cu}_4\text{O}_6$ which has a 2-leg spin ladder structure. The solid lines are fits (adapted from Kojima *et al* 1995a). Note that the horizontal scales are ~ 10 times larger than in figure 7.

3.3. Diamagnetic domains in beryllium

In general terms, we first note that the relation between induction, external field and magnetization for a given material is given by

$$\mathbf{B} = \mathbf{B}_{\text{ext}} - \mu_0(\mathbf{N} - \mathbb{1})\mathbf{M}, \quad (16)$$

where \mathbf{N} is the demagnetization factor tensor and $\mathbb{1}$ the unit tensor. Therefore if the external field \mathbf{B}_{ext} is applied perpendicular to an infinite plane, in practice to a platelike sample with extremely small thickness relative to radius, (16) yields (see section 2.3) $\mathbf{B} = \mathbf{B}_{\text{ext}}$, i.e. the induction should follow the external field.

It is well known that the magnetic response of a non-magnetic metal can oscillate as a function of B_{ext} . This is the de Haas-van Alphen (dHvA) effect which is used to study Fermi surfaces (Shoenberg 1984). Condon 1966 noticed that if the oscillating amplitude is large within some part of each dHvA oscillation period, i.e. for a given B_{ext} range, the conduction electron states in this range are thermodynamically unstable and cannot follow the electrodynamics relation $\mathbf{B} = \mathbf{B}_{\text{ext}}$. Therefore the electronic system should jump periodically over the forbidden intervals of B . A compromise could be the splitting of the magnetic energy in alternating diamagnetic (with induction smaller than B) and paramagnetic (with induction larger than B) domains. With such a domain structure the relation $\mathbf{B} = \mathbf{B}_{\text{ext}}$ is fulfilled as an average over the sample. The so-called Condon domains are spectacular manifestations of the collective behaviour of the electrons in quantized cyclotron orbits, i.e. Landau states.

The first direct observation of the Condon domain formation was made on silver by NMR measurements (Condon and Walstedt 1968). One had to wait 28 years for a second report on the domain formation: using transverse field μSR measurements,

Solt *et al* 1996a have reported the observation of domains in beryllium. Interestingly, the prediction of Condon was made for beryllium.

As a first step, Solt *et al* 1996a have analyzed their data using (7). The field dependence of λ_X is presented in figure 9. Any deviation from $\lambda_X(B_{\text{ext}}) \approx \text{constant}$ must reflect the influence of the dHvA effect. The function $\lambda_X(B_{\text{ext}})$ rises periodically, reaching values about 10 times as large as its minimum. The period is consistent with the expected dHvA value. The broadening model is practical to visualize the dHvA effect but not strictly justified. Solt *et al* 1996a have then performed a Fourier analysis. The results for the central peak region of figure 9 are presented in figure 10. As expected, within a given field range, B_{loc} , which is a measure of the induction, does not follow B_{ext} . The diamagnetic and paramagnetic signals are clearly seen, their respective populations changing smoothly as B_{ext} increases. Interestingly, the domains could not be visualized by NMR on beryllium because of the excessive linewidth produced by the electric field gradients. Since the muon does not have a quadrupolar moment, it does not couple to these gradients. The Condon domains have been detected by a point-like probe such as the muon because the volume occupied by the domains is much larger than the volume of the domain walls: at $B_{\text{ext}} = 1$ T, the domain and wall thicknesses are $\sim 30 \mu\text{m}$ and $\sim 1 \mu\text{m}$, respectively (Solt *et al* 1996b). Note that the observation of the domains means that they are pinned (static) for the time scale of the muon experiment ($\sim 1 \mu\text{s}$).

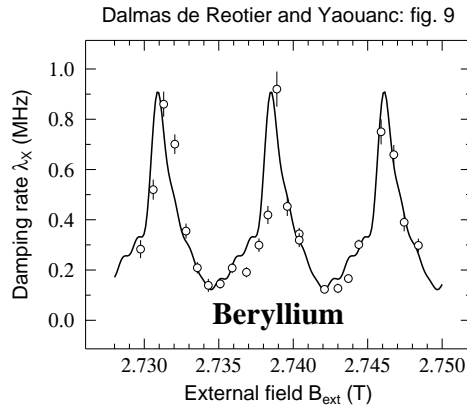


Figure 9. Exponential damping rate λ_X of the μSR signal as a function of the intensity of the external field measured on beryllium. The temperature is 0.8 K. The periodic sharp rises of λ_X mark the onset of line splitting due to the domain formation. For $\lambda_X \geq 0.4$ MHz the broadened line turns out to be a well resolved doublet. The solid line is a best fit to a truncated Fourier series (adapted from Solt *et al* 1996a).

The Condon domains discovered in silver and beryllium correspond to the simplest possibility. A variety of domain-like periodic structures have been predicted (for a review, see Solt *et al* 1996b). We expect that with the improvement of the high field transverse field μSR spectrometers, the investigation of magnetic domains in the bulk of non-magnetic metals will attract much interest in the future.

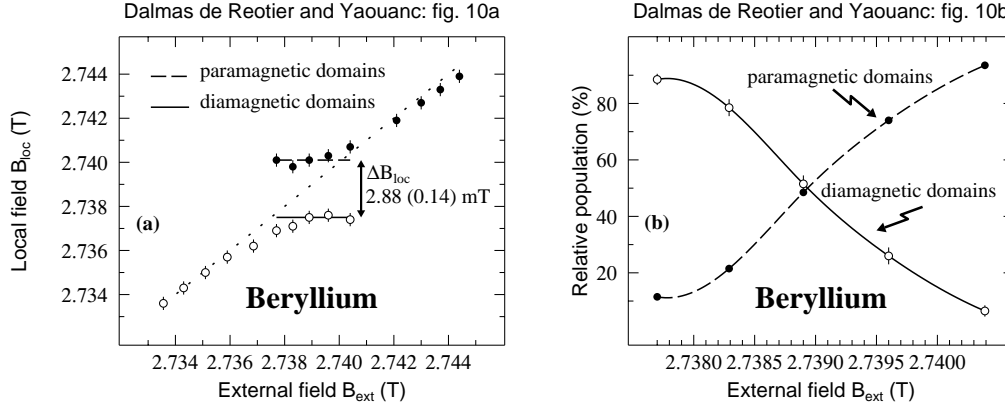


Figure 10. Analysis of the central peak of figure 9. The (a) panel displays the intensity of the local fields at the muon site versus the intensity of the external field. The difference between the fields in the paramagnetic and diamagnetic domains is clearly resolved. For reference the line whose equation is $B_{loc} = B_{ext}$ is plotted (dotted line). The (b) panel presents the relative populations of the paramagnetic and diamagnetic domains versus the intensity of the external field. The lines are guide to the eyes. (adapted from Solt *et al* 1996a).

3.4. Localized and itinerant f electrons in heavy fermion materials

In recent years the analysis of μ SR data recorded in some intermetallic compounds containing cerium or uranium atoms has suggested that two different substates of electrons of f character are present. In this section the available experimental evidence found recently is presented. We discuss in some detail results obtained for the heavy fermion superconductor UPd_2Al_3 and the heavy fermion metal CeRu_2Si_2 . We then mention the superconductor CeRu_2 and give a short discussion of the magnetic behaviour of these f electron magnets, pointing out the complementary nature of the information obtained by μ SR and inelastic neutron scattering.

UPd_2Al_3 belongs to the small family of heavy fermion superconductors; see for example Heffner and Norman 1996. It has a hexagonal crystal structure (space group $P6/mmm$) and exhibits a coexistence of superconductivity ($T_c \simeq 1.5 \text{ K}$) and antiferromagnetism ($T_N \simeq 14 \text{ K}$). The uranium atom carries a relatively large magnetic moment of $0.85 \mu_B$ as determined by neutron diffraction. The uranium moments are aligned ferromagnetically in the basal plane along the a axis and stacked antiferromagnetically along the c axis. The magnetic structure is not affected by the superconducting transition, which is intriguing in view of the unquestionable $5f$ character of both the heavy quasiparticles forming the Cooper pairs and the electrons responsible for the antiferromagnetic structure. The transverse field μ SR investigation of the superconducting phase by Feyerherm *et al* 1994 provides information on the $5f$ electrons involved in the Cooper pair formation.

Since the local field produced by the magnetic sublattices in the antiferromagnetic phase cancels at the muon localization site, a study of the muon frequency shift could be undertaken below T_N and in particular in the superconducting phase. The key point is the observation that the positive frequency shift along the c axis as well as the negative frequency shift in the basal plane are decreasing in absolute values when the temperature decreases below T_c as seen in figure 11. In discussing the possible

origins for this decrease, Feyerherm *et al* 1994 noticed that the diamagnetic shift due to the flux expulsion or a possible change of the hyperfine coupling cannot explain the data. Therefore, the observed partial reduction of the frequency shifts can only reflect a decrease of the susceptibility of the $5f$ electrons. Taking into account the strong anisotropy of the bulk susceptibility, these authors infer that the f electron susceptibility reduction due to superconductivity is isotropic. This, apparently surprising, result can be understood if the $5f$ electrons are viewed as two essentially independent electron subsets. The decrease of the susceptibility is associated with the electron system formed by the heavy quasiparticles condensing into Cooper pairs below T_c . Interestingly, this reduction suggests singlet pairing of the Cooper pairs. The residual susceptibility is ascribed to the electron subsystem associated with the local antiferromagnetism which is not affected by superconductivity. We mention that the analysis of NMR Knight shift data leads to the same physical picture if one assumes that the hyperfine coupling constant is temperature independent, in contrast to the μ SR analysis which does not need this assumption (Kyogaku *et al* 1993).

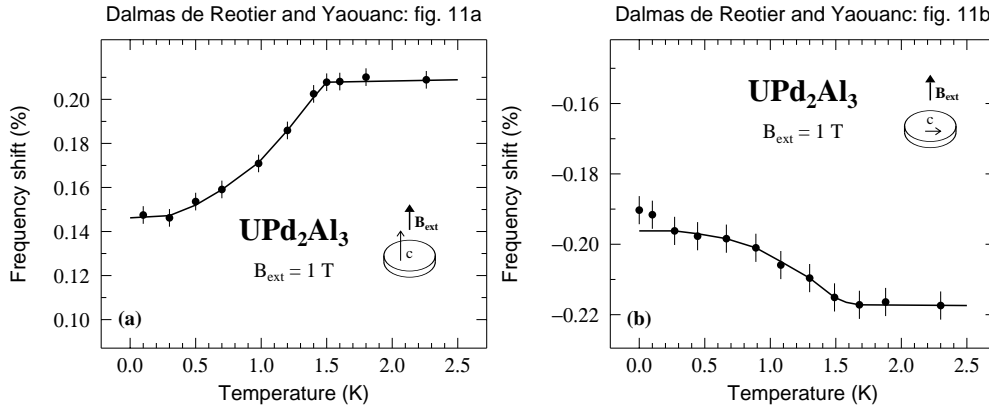


Figure 11. Temperature dependence of the muon frequency shift in UPd_2Al_3 measured in an external field of 1 T applied either along or perpendicular to the c axis. Note the strong reduction of the absolute value of the shifts below the superconducting transition ($T_c \simeq 1.5$ K). The solid lines are guides to the eyes. The data are not corrected for demagnetization and Lorentz fields. (adapted from Feyerherm *et al* 1994).

The picture of an isotropic itinerant $5f$ electron subset is supported by the μ SR observation of an almost isotropic London penetration depth (Feyerherm *et al* 1994). It is noteworthy that specific heat measurements under pressure indicate that the itinerant subset accounts for 80 % of the linear coefficient of the specific heat (Caspary *et al* 1993).

CeRu_2Si_2 has attracted considerable interest because it lies at the borderline of a magnetic instability, between long-range magnetic order and paramagnetic ground state (for a review, see Kambe *et al* 1996).

In figure 12 is presented the temperature dependence of the zero-field exponential damping rate measured on a CeRu_2Si_2 crystal (Amato *et al* 1993). The rate increases significantly below ~ 2 K, corresponding to an enhancement of the field spread at the muon site of the order of $20 \mu\text{T}$. The static nature of the local field is proved by the strong reduction of the damping rate measured in a longitudinal field as shown

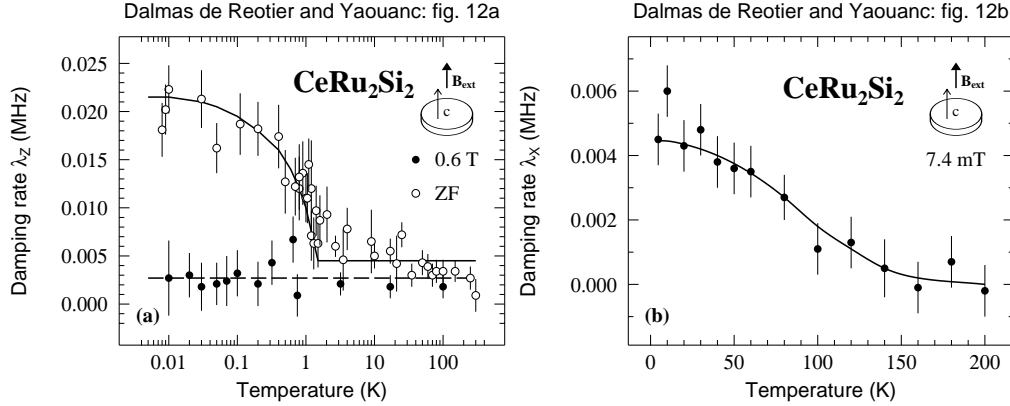


Figure 12. Temperature dependence of the damping rates measured with a single crystal of CeRu_2Si_2 . On the (a) and (b) panels are presented the rates recorded with the longitudinal and transverse geometry, respectively. These measurements show that CeRu_2Si_2 exhibits, in addition to a static magnetic field distribution below ~ 2 K, a dynamical magnetic component persisting up to ~ 150 K. The solid lines are guide to the eyes (adapted from Amato *et al* 1993)

in figure 12. The exponential shape of $P_Z(t)$ in zero-field is surprising as one would expect to observe a parabolic function for such small damping rates. Amato *et al* 1994 argue that the enhancement of the field distribution originates from a static electronic magnetic moment carried by the Ce atoms. The Ce magnetic moment is estimated to be $\simeq 10^{-3} \mu_B$. Because of this extremely small value, this magnetism is probably itinerant in nature. Since the value is found using a localized magnet model, there is quite a large uncertainty on the value of the magnetic moment deduced from the data. The small longitudinal damping rate which seems to exist at high magnetic field suggests the presence of fast electronic spin fluctuations. The existence of such fluctuations is confirmed by the transverse field measurements shown in figure 12. These fluctuations, which are observed up to ~ 150 K, have been related to the short-range dynamical magnetic correlations detected below ~ 60 K by inelastic neutron scattering (Regnault *et al* 1988). They involve a relatively large Ce magnetic moment ($0.6 \mu_B$, see Amato *et al* 1994) and an extremely short correlation time of $\sim 10^{-13}$ s (Amato *et al* 1993).

Recently, zero-field and longitudinal field measurements on a polycrystalline sample of the superconductor CeRu_2 ($T_c = 6.1$ K) have shown that this compound presents a magnetic phase transition at $\simeq 40$ K characterized by an extremely small magnetic moment of $\sim 10^{-4} \mu_B$ (Huxley *et al* 1996). Because of this extremely small value, the magnetism is itinerant in nature. We note that a high energy neutron scattering study of CeNi_2 , a compound which should have the same magnetic characteristics as CeRu_2 , has revealed a strong inelastic paramagnetic response of the Ce ion with a large Kondo temperature (Murani and Eccleston 1996). The combination of the μSR results on CeRu_2 and the neutron data on CeNi_2 suggests again the existence of a two component $4f$ electronic system: in this case, a $4f$ weakly polarized itinerant electron system and a paramagnetic $4f$ localized electron system.

The picture of two different substates of electrons of f character which emerges from the analysis of the UPd_2Al_3 , CeRu_2Si_2 and CeRu_2 data was already suggested for UCu_5 by Schenck *et al* 1990. Some years ago inelastic neutron scattering

measurements on CeCu_6 and CeRu_2Si_2 were analyzed in terms of two magnetic contributions (Aeppli *et al* 1986 and Regnault *et al* 1988). Amato *et al* 1993 have shown that the two contributions observed by neutron and μSR can be nicely related in the case of CeRu_2Si_2 . Clearly, it would be of interest to carry on this type of comparison keeping in mind that, contrary to the inelastic neutron scattering technique, the μSR method probes the spectral weight of the modes at extremely small energy transfer, i.e., quasi-static modes.

The two component picture which is proposed from the analysis of the data is in qualitative agreement with the duality model for heavy fermion (Kuramoto and Miyake 1990) which introduces two coupled electron components: itinerant and localized. The physical basis of such a picture is attributed to the fact that the one-particle density of states has a triple peak structure in strongly correlated fermion systems. This structure consists of two broad peaks corresponding to the upper and lower Hubbard bands and a narrow quasiparticle peak at the Fermi level. Interestingly, this type of structure is found by recent numerical works using the $d = \infty$ technique, d being the space dimension (see for example, Georges and Kotliar 1992). A recent theoretical discussion is given by Pépin and Lavagna 1997.

A high resolution photoemission study of CeRu_2 has found a substantial $4f$ electron density at the Fermi level, in agreement with the interpretation of the μSR result on this compound and the duality picture (Yang *et al* 1996).

4. Spin dynamics in magnets

The study of the spin dynamics in magnets has been a traditional subject of μSR . But it is only recently that quantitative information has been extracted, thanks to greatly improved experimental conditions and better data analysis. In section 4.1 and section 4.2, spectra recorded respectively in the critical regime of a ferromagnet and for a spin-glass are analyzed in terms of spin-spin correlation-functions. The first study has taken advantage of the possibility to carry out the measurements in truly zero field and the second one, of the large spectrum of fluctuations which can be probed. The discussion is partly based on the material presented in Appendix B and Appendix C.

4.1. Critical and low temperature spin dynamics in ferromagnets

The first detailed analysis of data recorded in the critical regime has been given for Ni and Fe by Yaouanc *et al* 1993a and 1993b and for Gd by Dalmas de Réotier and Yaouanc 1994. These works were restricted to the critical paramagnetic regime. In this section we present an analysis of the spin dynamics of the Gd^{3+} ion spins in the dipolar axial ferromagnet GdNi_5 covering the whole temperature range (Yaouanc *et al* 1996a). This zero-field study reveals the effect of the dipolar interaction on the physical properties of the spin-spin correlation-tensor $\tilde{\Lambda}^{\alpha\beta}(\mathbf{q})$, both in the paramagnetic and ferromagnetic state. This effect is expected to be strong since the measurements probe the fluctuation modes in the zone center where the long range nature of the dipolar interaction dominates the dynamics. This interaction introduces non-conserving terms in the Hamiltonian which prevents the slowing down of the longitudinal (to the wave vector) modes near the Curie temperature, T_C (Kötzler 1986). Therefore, if the measured relaxation rate reflects only these modes, it should saturate as the temperature approaches T_C .

GdNi₅ crystallizes in the hexagonal CaCu₅ crystal structure and exhibits a ferromagnetic phase transition at $T_C \simeq 32$ K characterized by a small magnetic dipolar anisotropy field as determined by magnetization measurements: $B_a(T = 5 \text{ K}) \simeq 0.21$ T. The muon localization site(s) is unknown.

An overview of the zero-field relaxation rate λ_Z is presented in figure 13a. This rate reflects the fluctuations of the Gd³⁺ ion spins. No signal is found in the ferromagnetic state when \mathbf{S}_μ is perpendicular to the crystal c axis since the spontaneous muon spin rotation is too fast to be resolved at the pulsed source (ISIS) where the data were recorded. Four temperature regions can be distinguished: far above or below the Curie temperature T_C and the critical paramagnetic and ferromagnetic regions.

Far above T_C , the wave vector dependent spin-spin correlation-tensor, $\tilde{\Lambda}^{\alpha\beta}(\mathbf{q})$, is expected to be isotropic and independent of the wave vector: $\tilde{\Lambda}^{\alpha\beta}(\mathbf{q}) = \tilde{\Lambda}^{\alpha\beta}$. The observed anisotropy of λ_Z , which reflects the anisotropy of the coupling tensor between the muon spin and the Gd³⁺ spins, can be explained if the muon occupies the interstitial site of coordinates $(1/2, 0, 0)$.

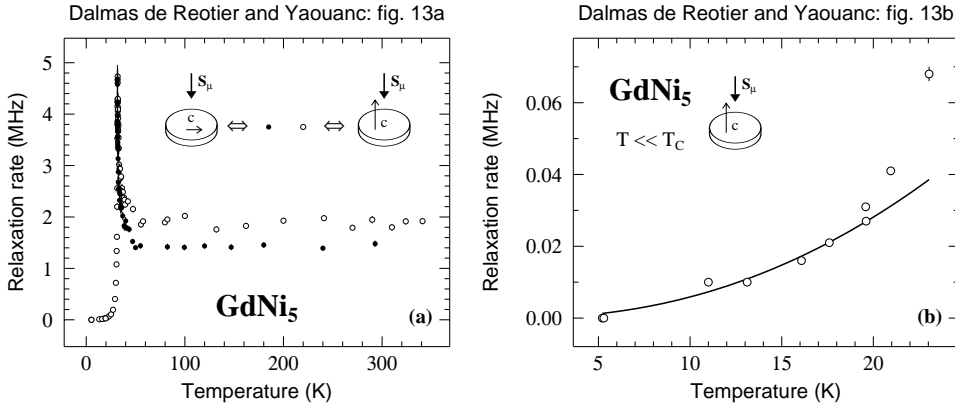


Figure 13. (a): an overview of the zero-field relaxation rate of GdNi₅ (Yaouanc *et al* 1996a). The two sets of data refer to measurements performed on two crystals which differ by the orientation of \mathbf{S}_μ relative to the c axis. (b): zero-field relaxation rate of GdNi₅ at low temperature (Yaouanc *et al* 1996b). The full line is the prediction for the relaxation induced by the Raman spin wave process (equation (17)).

Far below T_C , the spin-lattice relaxation rate increases with temperature as shown in figure 13b. Its thermal variation is interpreted as due to the relaxation of the muon spins by the magnons. Since the minimum magnon energy is much larger than the Zeeman muon energy $\hbar\omega_\mu$, a one magnon process cannot flip the muon spin because energy-conservation requirement would not be ensured. Therefore, the perturbation operator which induces the muon spin flip cannot contain the J^x and J^y operators (J denotes the Gd³⁺ spin). In terms of the correlation-tensor $\tilde{\Lambda}^{\alpha\beta}(\mathbf{q})$, this means that one does not have to consider the correlations with $\{\alpha\beta\} = \{x, y\}$. On the other hand, a two-magnon, or Raman, process does not present problems as regards energy conservation because the only requirement is that the energies of the annihilated and created magnons must be equal (we neglect $\hbar\omega_\mu$). Therefore the energy principle tells us that only the parallel (to the easy axis z ; the Z and z axes are parallel) fluctuations contributes to the relaxation, i.e. the measurements only probe the correlation-function $\tilde{\Lambda}^{zz}(\mathbf{q})$ (Yaouanc and Dalmas de Réotier 1991).

While in NMR the Raman process is almost never observed because the hyperfine interaction between the spin probe and the lattice spins is isotropic (therefore a perturbation operator such as $\sigma_{\pm}J^z$ does not exist; σ is the Pauli operator of the spin probe), this process is expected to be active in μ SR since the interaction between the spins is mainly due to the dipolar interaction which is spatially anisotropic.

The key parameter which determines if the muon spin is relaxed by the Raman process is the ratio of the minimum magnon energy over the thermal energy. The relaxation is effective only if this ratio is sufficiently small. This means that $\lambda_Z = 0$ at very low temperature as observed experimentally in figure 13b. For a small ratio, i.e. at high temperature, we expect $\lambda_Z \propto T^2$ since two magnons are involved. This quadratic law is a robust result in the sense that it does not depend on the details of the model.

Using the simple magnon dispersion relation $\hbar\omega_{\mathbf{q}} = D_m q^2 + \Delta$, where D_m is the magnon stiffness constant and Δ the anisotropy energy which is of dipolar origin, and the fact that $\Delta = g_L \mu_B B_a \ll k_B T$ for GdNi₅, the following approximate result holds (Dalmás de Réotier and Yaouanc 1995):

$$\lambda_Z = \frac{\mathcal{C} g_L^2 T^2}{D_m^3} \left[1 + \frac{15}{2} [(C^{xz}(\mathbf{q} = \mathbf{0}))^2 + (C^{yz}(\mathbf{q} = \mathbf{0}))^2] \right] \ln(k_B T / \Delta). \quad (17)$$

\mathcal{C} is the analytical part of the tensor describing the dipolar interaction between the muon spin and the Gd³⁺ spins; see (A10). Equation (17) accounts for the effect of the spin waves near the zone center. Note that λ_Z is independent of the characteristics of the muon localization site(s) if $C^{zx}(\mathbf{q} = \mathbf{0}) = C^{zy}(\mathbf{q} = \mathbf{0}) = 0$ as it is the case for the possible muon sites in GdNi₅. g_L is the Landé factor and k_B the Boltzmann constant. \mathcal{C} is a universal constant ($\mathcal{C} = 129.39 \text{ (meV)}^3 \cdot \text{\AA}^6 \cdot \text{s}^{-1} \cdot \text{K}^{-2}$). The fit to (17) presented in figure 13b yields $D_m = 3.2 \text{ (1) meV} \cdot \text{\AA}^2$. This estimate allows one to extract the value of an important parameter: namely the dipolar wave vector, q_D , which determines the relative strength of the dipolar and exchange interactions. The analysis gives $q_D = 0.19 \text{ \AA}^{-1}$. The simple linear magnon theory cannot describe the data above $\sim 20 \text{ K}$ because the magnon-magnon interactions are neglected.

We now analyze the paramagnetic critical behaviour of λ_Z . As shown in figure 14a, λ_Z is almost isotropic. This is expected for a dipolar Heisenberg paramagnet for which the correlation-tensor is

$$\tilde{\Lambda}^{\beta\gamma}(\mathbf{q}) = \tilde{\Lambda}^T(q) P_T^{\beta\gamma}(\mathbf{q}) + \tilde{\Lambda}^L(q) P_L^{\beta\gamma}(\mathbf{q}) \quad (18)$$

where $P_T^{\beta\gamma}(\mathbf{q})$ and $P_L^{\beta\gamma}(\mathbf{q})$ are the transverse and longitudinal (relative to \mathbf{q}) projector operators, respectively. This decomposition reflects the symmetry of the Hamiltonian at small \mathbf{q} value, i.e. of the long range dipolar interaction between the Gd³⁺ ions (Frey and Schwabl 1988, 1989 and 1994). Since the dynamics near T_C is driven by the modes at small \mathbf{q} , we need to consider the expansion of the muon-lattice coupling tensor $G^{\alpha\beta}(\mathbf{q})$ only near $\mathbf{q} = \mathbf{0}$: $G^{\alpha\beta}(\mathbf{q}) = -4\pi \left[P_L^{\alpha\beta}(\mathbf{q}) - C^{\alpha\beta}(0) - \frac{H^{\alpha\beta}(0)}{4\pi} \right]$. H is the hyperfine tensor. These functional forms of $\tilde{\Lambda}$ and G , together with the expression for λ_Z given in Appendix C, leads to the simple result

$$\lambda_Z = \mathcal{W} [a_L I^L(\varphi) + a_T I^T(\varphi)], \quad (19)$$

where \mathcal{W} is a nonuniversal constant, $a_{L,T}$ depends only on the muon localization site(s) and $I^{L,T}(\varphi)$ are universal fluctuation functions of the temperature through the angle φ . $I^L(\varphi)$ and $I^T(\varphi)$ account for the longitudinal and transverse fluctuations,

respectively. We have $\varphi = \arctan(q_D \xi)$ with $\xi = \xi_0 t^{-\nu}$. ξ is the correlation length, ξ_0 the correlation length extrapolated to $T = 2T_C$, $t \equiv |T - T_C|/T_C$ and ν the correlation length critical exponent ($\nu \simeq 0.69$). Therefore, in general, λ_Z is a weighted sum of $I^L(\varphi)$ and $I^T(\varphi)$. Experimentally, a saturation is observed when approaching T_C (see figure 14a). This is understood if $a_L I^L(\varphi) \gg a_T I^T(\varphi)$ since $I^L(\varphi)$ saturates as T_C is approached.

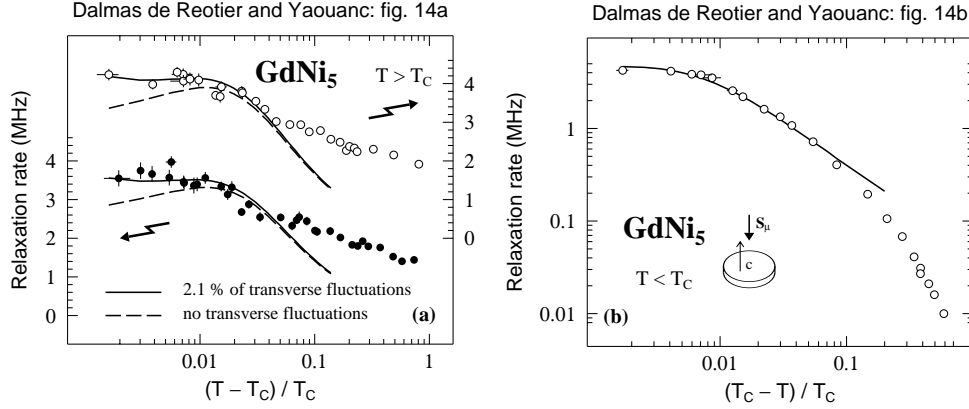


Figure 14. (a): zero-field relaxation rate measured in the critical paramagnetic state given as a function of the temperature relative to the Curie temperature and the orientation of \mathbf{S}_μ relative to the c axis (same symbol convention as in figure 13a). The full and dashed lines are predictions of the mode coupling theory for the critical behaviour of $\lambda_Z(T)$ in a dipolar Heisenberg ferromagnet (Frey and Schwabl 1988, 1989 and 1994). (b): zero-field relaxation rate measured in the ferromagnetic state near the Curie temperature. The full line is the prediction for the critical paramagnetic fluctuations. The relative weight of the longitudinal and transverse fluctuations is taken as given by the analysis of the paramagnetic fluctuations. Both figures are from Yaouanc *et al* 1996a.

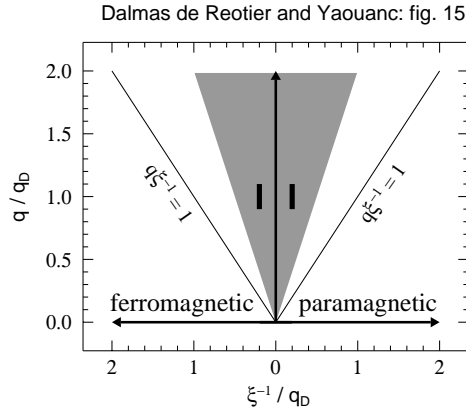


Figure 15. Halperin-Hohenberg diagram for the μ SR measurements of GdNi_5 at $|T_C - T|/T_C = 10^{-2}$ (from Yaouanc *et al* 1996b). Their locations are indicated by the two bars. They have been clearly performed in the critical regime delimited by the shaded region.

An interesting result of this study is the observed similarity between the paramagnetic and ferromagnetic longitudinal critical fluctuations as discovered when comparing figure 14a and figure 14b. Using the dynamical scaling theory of Halperin and Hohenberg (Halperin and Hohenberg 1967), it can be understood as follows. The basic quantity which distinguishes the different regions in the (q, ξ^{-1}) plot is the product $q\xi$. Since the measurements are mostly sensitive to longitudinal fluctuations, they probe the modes with $q \sim q_D$ (Dalmas de Réotier *et al* 1994). Therefore the relevant quantity is $q_D\xi$. Taking $\xi_0 = 1 \text{ \AA}$ one finds $q_D\xi \simeq 5$ at $t = 10^{-2}$. Despite this rough estimate for the correlation length, the measurements are still clearly in the critical regime of the paramagnetic and ferromagnetic dynamics as shown in figure 15. Thus the continuity of the dynamical behavior when crossing T_C and therefore the observed similarity is understood. Nevertheless this argument calls for a detailed theoretical justification : in a dipolar magnet two scaling variables are needed instead of one for the isotropic model of Halperin and Hohenberg.

We note that the relaxation rate of the points very close to T_C (namely the points which have been used for the determination of T_C and correspond to $t \leq 0.0015$) is significantly larger than the saturation value obtained for $0.002 \leq t \leq 0.02$. This can be seen by comparing the values of the damping rate in figure 14a and figure 14b with figure 13a. This increase of the damping rate near T_C could be due to the Ising crossover that has been observed in metallic Gd (Dalmas de Réotier and Yaouanc 1994).

We point out that systematic zero-field investigations of the dynamics in rare-earth metals would be of great interest: it could provide essential information for the determination of their universality class through the measurement of the dynamical critical exponent.

Recently Heffner *et al* 1996 have measured λ_Z in the ferromagnet $\text{La}_{0.67}\text{Ca}_{0.33}\text{MnO}_3$ which has attracted much interest because of its colossal magnetoresistance. Equation (17) fails to predict the order of magnitude of λ_Z . This may not be surprising since this oxide is an inhomogeneous mixed-valence compound. The results of Heffner *et al* 1996 reveal the presence of a density of states for magnetic excitations larger than expected, which has a strong influence on the correlations along the easy axis. Its origin could be related to the existence of a second d electron component in addition to the localized d component responsible for the conventional spin waves detected by inelastic neutron scattering (Perring *et al* 1996, Moussa *et al* 1996). This picture is identical to the one used to describe results obtained on some metallic compounds containing Ce or U atoms (see section 3.4). In order to characterize these unexpected excitations further, it would be of interest to extend the measurements to crystals and investigate the possible field dependence of λ_Z over the whole temperature range.

4.2. The correlation-function in spin-glasses

The intensive investigation of glass and spin-glass forming systems in the eighties has shown that the key to a comprehensive understanding of the transition lies in the dynamics (Fisher and Hertz 1991). The spin-spin self correlation-function is the most important quantity in the spin glass systems since cross correlations are zero, i.e. one can neglect the wave vector dependence of the correlation-function. Therefore for an isotropic spin glass system one should only consider the correlation-function $\Lambda(t) \equiv \Lambda(t, \mathbf{q} = \mathbf{0})$ (see Appendix C).

Below the spin glass transition temperature T_g , a μ SR study has shown that $\Lambda(t)$ decays as a power law after some microscopic time, of the order of 10^{-14} s (MacLaughlin *et al* 1983). However it is only recently that the form of $\Lambda(t)$ above T_g has been established (Keren *et al* 1996b). In this section we highlight this work.

The goal of the work by Keren *et al* 1996b was to distinguish, using the longitudinal field method, between three possible forms of $\Lambda(t)$ above T_g : the power law ($d \cdot |t|^{-\alpha}$), the stretched exponential ($d \exp[-(\zeta|t|)^\beta]$) and the cutoff power law ($d \cdot |t|^{-\alpha} f(\zeta|t|)$) which is often approximated by the Ogielski form ($d \cdot |t|^{-\alpha} \exp[-(\zeta|t|)^\beta]$). The exponents α and β are positive by definition. The difference between these forms is fundamental: the power law is time-invariant, the stretched exponential has a well-defined time scale given by $1/\zeta$ and the cutoff power law is time-invariant only at times shorter than $1/\zeta$.

Since the longitudinal field method does not probe directly $\Lambda(t)$ but only $P_Z(t)$, one has to determine the relation between these two quantities. Because the magnetic impurities are randomly distributed, the spin environment of each muon is different. We first consider an expression of $P_Z(t)$ for a given environment. As written in (10), for a crystal in the fast-fluctuation limit, $P_Z(t)$ is an exponential function with a relaxation rate $\lambda_Z = 2\Delta^2/\nu$. The field dependence of $1/\nu$ is given in terms of the correlation-function:

$$\frac{1}{\nu(B_{\text{ext}})} = \frac{1}{2\Lambda(0)} \int_{-\infty}^{\infty} \Lambda(t) \cos(\gamma_\mu B_{\text{ext}} t) dt. \quad (20)$$

This formula, valid for an isotropic system, can be deduced from Appendix B. $\Lambda(t)$ does not depend on B_{ext} if the electronic Zeeman energy is much smaller than the spin-spin coupling energy. The parameters Δ and ν can vary from one muon site to another, hence their average values should be considered. Most treatments have assumed that ν is site independent. In order to understand their data, Keren *et al* 1996b are forced to use a weaker assumption. They write $\nu(B_{\text{ext}}) = c l(B_{\text{ext}})$ where the site dependence enters through the prefactor c . Thus the measured depolarization, which is an average, is given by

$$P_Z(t) = \int \int \rho(\Delta, c) \exp \left[\frac{-2\Delta^2}{c l(B_{\text{ext}})} t \right] dc d\Delta, \quad (21)$$

where $\rho(\Delta, c)$ is the probability of occurrence of the values Δ and c . For the three possible forms of $\Lambda(t)$, $P_Z(t)$ obeys asymptotically the scaling relation

$$P_Z(t, B_{\text{ext}}) = P_Z(t/B_{\text{ext}}^\gamma), \quad (22)$$

where $\gamma = 1 - \alpha$ for the power law and the cutoff power law, and $\gamma = 1 + \beta$ for the stretched exponential form. Asymptotically means for the stretched exponential, $\gamma_\mu B_{\text{ext}} \gg \zeta$, and for the cutoff form, $\zeta|t| \ll 1$.

It is interesting to notice that (22) should be valid with $\gamma = 1$ for a conventional magnet if the spin dynamics is slow because $\Lambda(t)$ is an exponential function for such a magnet.

The measurements have been done on the canonical Heisenberg spin glass system AgMn(0.5 at. %). In figure 16a we present the field dependence of the spectra recorded at 3.2 K, i.e. just above T_g . In figure 16b the validity of the scaling law (22) is demonstrated for $\gamma = 0.76$ (5) over three orders of magnitude in t/B_{ext}^γ . The stretched exponential form is inconsistent with the measured γ value. According to (22), an instantaneous relaxation should occur as $B_{\text{ext}} \rightarrow 0$ since then $P_Z(t) \rightarrow 0$ at

any t . This is not observed as confirmed in figure 16a. But as $B_{\text{ext}} \rightarrow 0$ the exponential term of the cutoff power law provides a cutoff. Therefore, only the cutoff power law describes the field dependence of $P_Z(t)$. This conclusion is achieved without assuming a specific functional form of $P_Z(t)$.

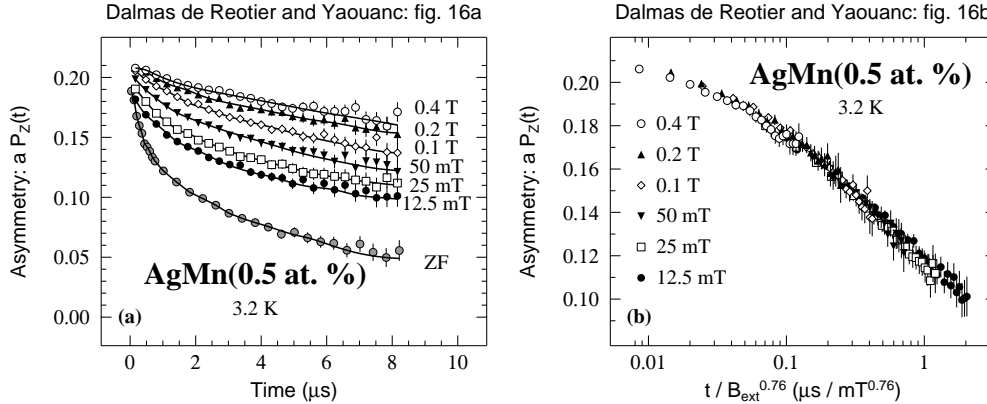


Figure 16. (a) Dependence of the μ SR spectra on the intensity of the longitudinal magnetic field recorded on the spin glass AgMn(0.5 at. %). The measurements have been performed at $T = 3.2$ K, i.e. above the spin glass transition temperature ($T_g = 2.95$ K). The solid lines are guides for the eyes. (b) The same spectra as presented on figure 16a but plotted as a function of the scaling variable $t/B_{\text{ext}}^{0.76}$ and for various values of B_{ext} . t is the time and B_{ext} the external magnetic field. Both figures are adapted from Keren *et al* 1996b.

A complementary approach is to test a functional form for $P_Z(t)$. One possibility, which has been tested with success at a high impurity concentration (Campbell *et al* 1994), is the stretched exponential function:

$$P_Z(t) = \exp [-(\lambda t)^\beta]. \quad (23)$$

Keren *et al* 1996b show that this function provides a very good description of the AgMn(0.5 at. %) spectra recorded at various temperatures around the spin glass transition temperature by cooling the sample in a longitudinal field of 12.5 mT. In figure 17 are plotted the two parameters characterizing the stretched exponential. The maximum of λ indicates the vicinity of the phase transition. As the temperature is lowered towards T_g , the exponent β saturates to $1/3$. This result holds for a wide range of concentration in AgMn.

Keren *et al* 1996b have been able to distinguish between three possible forms of the spin-spin self correlation-function with only a scaling argument. Using the neutron spin echo technique, Mezei and Murani 1979 could not achieve this result. Interestingly, the success of the μ SR work lies in the use of the spin correlation-function concept for the data analysis. It would be of interest to check if the limit $\beta \rightarrow 1/3$ as $T \rightarrow T_g$ is a universal characteristics of spin glasses.

5. Probing the magnetic properties of superconductors

μ SR spectroscopy has been intensively used in recent years to probe the magnetic properties of superconductors. Below we present three experimental works which

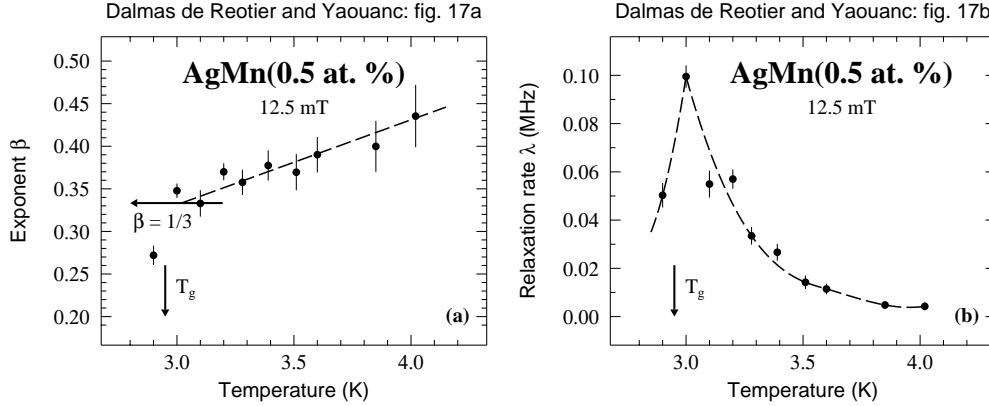


Figure 17. Temperature dependence of the two physical parameters characterizing the stretched exponential used to fit spectra recorded on AgMn(0.5 a. %) at various temperatures around the spin glass transition temperature ($T_g = 2.95$ K) by cooling the sample in a longitudinal field of 12.5 mT (adapted from Keren *et al* 1996b). The dashed lines are guides for the eyes.

have greatly benefited from the availability of high quality crystals. In these works the physical properties of the mixed state are probed but with quite different results. In section 5.1 and section 5.2 the field distribution due to the vortices is visualized for $\text{YBa}_2\text{Cu}_3\text{O}_{6.95}$ and $\text{Bi}_{2+x}\text{Sr}_{2-x}\text{CaCu}_2\text{O}_{8+\delta}$, respectively. Whereas the observation of a conventional 3D flux-line lattice for $\text{YBa}_2\text{Cu}_3\text{O}_{6.95}$ leads to the analysis of the data in terms of the symmetry properties of the superconducting order-parameter, the strong temperature and field dependence of the $\text{Bi}_{2+x}\text{Sr}_{2-x}\text{CaCu}_2\text{O}_{8+\delta}$ field distribution offers the possibility of investigating its phase diagram in the temperature-field plane. In section 5.3, the measurements in UPt_3 show that, in addition to the analysis of the field distribution in terms of the symmetry of its superconducting order-parameter, one is able to unravel some basic magnetic properties of the compound and their interplay with superconductivity.

5.1. The symmetry of the superconducting order-parameter in $\text{YBa}_2\text{Cu}_3\text{O}_{6.95}$

The symmetry of the superconducting order-parameter of the cuprate superconductors is the subject of ongoing research. A possible way of obtaining information on this symmetry is to investigate the excitation spectrum from the temperature dependence of the superconducting condensate density, n_s . The flux line lattice in $\text{YBa}_2\text{Cu}_3\text{O}_{6.95}$ is expected to be conventional, i.e. not to melt (at least for a usual magnetic field intensity; see section 5.2). Therefore the field distribution due to the flux line lattice is characterized by the coherence length and the London penetration depth, λ , which is directly related to n_s : namely $1/\lambda^2 \propto n_s$. An effective method to measure the field distribution is the muon spin rotation technique (see Appendix D). It probes the bulk of the material.

Early μSR measurements of the field distribution in sintered powders and low quality crystals concluded that $1/\lambda^2$ has a weak temperature dependence for $T \ll T_c$, suggesting the existence of an energy gap in the spectrum of excitations, in contradiction to the interpretation of other measurements. In particular, microwave data of Hardy *et al* 1993 on high quality crystals show that $1/\lambda_{ab}^2$ depends linearly on

temperature. λ_{ab} is defined as $(\lambda_a \lambda_b)^{1/2}$ where λ_a and λ_b are the penetration depths for currents flowing along the a and b axis, respectively. This is consistent with the expected line of nodes for the order-parameter from singlet $d_{x^2-y^2}$ wave pairing.

Although the microwave method has a high precision, it is not sensitive to the absolute value of $\lambda_{ab}(0)$ and probes only the skin depth at the surface. Sonier *et al* 1994 and 1997 and Riseman *et al* 1995 have performed μ SR measurements in a mosaic of single crystals. In figure 18 we present the Fourier transformation of two spectra which have been recorded using a field cooling procedure with $B_{\text{ext}} = 0.500$ T. But while the distribution on the left has been recorded with that field value, the distribution on the right was taken in a field of 0.489 T after initially cooling the sample in a field of 0.500 T. Whereas the signal from muons in the sample remains practically unchanged due to the strong pinning of the vortex lattice, the sharp peak attributed to the background (muons stopped in the sample holder and cryostat walls) shifts down by ~ 11.2 mT.

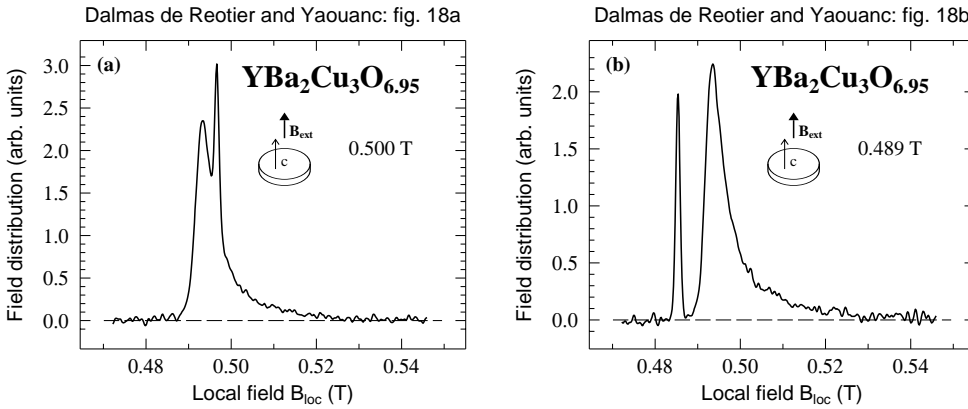


Figure 18. Typical field distributions recorded in $\text{YBa}_2\text{Cu}_3\text{O}_{6.95}$ after cooling the sample in a field of 0.500 T (adapted from Sonier *et al* 1994). While the distribution of figure 18a has been recorded at 5.4 K with that field value, the distribution of figure 18b was measured at 6 K after decreasing the field to 0.489 T. Because of the high superconducting temperature of this compound, the difference in temperature for the two measurements is expected not to be significant. The sharp lines below 0.50 and 0.49 T in figure 18a and 18b respectively represent the background contribution, i.e. muons which are not stopped in the sample. The other part of the distribution arises from the superconductor and is not affected by the field decrease. These measurements prove that the vortices are pinned.

From the measured field distribution, Sonier *et al* 1994 and 1997 have extracted λ_{ab} using the theory explained in Appendix D, with the restriction that they do not use a proper cutoff function to account for the finite size of the vortex cores (Yaouanc *et al* 1997a). In figure 19 we present $1/\lambda_{ab}^2(T)$ for $B_{\text{ext}} = 0.2$ T, 1.0 T and 1.5 T. The linear dependence of $1/\lambda_{ab}^2$ vs T , confirms the zero-field microwave measurements. We note that the weak field-dependence of $1/\lambda_{ab}^2(T=0)$ can probably be explained using a proper cutoff function (Yaouanc *et al* 1997a). In their analysis, Sonier *et al* 1997 take into account the in-plane anisotropy of the penetration depth discovered by μ SR (Tallon *et al* 1995, Bernhard *et al* 1995b) and infrared measurements (Basov *et al* 1995).

Measurements carried out by Riseman *et al* 1995 for $1.9 \text{ T} \leq B_{\text{ext}} \leq 6.5 \text{ T}$ show

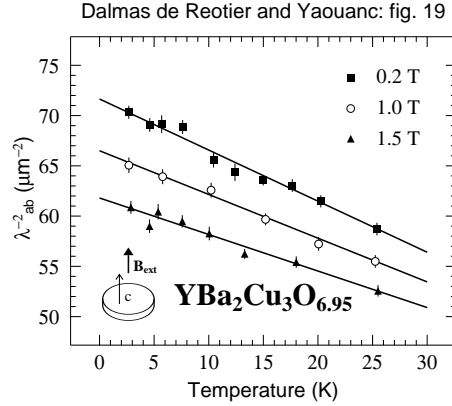


Figure 19. Temperature dependence of $1/\lambda_{ab}^2$ measured on $\text{YBa}_2\text{Cu}_3\text{O}_{6.95}$ for three values of the external field applied along the c axis (adapted from Sonier *et al* 1997). The measured linear temperature dependence is consistent with a d -wave superconducting order-parameter. The observed field dependence is probably explained if a proper proper cutoff function is used (Yaouanc *et al* 1997a).

that the Ginzburg-Landau parameter κ is constant between 30 K and 75 K with a value $\kappa \approx 70$. In addition, these authors find an upper critical field $B_{c2} = 90$ (10) T.

As pointed out by Sonier *et al* 1994, the sample quality seems to have a significant influence on the experimental results. This is understandable since λ is in fact expressed in terms of an integrated excitation spectrum over parts of the Fermi surface (see Gross *et al* 1986 and Gross-Alltag *et al* 1991). Therefore, additional methods of investigation of the symmetry of the order-parameter are highly desirable. A recent example is given by Bernhard *et al* 1996 who have determined by μSR the depression of n_s as a function of the level of Zn doping. They argue that the initial decrease of n_s is inconsistent with s -wave pairing and magnetic scattering but points rather towards d -wave pairing, in agreement with the microwave data of Hardy *et al* 1993, the μSR data of Sonier *et al* 1994 and 1997 and the micro-SQUID results of Tsuei *et al* 1994. However, this conclusion is disputed by Nachumi *et al* 1996. Therefore, until the dispute is settled, it is not possible to give a definite conclusion concerning the interpretation of the effect of Zn doping on n_s .

Since the discovery of the high T_c superconductors, trends in the relations between some of their parameters have been looked for. Some years ago a remarkable empirical relationship between T_c and the low-temperature variance of the vortex field distribution was found for some high T_c oxides (Uemura *et al* 1991). This experimental result was taken as evidence for a high-energy-scale pairing mechanism, consistent with the picture of real-space paired bosons. It was suggested that this scaling was valid for all the high T_c materials. This suggestion has triggered an important experimental activity. The recent reports (Uemura *et al* 1993, Niedermayer *et al* 1993, Weber *et al* 1993, Bernhard *et al* 1995b, Zimmermann *et al* 1995, Tallon *et al* 1995) show that the simple universal scaling-law is only partially valid. For example, T_c is not solely a function of the hole concentration: the oxides with and without Cu chains do not belong to the same class.

We note that practically all these works have been performed in powder samples and the μSR spectra have been analyzed supposing a Gaussian field distribution.

Although this methodology may not be completely safe (Sonier *et al* 1994 and Harshman and Fiory 1994), it has nevertheless been able to provide the first proof of the in-plane anisotropy of the London penetration depth in $\text{YBa}_2\text{Cu}_3\text{O}_{z-\delta}$ (Tallon *et al* 1995).

From the μSR technical point of view, the works of Sonier *et al* 1994 and 1997 and Riseman *et al* 1995 are remarkable since they have been performed both at high fields and with small samples (one of the Sonier's sample covers an area of $5 \times 5 \text{ mm}^2$ perpendicular to the c axis). In a near future one may foresee routine μSR measurements on even smaller samples and therefore on samples of even higher quality.

5.2. The vortex state in highly anisotropic high T_c superconductors

The state of the vortices in some of the highly anisotropic superconducting oxides is still a subject of discussion (see Bishop 1996a and 1996b, Nelson 1997 and Crabtree and Nelson 1997 for reviews). In these compounds such as $\text{Bi}_{2+x}\text{Sr}_{2-x}\text{CaCu}_2\text{O}_{8+\delta}$, the vortices are best described as layered systems of 2D pancake vortices interacting via a combination of tunneling Josephson currents and electromagnetic interactions. Increasing the field or the temperature, one expects to observe changes in the typical 3D flux line lattice field distribution due to either disordering of the vortex lattice, a reduction of its dimensionality or its melting.

In this section we focus on results obtained by Lee *et al* 1993, 1995 and 1997, Aegerter *et al* 1996 and Bernhard *et al* 1995a.

At low temperature and for a field less than the crossover field B_{cr} , a lattice of extended flux lines is observed. As seen in figure 18 and figure 20, its μSR signature is a typical strongly asymmetric field distribution with a pronounced tail towards high fields, showing that some of the muon spins precess in the local field caused by flux cores that are extended in the c direction. This interpretation is supported by the occurrence of Bragg peaks in the neutron scattering experiments (Cubitt *et al* 1993). Drastic changes occurs when B_{ext} exceeds B_{cr} . The field distribution becomes more symmetric as shown in figure 20. Simultaneously the neutron Bragg peaks disappear indicating that the long-range coherence of the flux lattice is destroyed. The change of the shape of the field distribution is quantified by the skewness parameter α (see Appendix D). Its field dependence is presented in figure 20. α is definitively smaller above B_{cr} than below, reflecting the truncation of the high-field tail. This reduction is either due to the motion of the vortices (Harshman *et al* 1991, Inui and Harshman 1993), a reduced dimensionality of the vortex structure (Brandt 1991 and Harshman *et al* 1993) or a transition to a glass phase (Ryu *et al* 1996, Ryu and Stroud 1996 and Gingras and Huse 1996). The last two statements have common features and it may not be easy to distinguish between them (Gingras and Huse 1996). Lee *et al* 1993 suggest that their data points to a reduction of the dimensionality of the vortex system: in a high field, the system consists of an array of pancake vortices that are uncorrelated in the c direction but ordered two-dimensionally within each stack of CuO_2 planes. This interpretation is supported by the numerical results of Schneider *et al* 1995. Such a dimensional crossover has been predicted to occur at B_{cr} (Vinokur *et al* 1990 and Glazman and Koshelev 1991). Additional measurements (Bernhard *et al* 1995a) on underdoped and strongly overdoped crystals support this interpretation. Recently Aegerter *et al* 1996 have discovered that $B_{\text{cr}} = \Phi_0/\lambda_{ab}^2$ where $\Phi_0 = 2.07 \times 10^{-15} \text{ Tm}^2$ is the quantum of flux. This latter result is understood in terms of a system of vortices controlled predominantly by electromagnetic interactions. This is

in contrast to other materials, such as $\text{HgBa}_2\text{Ca}_3\text{Cu}_4\text{O}_{10+\delta}$, where Josephson coupling plays a more significant role.

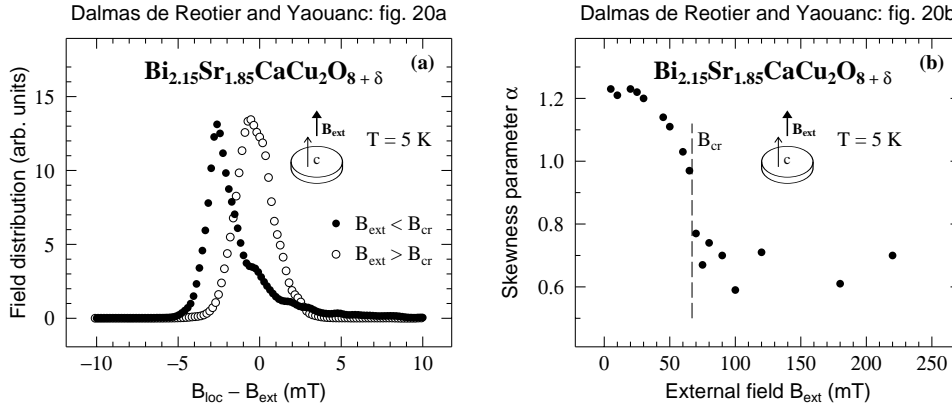


Figure 20. The vortex state in the highly anisotropic material $\text{Bi}_{2.15}\text{Sr}_{1.85}\text{CaCu}_2\text{O}_{8+\delta}$ as the intensity of the external magnetic field is increased. The temperature is kept fixed far below T_c . As shown in figure 20a, the shape of the field distribution becomes more symmetric at high field. The field dependence of the skewness parameter, which allows one to quantify the change in the shape of the distribution, is presented in figure 20b (Aegerter 1997 and adapted from Aegerter *et al* 1996). Note the sharpness of the crossover at B_{cr} .

There is much interest in investigating the vortex state as a function of the temperature since it is expected that, at sufficiently high temperature, the vortex lattice should melt (Bishop 1996). In figure 21 we compare field distributions recorded at low and high temperature for a given field intensity. The high temperature distribution is very narrow and the shapes at low and high temperature are distinctly different. The temperature dependence of the skewness parameter indicates a sharp change at T_m . α is even negative above T_m , whereas in figure 20 it is always positive. Comparing these results with the numerical calculations of the field distribution by Schneider *et al* 1995, T_m is found to be the fusion temperature of the vortex lattice. A thorough analysis is presented by Lee *et al* 1997 which supports this interpretation. In addition, this analysis points out the determinant role of the electromagnetic coupling between the superconducting layers, In fact, it is this coupling rather than the Josephson coupling which determines the phase diagram below $\sim 70\text{ K}$, a rather high temperature relative to the superconducting temperature ($T_c \sim 80\text{ K}$).

The detailed characterization of the vortex state in the highly anisotropic oxides is a complex problem. The microscopic methods like μSR and small angle neutron scattering, in combination with magnetization measurements, can lead to an improved understanding of the physics involved. For example, in $\text{Bi}_2\text{Sr}_2\text{CaCu}_2\text{O}_{8+\delta}$, the “second peak” observed in the hysteresis loops and the sharp change in the field distribution detected by μSR both occur at the same field, the crossover field B_{cr} , allowing the origin of the “second peak” to be understood (Bernhard *et al* 1995a).

5.3. Anisotropy of the magnetic response in UPt_3

The hexagonal heavy fermion superconductor UPt_3 has the unique physical property of showing two Meissner phases, at $T_{c1} \simeq 0.48\text{ K}$ and $T_{c2} \simeq 0.53\text{ K}$, and three

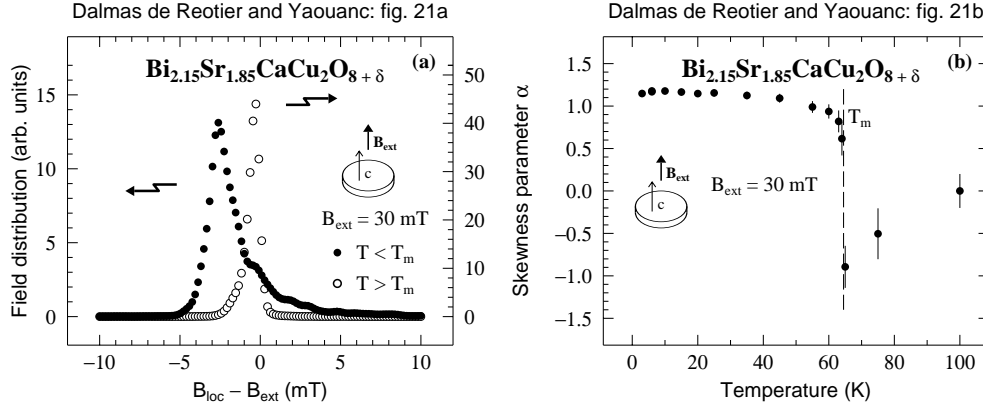


Figure 21. The vortex state in the highly anisotropic material $\text{Bi}_{2.15}\text{Sr}_{1.85}\text{CaCu}_2\text{O}_{8+\delta}$ as the temperature is increased. The intensity of the external magnetic field is kept fixed. As shown in figure 21a, the shape of the field distribution changes and becomes narrow at high temperature. The temperature dependence of the skewness parameter is presented in figure 21b (Aegerter 1997 and adapted from Lee *et al* 1997). Note the sharp change of α at T_m and the negative value of α for $T > T_m$.

flux phases. In addition, neutron and magnetic X-ray diffractions have indicated an antiferromagnetic phase transition at $T_N \sim 6$ K characterized by a tiny magnetic moment of 0.02 (1) $\mu_B/\text{U-atom}$ at low temperature, lying in the basal plane along the b axis. This transition has never been detected by macroscopic measurements. The origin of the magnetic and superconducting phases of UPt_3 is one of the most debated subjects in condensed matter physics. The superconducting multiphases identify UPt_3 has a candidate for unconventional superconductivity. The term “unconventional” refers to the fact that the order-parameter has a lower rotational symmetry in the superconducting phases than in the normal state. More information on UPt_3 can be found in the reviews of Sauls 1994 and of Heffner and Norman 1996. A review on unconventional superconductivity has been recently published (Muzikar 1997).

We first present some recent zero-field measurements (Dalmas de Réotier *et al* 1995). They have been performed with two purposes: to detect the magnetic phase transition at T_N and a signature of an eventual internal magnetic field induced by the Cooper pairs in the low temperature superconducting B phase (below T_{c1}). The results are presented in figure 22. For the large temperature range probed and the two crystals investigated (\mathbf{S}_μ either parallel or perpendicular to the c axis), $P_Z(t)$ is simply described by a Kubo-Toyabe function. The values of the damping rates are consistently explained as arising from the ^{195}Pt nuclear magnetic moments. Therefore neither the phase transition at T_N , nor an additional magnetic field in the superconducting B phase is observed.

Since neutron diffraction measurements performed on some of the slices of the μSR samples show that the antiferromagnetic phase transition still exists, one must conclude that either the electronic dipolar fields at the muon site cancel out exactly or the electronic uranium magnetic moments fluctuate too fast to be detected, i.e. their characteristic time is shorter than $\sim 10^{-7}$ s. From neutron diffraction (Aeppli *et al* 1988) we know that this time is longer than $\sim 10^{-11}$ s.

The zero-field measurements (Dalmas de Réotier *et al* 1995) indicate that a

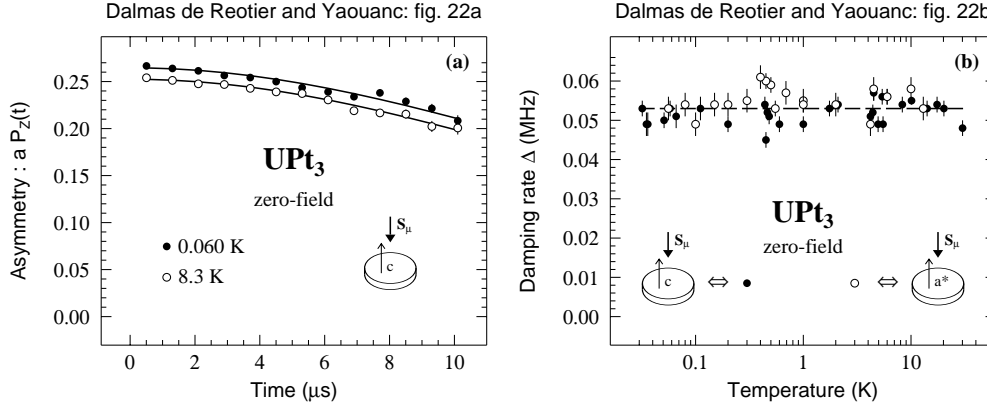


Figure 22. (a): Typical zero field spectra measured for UPt_3 . The full lines are fits. This figure shows that there is no additional local field at the magnetic phase transition and in the low temperature superconducting phase. (b): Temperature dependence of the Kubo-Toyabe damping rate Δ . The dashed straight line indicates its average. These results show that Δ is independent of the temperature and orientation of the crystal axes relative to \mathbf{S}_μ . Both figures are from Dalmas de Réotier *et al* 1995.

possible change in B_{loc} induced by magnetism or superconductivity, if any, has to be smaller than approximately $3 \mu\text{T}$. Recently high precision magnetization measurements have shown that the possible change in bulk magnetization (rather than in the local field as observed by μSR) in the superconducting B phase is smaller than $0.2 \mu\text{T}$ (Kambara *et al* 1996). A Cooper pair produces an orbital magnetic field at the muon site. If it has a spin, a spin density has to be added to the orbital density. Since the orbital moment is expected to be much smaller than the spin moment, the measurements put a limit on the possible value of the spin density at the muon site. Taking into account the available theoretical estimates for the spin density, Dalmas de Réotier *et al* 1995 conclude that their results do not support models predicting a triplet spin state for the Cooper pair.

Lussier *et al* 1996 have investigated the magnetic field response of UPt_3 by single crystal neutron diffraction. Their results show that a field in the basal plane of up to 3.2 T has no effect on the magnetic Bragg peaks. Since the intensity of these peaks is extremely small, the precision of the measurements is limited: it is only known that the angle of rotation of the magnetic moment in the hexagonal plane is smaller than 26° . Taking into account that the μSR technique is well adapted to study small moment systems, Yaouanc *et al* 1997c have performed transverse high field μSR measurements. They detect the magnetic phase transition if a large field is applied in the basal plane. As expected, the phase transition is not observed for a field applied along the c axis. Therefore the magnetic properties of UPt_3 are found to be field dependent if probed at high field by a sufficiently sensitive method.

The magnetic properties of UPt_3 are remarkably sensitive to alloying. In the case of the pseudobinaries $\text{U}(\text{Pt}_{1-x}\text{Pd}_x)_3$, large uranium magnetic moments have been detected for $0.02 \leq x \leq 0.07$. Neutron diffraction experiments on $\text{U}(\text{Pt}_{0.95}\text{Pd}_{0.05})_3$ show that the size of ordered magnetic moment equals $0.6 (2) \mu_B/\text{U-atom}$, much larger than in the pure sample ($0.02 (1) \mu_B/\text{U-atom}$). In the zero-field μSR measurements of deVisser *et al* 1997 on this compound, two frequencies (or one frequency and

a strongly damped Kubo-Toyabe signal; Amato 1997) are observed, indicating two magnetically inequivalent muon stopping sites. On the other hand, the zero-field signal in $U(\text{Pt}_{0.998}\text{Pd}_{0.002})_3$ and in the pure sample are the same, i.e. no electronic magnetic signal is observed.

The preliminary data of deVisser *et al* 1997 demonstrate a salient difference in the μSR response between compounds with small and large magnetic moments in the $U(\text{Pt}_{1-x}\text{Pd}_x)_3$ series. It is still not possible to extract reliable physical information from the limited amount of available experimental μSR data. An important issue that could be resolved by combining these measurements with neutron measurements on the same samples concerns origin of the large difference between the intensity of the low temperature magnetic moment for UPt_3 and $U(\text{Pt}_{0.95}\text{Pd}_{0.05})_3$.

The temperature dependence and the anisotropy of the magnetic field penetration lengths in the superconducting phases of UPt_3 have been studied by muon spin rotation measurements (Yaouanc *et al* 1997b). The analysis of the temperature dependence of the penetration length parallel and perpendicular to the c axis has shown that the superconducting order-parameter in the B phase cannot just have a line of nodes in the equatorial plane of the Fermi surface. The analysis supports an hybrid order-parameter with point nodes at the poles and a line of nodes at the equatorial plane. A remarkable result of the measurements is the observation of a strong axial anisotropy of the penetration length. As explained at Appendix D, this anisotropy is directly related to the opening angle of the vortex lattice. In figure 23 we present the temperature dependence of this angle for \mathbf{B}_{ext} applied along the a axis. If the penetration lengths were isotropic, it would be equal to 60° . It has already been measured by small angle neutron scattering (Kleiman *et al* 1992). But, because the neutron cross-section decreases dramatically as the temperature is increased, it could only be measured at 0.05 K. We note that the angle is practically temperature independent. When \mathbf{B}_{ext} is applied along the c axis of the crystal lattice, the angle is found to be temperature independent with a value of $\simeq 60^\circ$, i.e. the vortex lattice is a traditional hexagonal lattice.

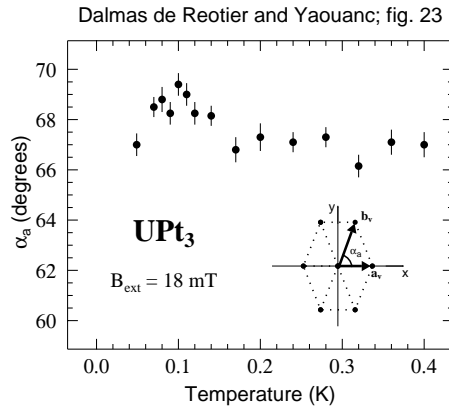


Figure 23. Temperature dependence of the angle characterizing the vortex lattice of UPt_3 for the external field applied along the a axis. The angle of the real space vortex lattice is defined in the insert. (adapted from Yaouanc *et al* 1997b).

6. Summary and perspectives

In this review we have attempted to detail the possibilities offered by the μ SR technique for the study of the magnetic properties of materials. A quick look at all the examples described in this work shows that the prominently used properties of the technique are its high sensitivity to local fields, and its capability to characterize the time scale of their fluctuations. Interestingly, information can be extracted from compounds which do not display long range magnetic correlations. In fact, many μ SR investigations concern disordered or frustrated magnetic compounds. Two examples are given in this review. The typical spot size of a muon beam is some millimetres at a continuous source. Although this means that extremely small samples can not be studied, this macroscopic size allows one to probe magnetic structure with nanometre or micrometre scales. We have presented four examples of such studies.

The μ SR technique has many attractive features which explain its present fast development. Although we have not explained in any detail how a μ SR experiment is performed (this information is found in the general references provided at the beginning of section 2), relative to other non local microscopic techniques, a μ SR experiment is relatively straightforward. The μ SR spectroscopy is of general use: the sample does not need to contain special nuclei. A relatively involved sample environment can be used as illustrated, for example, by the high number of measurements performed in the 30 mK - 1 K range using dilution refrigerators. Measurements have been performed up to $B_{\text{ext}} = 6.5$ T (Riseman *et al* 1995). The recording of a μ SR spectrum requires in most cases less than an hour. Therefore, in a reasonable amount of time, it is possible to map out the temperature and magnetic field μ SR response of a compound.

As does any experimental technique, the μ SR method has its own limitations. One of the major drawbacks is that the sample has to be sufficiently big. If a disk is used and if the muon beam is perpendicular to its plane, in the most favourable cases, the diameter of the disk should not be smaller than ~ 5 mm. A larger diameter is unfortunately required at a pulsed source such as ISIS, where the diameter has to be at least 20 mm. For the more widely used beamlines, the so-called surface muon beams (i.e. relatively slow muon beams), 150 mg of material per cm^2 of beam cross section is required to stop the muons. This means that the sample thickness needs not to be much larger than ~ 1 mm for organic materials (density $\gtrsim 1$) and even much less (one to three hundred micrometres) for denser material such as oxides or metals.

A priori, the muon diffusion and localization site(s) properties are unknown. This can turn out to be a problem to extract detailed information from the measurements. In this respect, it has recently been shown that frequency shift measurements may be of great help (see section 2.3).

In order to respond to the demand of the users, major technical developments are scheduled at the μ SR facilities.

The investigation of the vortex state in superconductors is at present one of the main subject of μ SR research. Optimized spectrometers in transverse geometry with intense magnetic fields at relatively high temperature are needed for this type of work. They should be available in a few years time both at TRIUMF and PSI.

Surface science is a major topic of modern physics which, so far, is untouched by μ SR. The reason is that the momentum of the muons in presently available beam is too large and therefore the muons are stopped at best in a few hundred micrometres. Ultra slow muon beams are being developed at facilities. The challenge is to keep a

high degree of polarization in the slowing down process together with a reasonable efficiency. The possibility to moderately reaccelerate the ultra slow muons provides the opportunity of fine tuning the stopping range of the muons. For instance, such a beam will allow the study of magnetic multilayers which are of interest both for basic research and technological applications.

The possibility of building an intense pulsed neutron facility in Europe, the European Spallation Source, is also being considered. As at the ISIS Facility, where pulsed neutrons and muons are available, many muon beams are scheduled to be introduced at this future facility. The experience gained at ISIS has shown that having beams of both particles at the same institution is a real advantage: it provides opportunities for the neutron and muon communities to interact.

7. List of works published from July 1993

The tables provide a list of published works. When a given work has been described in short articles and later on in an extended paper, we only refer to the latter report.

Table 1. A selection of work carried out on conventional magnets

Chemical formula	Comments	References
Magnetic correlations in magnets		
$(\text{Mn}_{1-x}\text{Fe}_x)\text{Pt}_3$	dynamical crossover from ferromagnetism to asperomagnetism	Barsov <i>et al</i> 1993 and 1994
MnSi	strong correlation between the ^{55}Mn electric field gradient and magnetic susceptibility	Kadono <i>et al</i> 1993
$\text{Ag}_{1-x}\text{Mn}_x$	spin correlation-function in a spin-glass see section 4.2	Campbell <i>et al</i> 1994 Keren <i>et al</i> 1996b
Gd	critical paramagnetic fluctuations and correlation-functions; effect of dipolar interaction	Dalmas de Réotier and Yaouanc 1994
Ni and Fe	evaluation of the Brillouin zone probed by μSR study of critical paramagnetic fluctuations	Dalmas de Réotier <i>et al</i> 1994
$\text{Gd}_{0.696}\text{Y}_{0.304}$	magnetic phase diagram investigation	Eccleston <i>et al</i> 1995
CeB_6	field response in disagreement with the hypothesis of an antiferroquadrupolar phase	Feyerherm <i>et al</i> 1995c
PrCo_2Si_2	spin dynamics in an axial magnet	Gubbens <i>et al</i> 1995
$\text{Y}_6(\text{Mn}_{1-x}\text{Fe}_x)_{23}$	static and dynamical magnetism in competition	Kilcoyne and Telling 1995
CeSb	slow spin dynamics below T_N	Klauss <i>et al</i> 1995
EuO, EuS	theoretical prediction of the thermal behaviour of the relaxation rate; see Yaouanc <i>et al</i> 1993b	Lovesey and Engdahl 1995
RbMnF_3	theoretical prediction of the thermal behaviour of the relaxation rate	Lovesey <i>et al</i> 1995
$\text{Y}_{0.97}\text{Sc}_{0.03}\text{Mn}_2$	a spin liquid ground state is suggested	Mekata <i>et al</i> 1995
Al-Mn-Si quasicrystal	study of the spin-glass state	Noakes <i>et al</i> 1995
UNiGa	magnetic phase diagram investigation	Prokes <i>et al</i> 1995
YMn_2	comparison between neutron and μSR results	Rainford <i>et al</i> 1995a
Ni	temperature and pressure dependence of the Fermi contact field	Stammler <i>et al</i> 1995
$\text{Cr}_{1-x}\text{Fe}_x$	spin correlation-function in a spin-glass	Telling and Cywinski 1995
$\beta\text{-(NH}_4)_2\text{FeF}_5$	combined Mössbauer and μSR analysis	Attenborough <i>et al</i> 1996
MnF_2	first proof of Ising dynamical critical behaviour	Brown <i>et al</i> 1996
CeRh_3B_2	investigation of the magnetic state	Cooke <i>et al</i> 1996
$\text{La}_{0.67}\text{Ca}_{0.33}\text{MnO}_3$	ferromagnet with colossal magnetoresistance; unusual spin dynamics; see section 4.1	Heffner <i>et al</i> 1996
YMn_2D_x	effect of deuterium on spin dynamics and magnetic phase diagram	Latroche <i>et al</i> 1996
ReGa_6	combined μSR and neutron study of these quasi-two-dimensional magnets	Lidström <i>et al</i> 1996a
GdNi_5	effect of the dipolar interaction on the critical ferromagnetic fluctuations; see section 4.1	Yaouanc <i>et al</i> 1996a
Ho	study of the incommensurate helicoidal structure	Krivosheev <i>et al</i> 1997

Table 2. A selection of work carried out on conventional magnets (continuation of Table 1)

Chemical formula	Comments	References
Magnetic phase diagrams in organic magnets		
(TMTSF) ₂ -X X = PF ₆ , NO ₃ , ClO ₄	collective low-energy spin-density-wave in addition to single-particle excitations	Le <i>et al</i> 1993a
<i>p</i> -NPNN	3D Heisenberg ferromagnet with $T_C \simeq 0.67$ K; effect of a longitudinal field; see section 3.1	Le <i>et al</i> 1993b Blundell <i>et al</i> 1995
<i>p</i> -PYNN	magnetic phase transition at $\simeq 0.09$ K see section 3.1	Blundell <i>et al</i> 1994
3-QNNN	magnetic phase transition at $\simeq 0.21$ K see section 3.1	Pattenden <i>et al</i> 1995
α -(BEDT-TTF) ₂ KHg(SCN) ₄	detection of two spin density wave transitions	Pratt <i>et al</i> 1995
1-NAPNN, 2-NAPNN	1-NAPNN has a magnetic transition below 0.1 K and 2-NAPNN does not order magnetically	Blundell <i>et al</i> 1996
MEM(TCNQ) ₂	spin dynamics in this spin-Peierls system	Blundell <i>et al</i> 1997a
<i>p</i> -CNPNN, 4-QNNN	<i>p</i> -CNPNN has a magnetic transition at $\simeq 0.17$ K and 4-QNNN does not order magnetically	Blundell <i>et al</i> 1997b
Borocarbide materials		
YNi ₂ B ₂ C	characterization of the vortex state of this conventional superconductor	Cywinski <i>et al</i> 1994
YNi ₄ BC _{0.2}	proof that it is not a bulk superconductor	Süllow <i>et al</i> 1994
TmNi ₂ B ₂ C	coexistence of magnetism and superconductivity	Cooke <i>et al</i> 1995 Le <i>et al</i> 1995
ErNi ₂ B ₂ C	observation of one frequency below T_N	Le <i>et al</i> 1995
SmNi ₂ B ₂ C	exhibits a magnetic phase transition	Prassides <i>et al</i> 1995
YNi ₂ B ₂ C	no magnetic correlations	
HoNi ₂ B ₂ C	observation of two magnetic transitions : one commensurate and one incommensurate	Le <i>et al</i> 1996a

Table 3. A selection of work carried out on strongly correlated electronic systems

Chemical formula	Comments	References
Non-superconducting compounds		
CeRu ₂ Si ₂	a two component <i>4f</i> system; see section 3.4	Amato <i>et al</i> 1993 and 1994
Y _{1-x} U _x Pd _y	competition between Kondo, RKKY and crystal field interactions: effect on the magnetic phase diagram	Wu <i>et al</i> 1994
CeCu _{5.9} Au _{0.1}	no magnetic ordering in this non-Fermi-liquid system; Kondo disorder is maybe negligible	Amato <i>et al</i> 1995 Bernal <i>et al</i> 1996 MacLaughlin <i>et al</i> 1996
CeCu _{5.5} Au _{0.5}	phase transition at $T_N = 0.95$ K	Chattopadhyay <i>et al</i> 1995
CeNiSn	magnetic correlations with surprising temperature dependence (the analysis yields a too small Kondo temperature; see Dalmas de Réotier <i>et al</i> 1996)	Kalvius <i>et al</i> 1995a
CeTrSn, Tr = Pt, Pd	CePdSn exhibits a simple second order transition; the transition in CePtSn is unusual	Kalvius <i>et al</i> 1995b and 1995c
CePt ₂ Sn ₂	investigation of magnetic correlations; see comments of Dalmas de Réotier <i>et al</i> 1996	Luke <i>et al</i> 1995
UNi ₄ B	study of the magnetic phase diagram	Nieuwenhuys <i>et al</i> 1995
CeRhSb	spin correlations below ≈ 0.6 K	Rainford <i>et al</i> 1995b
CeCu _{5-x} Al _x	magnetic phase diagram investigation	Wiesinger <i>et al</i> 1995
UCu _{5-x} Pd _x	non-Fermi-liquid alloy; strong Kondo disorder	Bernal <i>et al</i> 1996 Maclaughlin <i>et al</i> 1996
YbAuCu ₄	effect of crystal field on Kondo-type fluctuations; possible muon induced crystal field effect	Bonville <i>et al</i> 1996
Ce _{1-x} Re _x Ni _{1-y} Tr _y Sn	effect of doping on the electronic ground state	Flaschin <i>et al</i> 1996
CeTr ₂ Sn ₂ Tr = Cu, Pt, Pd	Investigation of the magnetic correlations in heavy fermion antiferromagnets	Lidström <i>et al</i> 1996b
YbPdSb	a spin liquid system	Bonville <i>et al</i> 1997
CePt ₂ Si ₂	Kondo lattice compound with no magnetic ordering	Dalmas de Réotier <i>et al</i> 1997
CeRuSi ₂	ferromagnetic phase transition at $T_C = 11.6$ K; very small ordered Ce magnetic moment	Duginov <i>et al</i> 1997
Superconductors		
UPd ₂ Al ₃	London penetration depth approximately isotropic; a two component <i>5f</i> system; see section 3.4	Feyerherm <i>et al</i> 1994
Ce _{1+x} Cu _{2+y} Si ₂	competition between superconductivity and magnetism	Luke <i>et al</i> 1994 Feyerherm <i>et al</i> 1995a
UPt ₃	absence of electronic magnetic signal in zero-field; study of London penetration depths; see section 5.3	Dalmas de Réotier <i>et al</i> 1995 Yaouanc <i>et al</i> 1997b
U _{1-x} Re _x Ru ₂ Si ₂ Re = La, Y	magnetic phase diagram investigation	Cywinski <i>et al</i> 1995 Park <i>et al</i> 1996
CeRu ₂	detection of a magnetic phase transition with very small magnetic moments; see section 3.4	Huxley <i>et al</i> 1996
U(Pt _{1-x} Pd _x) ₃	study of effect of doping on magnetism; see section 5.3	de Visser <i>et al</i> 1997

Table 4. A selection of miscellaneous studies

Chemical formula	Remarks	Reference
$\text{AMo}_6\text{S}_{8-x}\text{Se}_x$, A= Sn, Pb	Penetration depth measurements	Birrer <i>et al</i> 1993
$\kappa\text{-[BEDT-TTF]}_2\text{Cu[NCS]}_2$	Penetration depth measurement and fluxon dynamics	Harshman <i>et al</i> 1994
Bi	theoretical investigation of line broadening due to inhomogeneity of the Landau orbital magnetization	Solt 1994
$\alpha\text{-O}_2$	characterization of the magnetic phase transition below the $\alpha\text{-}\beta$ transition temperature	Storchak <i>et al</i> 1994
Sb	investigation of the anomalous Knight shift	Birrer <i>et al</i> 1995
PrNi ₅	observation of muon induced crystal field effects	Feyerherm <i>et al</i> 1995b
RbC ₆₀	magnetic phase diagram investigation	Cristofolini <i>et al</i> 1995 MacFarlane <i>et al</i> 1995 Uemura <i>et al</i> 1995
Be	diamagnetic domains; see section 3.3	Solt <i>et al</i> 1996a

Table 5. A selection of work carried out on superconducting and non-superconducting oxides

Chemical formula	Remarks	Reference
Superconducting oxides		
$\text{Bi}_{2+x}\text{Sr}_{2-x}\text{CaCu}_2\text{O}_{8+\delta}$	flux-line lattice study ; possible observation of melting; see section 5.2	Lee <i>et al</i> 1993, 1995 and 1997 Bernhard <i>et al</i> 1995a Aegerter <i>et al</i> 1996
$\text{HgBa}_2\text{Ca}_3\text{Cu}_4\text{O}_{10+\delta}$	test of the universal behaviour; see section 5.1	Niedermayer <i>et al</i> 1993
$\text{Bi}_2\text{Sr}_2\text{Ca}_{1-x}\text{Y}_x\text{Cu}_2\text{O}_{8+\delta}$ $\text{Bi}_{2-x}\text{Pb}_x\text{Sr}_2\text{CaCu}_2\text{O}_{8+\delta}$	results inconsistent with universal behaviour; see section 5.1	Weber <i>et al</i> 1993
$\text{YBa}_2\text{Cu}_3\text{O}_y$	theoretical analysis of the damping of the precession component	Aristov and Maleyev 1994
$\text{YBa}_2\text{Cu}_3\text{O}_{6.6}$	investigation of effect of sulfur substitution through measurement of the penetration depth	Cloots <i>et al</i> 1994
$\text{YBa}_2(\text{Cu}_{0.96}\text{Zn}_{0.04})_3\text{O}_x$	mapping of the magnetic phase diagram for $6.00 \leq x \leq 6.92$	Mendels <i>et al</i> 1994
La_2CuO_4	computation of the hyperfine field	Shukri B Sulaiman <i>et al</i> 1994
$\text{YBa}_2\text{Cu}_3\text{O}_{6.95}$	study of the flux-line lattice field distribution for a mosaic of single crystals; see section 5.1	Sonier <i>et al</i> 1994 and 1997 Riseman <i>et al</i> 1995
$\text{La}_{2-x}\text{Sr}_x\text{CuO}_4$	NMR and μSR study of the weakly doped region; possible evidence for phase separation	Borsa <i>et al</i> 1995
$\text{La}_2\text{Cu}_{1-x}\text{Zn}_x\text{O}_4$	NMR and μSR study of the effects of substitution of magnetic Cu^{2+} with diamagnetic Zn^{2+}	Corti <i>et al</i> 1995
$\text{YBa}_2\text{Cu}_4\text{O}_8\text{H}_x$	study of the antiferromagnetic order	Glückler <i>et al</i> 1995
$\text{YBa}_x\text{Cu}_y\text{O}_{z-\delta}$	in-plane London penetration depth anisotropic due to superconductivity in chains; see section 5.1	Tallon <i>et al</i> 1995 and 1996 Bernhard <i>et al</i> 1995b
$\text{YBa}_2\text{Cu}_3\text{O}_y$	sintered samples; inconsistent with results of Sonier <i>et al</i> 1994 and 1997 and Riseman <i>et al</i> 1995 for $y = 6.95$; see section 5.1	Zimmermann <i>et al</i> 1995
$\text{Y}_{0.8}\text{Ca}_{0.2}\text{Ba}_2(\text{Cu}_{1-y}\text{Zn}_y)_3\text{O}_{7-\delta}$	dependence of the condensate density on Zn doping points towards d -wave pairing; see section 5.1	Bernhard <i>et al</i> 1996
$\text{La}_{2-x}\text{Sr}_x\text{NiO}_{4+\delta}$	magnetic phase diagram investigation	Chow <i>et al</i> 1996
$\text{Nd}_{2-x}\text{Ce}_x\text{CuO}_4$	no magnetic order but spin fluctuations for $x = 0.02$; ordering of the Nd moments at low T for $x = 0$	Hillberg <i>et al</i> 1997
$\text{YBa}_2(\text{Cu}_{1-y}\text{Zn}_y)_3\text{O}_x$ $\text{La}_{2-x}\text{Sr}_x(\text{Cu}_{1-y}\text{Zn}_y)\text{O}_4$	effect of Zn doping on the superconducting electron density; see section 5.1	Nachumi <i>et al</i> 1996
$\text{La}_2\text{CuO}_{4+y}$	investigation of the spin-glass state	Pomjakushin <i>et al</i> 1996

Table 6. A selection of work carried out on superconducting and non-superconducting oxides (continuation of Table 5)

Chemical formula	Comments	References
Non superconducting oxides		
Ca _{0.86} Sr _{0.14} CuO ₂ , Sr ₂ CuO ₃	magnetic order in infinite-layer and chain	Keren <i>et al</i> 1993 and 1995
CuGeO ₃ and Cu _{1-x} Zn _x GeO ₃	possible spin-glass ground state of the doped compound; see comments of Kadono 1997	Lappas <i>et al</i> 1994 García-Muñoz <i>et al</i> 1995b Sohma <i>et al</i> 1995 Tchernyshyov <i>et al</i> 1995
SrCr ₈ Ga ₄ O ₁₉	a spin-liquid ground state is proposed; see comments of Dunsiger <i>et al</i> 1996	Uemura <i>et al</i> 1994
Y ₂ Cu ₂ O ₅	magnetic phase diagram investigation	Duginov <i>et al</i> 1995
RNiO ₃	characterization of the magnetic order in the low-temperature insulating phase	García-Muñoz <i>et al</i> 1995a
Sr _{n-1} Cu _{n+1} O _{2n}	magnetic phase diagram of spin ladder systems; see section 3.2	Kojima <i>et al</i> 1995a
(Y _{2-x} Ca _x)Ba(Ni _{1-y} Mg _y)O ₅	Haldane system; chain length controlled by doping; effect of doping on the ground state	Kojima <i>et al</i> 1995b
La ₂ Co _x Cu _{1-x} O _{4+δ}	magnetic phase diagram investigation	Lappas <i>et al</i> 1995
Y ₂ Mo ₂ O ₇ , Tb ₂₂ Mo ₂ O ₇	spin dynamics of geometrically frustrated magnets; large density of states near zero energy	Dunsiger <i>et al</i> 1996
CuO	magnetic phase diagram investigation	Grebinnik <i>et al</i> 1996
LaCuO _{2.5}	the ground state is magnetically ordered rather than spin-liquid	Kadono <i>et al</i> 1996
KTr ₃ (OH) ₆ (SO ₄) ₂ Tr = Cr, Fe	long range ordering in the Fe compound; no such ordering in the Cr compound	Keren <i>et al</i> 1996a
La ₂ Cu _{1-x} Li _x O ₄	magnetic phase diagram; formation of a singlet ground state at large doping	Le <i>et al</i> 1996b
Ca ₂ CuO ₃ , Sr ₂ CuO ₃	infinite-chain cuprates; see section 3.2	Kojima <i>et al</i> 1997
LiV ₂ O ₄	heavy fermion oxide with no magnetic ordering	Kondo <i>et al</i> 1997
SrCuO ₂	magnetic phase transition at ~ 2 K in this zigzag chain compound	Matsuda <i>et al</i> 1997

Appendix A. The magnetic field at the muon site

We first express the measured local magnetic field in terms of the field components in the crystal reference frame. Then we write these field components in terms of their spatial Fourier components. Finally, we complete this appendix by providing a method of computing the field distribution at the muon site for a given magnetic structure.

Appendix A.1. The magnetic field in the laboratory and crystal reference frames

Whereas we are interested in the characterization of the magnetic field components at the muon site in terms of parameters of the crystal under study, the measurements are done in the laboratory reference frame. Here we express the linear relation between the field components in the two frames.

For simplicity we suppose that the magnet has only one type of localized magnetic moment and that the muon occupies only one interstitial site. We must consider two orthonormal reference frames: the laboratory reference frame $(\mathbf{X}, \mathbf{Y}, \mathbf{Z})$ where \mathbf{X} , \mathbf{Y} , and \mathbf{Z} are unit vectors and a reference frame $(\mathbf{x}, \mathbf{y}, \mathbf{z})$ attached to the crystal axes. Its unit vectors are chosen parallel to the crystal axes according to the symmetry of the compound. $(\mathbf{X}, \mathbf{Y}, \mathbf{Z})$ are defined in the $(\mathbf{x}, \mathbf{y}, \mathbf{z})$ frame through the Euler angles θ , φ and ψ . Note that θ and φ are also the polar angles of the \mathbf{Z} axis in the $(\mathbf{x}, \mathbf{y}, \mathbf{z})$ frame. The components of the local field in the laboratory frame are written as a function of the components in the crystal frame: $B_{\text{loc}}^{\rho} = \sum_{\alpha} R_{\rho\alpha}(\theta, \varphi, \psi) \tilde{B}_{\text{loc}}^{\alpha}$. We list the nine $R_{\rho\alpha}$ components:

$$R_{xx} = \cos \psi \cos \varphi \cos \theta - \sin \psi \sin \varphi, R_{xy} = \cos \psi \sin \varphi \cos \theta + \sin \psi \cos \varphi, \quad (\text{A1})$$

$$R_{yx} = -\sin \psi \cos \varphi \cos \theta - \cos \psi \sin \varphi, R_{yy} = -\sin \psi \sin \varphi \cos \theta + \cos \psi \cos \varphi, \quad (\text{A2})$$

$$R_{xz} = -\cos \psi \sin \theta, R_{yz} = \sin \psi \sin \theta, \quad (\text{A3})$$

$$R_{zx} = \cos \varphi \sin \theta, R_{zy} = \sin \varphi \sin \theta, R_{zz} = \cos \theta. \quad (\text{A4})$$

Since R is a unitary matrix, it is easy to express $\tilde{B}_{\text{loc}}^{\alpha}$ in terms of B_{loc}^{ρ} using the matrix elements listed above.

Appendix A.2. The Fourier components of the magnetic field

This appendix is based on an extension of the work of Yaouanc *et al* 1993b. The reader will consult with profit the paper of Lovesey and Engdahl 1995.

We express the local field in the crystal frame as a function, on one hand, of a tensor which describes the coupling between the localized spins of the magnet and the muon spin and, on the other hand, of the localized spins components themselves. The α component of the field is given by

$$\tilde{B}_{\text{loc}}^{\alpha} = \frac{\mu_0}{4\pi} \frac{g_L \mu_B}{n_d v} \sum_{\beta=x,y,z} \sum_{i,d} G_{\mathbf{r}_{i+d}}^{\alpha\beta} J_{i+d}^{\beta}. \quad (\text{A5})$$

v is the volume per magnetic atom, n_d the number of magnetic atoms in the cell used for the description of the magnet, g_L the Landé factor of spin \mathbf{J}_{i+d} which is at the distance vector \mathbf{r}_{i+d} from the muon, μ_B the Bohr magneton, μ_0 the permeability of free space and $\{\alpha, \beta\}=\{x, y, z\}$. \mathbf{r}_0 defines the location of the muon relative to the origin of the crystal lattice; see figure A1. *Note that the equivalent crystallographic sites allowed by the point group symmetry at the muon may give rise to different $G_d^{\alpha\beta}(\mathbf{q})$ and therefore to inequivalent magnetic sites, each characterized by a given \mathbf{r}_0 .* The index i runs over the cells and d over the sites inside a cell. Since one of the most important characteristics of a magnetic structure is its periodicity, we introduce the spatial-Fourier component $J_d^\alpha(\mathbf{q})$. Using the vectors defined in figure A1 we derive

$$\tilde{B}_{\text{loc}}^\alpha = \frac{\mu_0 g_L \mu_B}{4\pi n_d v} \sum_{\beta=x,y,z} \sum_d \sum_{\mathbf{q}} G_d^{\alpha\beta}(\mathbf{q}) \exp(-i\mathbf{q} \cdot \mathbf{r}_0) J_d^\beta(\mathbf{q}), \quad (\text{A6})$$

where we have defined

$$G_d^{\alpha\beta}(\mathbf{q}) = \sum_i G_{\mathbf{r}_{i+d}}^{\alpha\beta} \exp(i\mathbf{q} \cdot \mathbf{r}_{i+d}), \quad (\text{A7})$$

and

$$J_d^\beta(\mathbf{q}) = \sum_i J_{i+d}^\beta \exp[-i\mathbf{q} \cdot (\mathbf{i} + \mathbf{d})]. \quad (\text{A8})$$

Dalmas de Reotier and Yaouanc: Fig. A1

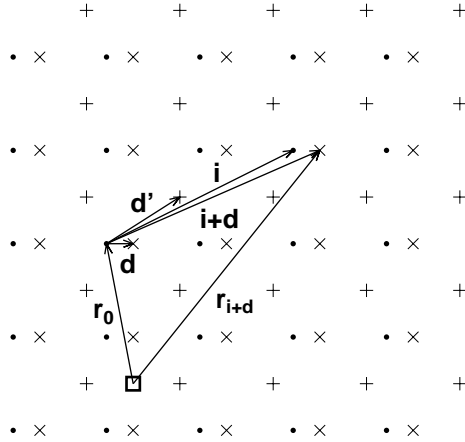


Figure A1. Definition of vectors relative to the crystallographic (+, ×) and muon (□) sites. The points (•) specify the origin of each cell. The point at the extremity of \mathbf{r}_0 is the origin of the crystal lattice. The drawing is done for a two dimensional square lattice with two magnetic atoms per cell. See the text for the definitions of the different vectors.

The tensor $G_d^{\alpha\beta}(\mathbf{q})$ is the sum of two tensors: $G_d^{\alpha\beta}(\mathbf{q}) = D_d^{\alpha\beta}(\mathbf{q}) + H_d^{\alpha\beta}(\mathbf{q})$. Whereas $D_d^{\alpha\beta}(\mathbf{q})$ describes the dipolar interaction between the spins of the magnet and the muon spin, $H_d^{\alpha\beta}(\mathbf{q})$ accounts for their hyperfine interaction. It is convenient

to rewrite

$$D_d^{\alpha\beta}(\mathbf{q}) = -4\pi \left[P_L^{\alpha\beta}(\mathbf{q}) - C_d^{\alpha\beta}(\mathbf{q}) \right], \quad (\text{A9})$$

where $P_L^{\alpha\beta}(\mathbf{q})$ is the longitudinal projection operator and $C_d^{\alpha\beta}(\mathbf{q})$ a symmetric tensor which reflects the point group symmetry at the muon site. The expression of $C_d^{\alpha\beta}(\mathbf{q})$ is computed using Ewald's method:

$$\begin{aligned} C_d^{\alpha\beta}(\mathbf{q}) &= \frac{q_\alpha q_\beta}{q^2} \left[1 - \exp\left(\frac{-q^2}{4\varrho^2}\right) \right] \\ &- \frac{1}{4\varrho^2} \sum_{\mathbf{K} \neq \mathbf{0}} (K_\alpha + q_\alpha)(K_\beta + q_\beta) \varphi_0\left(\frac{(\mathbf{q} + \mathbf{K})^2}{4\varrho^2}\right) \exp(-i\mathbf{K} \cdot \mathbf{r}_{0+d}) \\ &+ \frac{n_d v \varrho^3}{2(\pi)^{3/2}} \sum_i \left[2\varrho^2 r_{i+d, \alpha} r_{i+d, \beta} \varphi_{3/2}(\varrho^2 r_{i+d}^2) - \delta^{\alpha\beta} \varphi_{1/2}(\varrho^2 r_{i+d}^2) \right] \exp(i\mathbf{q} \cdot \mathbf{r}_{i+d}), \quad (\text{A10}) \end{aligned}$$

where we use the Misra functions:

$$\varphi_m(x) = \int_1^\infty d\beta \beta^m \exp(-\beta x). \quad (\text{A11})$$

\mathbf{K} is a vector of the reciprocal lattice. Expression (A10) gives the same result for all values of the Ewald parameter ϱ , but for numerical applications a value of ϱ is chosen which ensures that both series of (A10) converge rapidly.

Whereas $P_L^{\alpha\beta}(\mathbf{q})$ is only piecewise continuous at $\mathbf{q} = \mathbf{0}$, reflecting the long range nature of the dipolar interaction, $C_d^{\alpha\beta}(\mathbf{q})$ is analytical. The presence of the projection operator in (A9) is important for understanding the critical behaviour of the relaxation rate in ferromagnets and the temperature dependence of this rate in the spin wave regime (see section 4.1).

In section 2.3 we have noted that \mathbf{B}_{loc} can be written as a sum of seven terms. We can identify the first five terms. $(\mathbf{B}_{\text{con}} + \mathbf{B}_{\text{trans}})$ results from the polarized conduction electrons and the transferred fields. To first approximation, these two fields are isotropic in metals. The $(\mathbf{B}_{\text{con}} + \mathbf{B}_{\text{trans}})$ contribution to the local field is obtained by substituting H for G in (A6). In the same way, the $(\mathbf{B}'_{\text{dip}} + \mathbf{B}_L)$ and \mathbf{B}_{dem} contributions are derived from (A6) by substituting $4\pi C$ and $-4\pi P_L$ for G, respectively.

Although the spatial-Fourier transform may seem a complicated procedure for a result which can be obtained by a simple lattice sum, Appendix A.3 and Appendix C will show its unique possibilities.

Appendix A.3. The field distribution at the muon site

Even for a simple magnetic structure, crystallographically equivalent sites may not be magnetically equivalent, i.e. more than one local magnetic field may exist. This is nicely explained for the case of Fe by Seeger 1978. If the number of fields is sufficiently large and their values are close, the muons will probe a field distribution which may be far from Gaussian as supposed in section 2. The relation between a magnetic model and the field distribution at the muon site, $D(\mathbf{B}_{\text{loc}})$, was first investigated by Szeto 1987.

In an experiment the several million implanted muons may enter different crystal sites which are related by the lattice translation periodicity. Therefore an average over these \mathbf{r} sites is required: $\mathbf{r} = \mathbf{r}_0 + l\mathbf{x} + m\mathbf{y} + n\mathbf{z}$ where $\{l, m, n\}$ are integers. We

recall here that if the point group symmetry of the muon site gives several equivalent positions, one has to consider each of these as they may give rise to different coupling tensors $\mathbf{G}_d(\mathbf{q})$ i.e. to non equivalent magnetic sites.

For the sake of simplicity, we consider a magnetic structure described by a single propagation vector \mathbf{k} . This represents the majority of structures found in nature, and the extension to multi- \mathbf{k} structures is easily performed. Then the Fourier components of the magnetic moment may be written as

$$\mathbf{M}_d(\mathbf{q}) = \sum_p \mathbf{M}_d(p\mathbf{k})\delta(\mathbf{q} - p\mathbf{k}), \quad (\text{A12})$$

where δ is the Kronecker symbol. The sum is over the harmonics of the magnetic structure; $p = \pm 1$ for a sinusoidal modulation. Note that $\mathbf{M}_d(\mathbf{q})$ is related to $\mathbf{J}_d(\mathbf{q})$ via the relation $\mathbf{M}_d(\mathbf{q}) = g_L\mu_B\mathbf{J}_d(\mathbf{q})$. Using (A12) and (A6), we derive

$$\tilde{B}_{\text{loc}}^\alpha(\mathbf{r}) = \frac{\mu_0}{4\pi} \frac{1}{n_d v} \sum_d \sum_p \sum_{\beta=x,y,z} G_d^{\alpha\beta}(p\mathbf{k}) M_d^\beta(p\mathbf{k}) \exp(-ip\mathbf{k} \cdot \mathbf{r}) \quad (\text{A13})$$

For a commensurate magnetic structure $\mathbf{k} = (r/s)\mathbf{G}$ where r and s are integers with $r \leq s$ and \mathbf{G} a reciprocal lattice vector. From the well known properties of \mathbf{G} , we derive $\mathbf{k} \cdot \mathbf{r} = \mathbf{k} \cdot \mathbf{r}_0 + 2\pi(r/s)u$ where u is an integer. Using this result, the exponential term of (A13) is rewritten as

$$\exp[-ip\mathbf{k} \cdot \mathbf{r}] = \exp(-ip\mathbf{k} \cdot \mathbf{r}_0) \left[\exp\left(i\frac{2\pi pr}{s}\right) \right]^u. \quad (\text{A14})$$

During a measurement, an ensemble average is made, so that the integer u takes an enormous number of values. But, since $\{\exp[i(2\pi pr)/s]\}^u$ as a function of u is a periodic function of period s , this phase factor takes a maximum of s different values.

Since $\mathbf{B}_{\text{loc}}^\alpha(\mathbf{r})$ depends linearly on $\tilde{B}_{\text{loc}}^\alpha(\mathbf{r})$ and this latter field is a sum of Fourier components, $\mathbf{B}_{\text{loc}}(\mathbf{r})$ is a sum Fourier components. Taking into account the property of the phase factor, we deduce that each component can take many different values.

We discuss this important result. For simplicity we consider a primitive Bravais lattice ($n_d = 1$), a sinusoidal modulation and suppose that the laboratory and crystal frames are aligned with \mathbf{Z} and \mathbf{z} parallel. For instance, if $r = 1$ and $s = 3$, up to three different fields can exist. If s is big, a large number of fields can result and in the limit, a quasi-continuous distribution is generated.

To proceed further analytically we consider this limit and write $\mathbf{B}_{\text{loc}}(\mathbf{r}) = \cos[2\pi w(\mathbf{r})]\mathbf{B}_m$ with $0 \leq w \leq 1$. This form is strictly valid for an incommensurate magnetic structure. Using the well known formula for a distribution

$$D(\mathbf{B}_{\text{loc}}) = \langle \langle \delta[\mathbf{B}_{\text{loc}} - \mathbf{B}_{\text{loc}}(\mathbf{r})] \rangle \rangle, \quad (\text{A15})$$

where $\langle \langle \dots \rangle \rangle$ stands for the spatial average over \mathbf{r} , we derive (Le *et al* 1993a)

$$D(\mathbf{B}_{\text{loc}}) = \frac{2}{\pi} \frac{1}{\sqrt{B_m^2 - B_{\text{loc}}^2}}, \quad (\text{A16})$$

for $0 \leq B_{\text{loc}} \leq B_m$ and $D(\mathbf{B}_{\text{loc}}) = 0$ otherwise. If we suppose that \mathbf{B}_{loc} is perpendicular to Z , we find using (3)

$$P_Z(t) = J_0(\gamma_\mu B_m t), \quad (\text{A17})$$

where J_0 is a Bessel function. When $\gamma_\mu B_m t$ is large, the model predicts $P_Z(t) = \sqrt{2/(\pi\gamma_\mu B_m t)} \cos(\gamma_\mu B_m t - \pi/4)$ instead of the usual $P_Z(t) = \cos(\gamma_\mu B_m t)$, i.e. the depolarization function presents at large t a damped oscillation shifted by 45° .

If the muon site is known, using the $\tilde{B}_{\text{loc}}^\alpha(\mathbf{r})$ expression (A13) it is possible to compute numerically the field distribution for any magnetic structure. While with the μSR technique it is not possible to determine in detail a magnetic structure, one can test proposed structures.

Appendix B. Muon spin relaxation in a longitudinal field

When the dynamics of the magnetic field at the muon site is sufficiently rapid, $P_Z(t)$ takes the form (McMullen and Zaremba 1978 and Dalmas de Réotier and Yaouanc 1992)

$$P_Z(t) = \exp[-\psi_Z(t)], \quad (\text{B18})$$

with

$$\begin{aligned} \psi_Z(t) = \gamma_\mu^2 \int_0^t d\tau (t - \tau) \{ & \cos(\omega_\mu \tau) [\Phi^{XX}(\tau) + \Phi^{YY}(\tau)] \\ & + \sin(\omega_\mu \tau) [\Phi^{XY}(\tau) - \Phi^{YX}(\tau)] \}. \end{aligned} \quad (\text{B19})$$

$\Phi(\tau)$ is the symmetrized correlation-tensor of the magnetic field at the muon site:

$$\Phi^{\alpha\beta}(\tau) = \frac{1}{2} \left[\left\langle B_{\text{loc}}^\alpha(\tau) B_{\text{loc}}^\beta \right\rangle + \left\langle B_{\text{loc}}^\beta B_{\text{loc}}^\alpha(\tau) \right\rangle \right] \quad (\text{B20})$$

$\langle \dots \rangle$ stands for the thermal average.

If the fluctuations are sufficiently rapid, one neglects τ in the $(t - \tau)$ factor and extends the integral to infinity. Then $P_Z(t)$ is an exponential function characterized by the relaxation rate $\lambda_Z = \psi_Z(t)/t$.

In zero-field $\Phi^{\alpha\beta}(\tau)$ is an even function of t . In an applied field, this may not be true because time reversal symmetry is broken. However, in many cases the breaking terms in the Hamiltonian are so small that the effect of the field is negligible. Then, even in an applied field, $\Phi^{\alpha\beta}(\tau)$ is an even function of t . We will suppose that this property holds. This enables the integration over τ in (B19) to be extended from $-\infty$ to ∞ .

In zero field λ_Z is given by

$$\lambda_Z = \frac{\gamma_\mu^2}{2} \int_{-\infty}^{\infty} d\tau [\Phi^{XX}(\tau) + \Phi^{YY}(\tau)]. \quad (\text{B21})$$

This simple result can be derived from the Fermi golden rule (Lovesey *et al* 1992).

In a longitudinal field, a term proportional to $\sin(\omega_\mu \tau)$ is present as seen in (B19). In most cases this term is zero either because time reversal symmetry is not broken or $\omega_\mu \tau_c \ll 1$ where τ_c is a characteristic time of the fluctuations. Then we have

$$\lambda_Z = \frac{\gamma_\mu^2}{2} \int_{-\infty}^{\infty} d\tau \cos(\omega_\mu \tau) [\Phi^{XX}(\tau) + \Phi^{YY}(\tau)]. \quad (\text{B22})$$

As stressed by Dalmas de Réotier *et al* 1996, $P_Z(t)$ is, in general, an exponential function only if no spatial average of the depolarization function is needed. This means that $P_Z(t)$ has, in general, no reason to be an exponential function for measurements on a polycrystalline sample.

Appendix C. Longitudinal relaxation rate and correlation-functions

In this section we analyze the relaxation rate in terms of the spin-spin correlation-tensor of the magnet.

Using the results presented in the two previous sections, $\Phi(\tau)$ can be written in terms of correlation-functions of the spatial Fourier components of the lattice spins. It is useful to introduce the time-Fourier transform of a function $f(\tau)$:

$$f(\omega) = \frac{1}{2\pi} \int_{-\infty}^{\infty} d\tau \exp(-i\omega\tau) f(\tau). \quad (\text{C23})$$

Using (A6) and (B22), λ_Z can be expressed in terms of the spin-spin correlation-tensor between spins belonging to sublattices d and d' , $\Lambda_{d,d'}(\mathbf{q}, \omega)$. With the definition

$$\Lambda_{dd'}^{\gamma\gamma'}(\mathbf{q}, \omega) = \frac{1}{2} \left[\left\langle J_d^{\gamma}(\mathbf{q}, \omega) J_{d'}^{\gamma'}(-\mathbf{q}) \right\rangle + \left\langle J_{d'}^{\gamma'}(-\mathbf{q}) J_d^{\gamma}(\mathbf{q}, \omega) \right\rangle \right], \quad (\text{C24})$$

the λ_Z expression writes

$$\lambda_Z = \frac{\pi\mathcal{D}}{V} \sum_{\beta,\alpha} L_{\beta\alpha}(\theta, \varphi) \int \frac{d^3\mathbf{q}}{(2\pi)^3} \sum_{\gamma,\gamma'} \sum_{d,d'} G_{dd'}^{\alpha\gamma}(\mathbf{q}) G_{dd'}^{\gamma'\beta}(-\mathbf{q}) \Lambda_{dd'}^{\gamma\gamma'}(\mathbf{q}, \omega_\mu). \quad (\text{C25})$$

The sum over \mathbf{q} in (A6) has been replaced by an integral over the first Brillouin zone following the usual rule $\sum_{\mathbf{q}} \rightarrow \int V/(2\pi)^3 d^3\mathbf{q}$ where V is the volume of the sample.

We define $\mathcal{D} = (\mu_0/4\pi)^2 \gamma_\mu^2 (g_L \mu_B)^2$. $L(\theta, \varphi)$ is a symmetric matrix which accounts for the fact that the symmetry axes of the magnet do not necessarily coincide with the laboratory frame axes. θ and φ have been defined in Appendix A.1. We have

$$L_{xx} = \cos^2 \varphi \cos^2 \theta + \sin^2 \varphi, L_{yy} = \sin^2 \varphi \cos^2 \theta + \cos^2 \varphi, L_{zz} = \sin^2 \theta, \quad (\text{C26})$$

$$L_{xy} = -\cos \varphi \sin \varphi \sin^2 \theta, L_{xz} = -\cos \varphi \cos \theta \sin \theta, L_{yz} = -\sin \varphi \cos \theta \sin \theta. \quad (\text{C27})$$

It is often useful to consider $\tilde{\Lambda}(\mathbf{q}) = \sum_{d,d'} \tilde{\Lambda}_{d,d'}(\mathbf{q})$ and the average coupling tensor $\mathbf{G}(\mathbf{q}) = 1/n_d \sum_d \mathbf{G}_d(\mathbf{q})$ since for some non Bravais crystal structures such as the hexagonal closed compact structure (Dalmas de Réotier and Yaouanc 1994) (C25) can be written in terms of $\tilde{\Lambda}(\mathbf{q})$ and $\mathbf{G}(\mathbf{q})$, i.e. the sum over d and d' disappears in the expression of λ_Z .

The symmetry properties at the muon site and of the magnet itself leads to considerable simplification. Examples are found in Yaouanc *et al* 1993a and 1993b, Dalmas de Réotier and Yaouanc 1994, Bonville *et al* 1996, Dalmas de Réotier *et al* 1996, Yaouanc *et al* 1996a and in section 4.1.

As an example of the drastic simplifications which can occur, we suppose that only one spin-spin correlation matters. This is the case for an Ising system or a magnet with its magnetic ions in a cubic environment. Then the following formula can be derived:

$$\lambda_Z = v \int \frac{d^3\mathbf{q}}{(2\pi)^3} \Delta^2(\mathbf{q}) \frac{\int_{-\infty}^{\infty} d\tau \cos(\omega_\mu\tau) \langle J^z(\mathbf{q}, \tau) J^z(-\mathbf{q}) \rangle}{J(J+1)/3}. \quad (\text{C28})$$

λ_Z depends on the function $\Delta^2(\mathbf{q})$ which accounts for the coupling between the muon and the lattice spins. In zero-field, when the intersite correlations are neglected ($\Delta^2(\mathbf{q}) = \Delta^2 \delta(\mathbf{q})$) and the spin-spin-correlation is an exponential function characterized by a fluctuation rate ν , we recover the motional narrowing result: $\lambda_Z = 2\Delta^2/\nu$, see (10).

Appendix D. The μ SR response function for hard superconductors

In this appendix we calculate the magnetic field inside the mixed state of a hard superconductor. For such a superconductor the Ginzburg-Landau parameter κ is much larger than 1 ($\kappa = \lambda/\xi$ where λ is the penetration length and ξ the coherence length).

It is well known that a vortex lattice is formed in the mixed state. We suppose that this lattice is ideal. This means we disregard pinning and vortex “phases” such as the glassy or liquid states (Blatter *et al* 1994, Brandt 1995). Pinning can strongly influence the results of a μ SR experiment as shown in details by Wu *et al* 1993. We consider the case where the field \mathbf{B}_{ext} is parallel to one of the three main axes \mathbf{a} , \mathbf{b} and \mathbf{c} of the penetration-length tensor. With these simple conditions, the vortices are straight field tubes parallel to \mathbf{B}_{ext} and form a regular lattice. We define an orthonormal reference frame $(\mathbf{x}, \mathbf{y}, \mathbf{z})$ such that the vortex tubes are also along z . We denote λ_a , λ_b and λ_c , the penetration lengths for currents flowing along the a , b and c axes, respectively.

As shown by Kogan (Kogan 1981), for a conventional vortex lattice and $B_{\text{ext}} \gg B_{c1}$ where B_{c1} is the lower critical field, the angle characterizing the lattice depends only on the penetration-length ratio :

$$\tan \alpha_v = \sqrt{3}(\lambda_x/\lambda_y). \quad (\text{D29})$$

As expected, if the penetration length is isotropic, $\alpha_v = 60^\circ$. Therefore, although α_v is most naturally measured by small angle neutron scattering (SANS), one can determine this angle by μ SR. An example is given in section 5.3.

It is convenient to introduce the Fourier components

$$\mathbf{B}(\mathbf{G}) = \int \mathbf{B}(\mathbf{r}) \exp(-i\mathbf{G} \cdot \mathbf{r}) d^2\mathbf{r}/S \quad (\text{D30})$$

of the periodic magnetic field

$$\mathbf{B}(\mathbf{r}) = \sum_{\mathbf{G}} \mathbf{B}(\mathbf{G}) \exp(i\mathbf{G} \cdot \mathbf{r}), \quad (\text{D31})$$

where \mathbf{G} are the vectors of the vortex reciprocal lattice and S the surface of the vortex lattice unit cell. Since $B_x(\mathbf{G}) = B_y(\mathbf{G}) = 0$, there is no transverse field component. Interestingly, the only non-zero component, $B_z(\mathbf{G})$, is the form factor measured by SANS.

Using Kogan’s formula, the form factor factorizes (Yaouanc *et al* 1997a), $B_z(G_{pq}) = B_0 \cdot c_{pq}(b)$, where

$$B_0 = \frac{1}{\pi^2} \left(\frac{3}{64} \right)^{1/2} \frac{\Phi_0}{\lambda_x \lambda_y}. \quad (\text{D32})$$

$c_{pq}(b)$ are universal functions of $b = B/B_{c2}$ where B is the mean induction, which for $2b\kappa^2 > 1$ may be equated to B_{ext} . $\{p, q\}$ are the two indices denoting a Bragg peak. Recently the $c_{pq}(b)$ functions have been computed numerically in the framework of the conventional Ginzburg-Landau theory (Brandt 1997). In terms of the functions $b_{pq}(b)$ defined by Brandt, we have $c_{pq}(b) = b_{pq}(b)/(p^2 - pq + q^2)$.

Since a typical penetration length is much larger than a crystal lattice parameter which is the characteristic distance between adjacent muon stopping sites, the muon is

a good probe for the vortex field distribution. Then it is straightforward to compute the distribution using (A15). This has been done by many authors (for example, Sonier *et al* 1994 and Greer and Kossler 1995). A characteristic of the flux line lattice observed in many experiments (for example, see figure 18 and figure 20) is the pronounced tail towards high fields due to the vortex cores. A useful method to characterize a distribution is to consider its moments or, since $\langle B_z \rangle \neq 0$, $\Delta_v^n = \langle (B_z - \langle B_z \rangle)^n \rangle$. The variance which is a measure of the width of the distribution separates into two factors, $\sqrt{\Delta_v^2} = \Delta_0 \cdot f_v(b)$ where

$$\Delta_0 = 0.06092 \frac{\Phi_0}{\lambda_x \lambda_y} \quad (\text{D33})$$

is the London limit ($\xi_x, \xi_y \rightarrow 0$) (Barford and Gunn 1988) and $f_v(b)$ a universal function which accounts for the core size. $\Phi_0 = 2.07 \times 10^{-15} \text{ Tm}^2$ is the quantum of flux and the prefactor 0.06092 is a pure number. $f_v(b)$ computed using the data of Brandt 1997 is plotted in figure A2. It is strongly field dependent even at low reduced fields b . The shape of a distribution is characterized by its skewness parameter : $\alpha = (\Delta_v^3)^{1/3} / (\Delta_v^2)^{1/2}$. For a symmetric distribution $\alpha = 0$. $\alpha(b)$ is also presented in figure A2. Note the strong field dependence of α near $b = 0$. We have $\alpha(b = 0) = 1.446$.

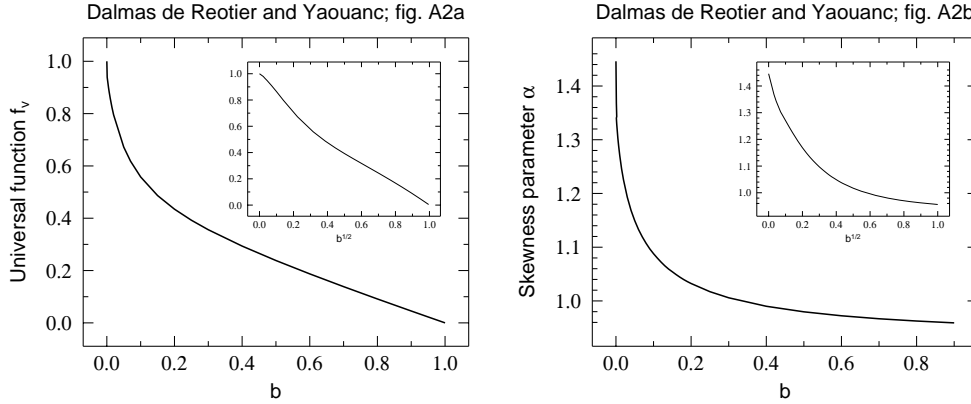


Figure A2. Field dependence of the functions f_v and α . $b \equiv B/B_{c2}$ where B is the mean induction, which for $2b\kappa^2 > 1$ may be equated to B_{ext} . In the inserts we present the functions versus $b^{1/2}$ to extend the low b part. (adapted from Yaouanc *et al* 1997a and Brandt *et al* 1997).

The results presented in figure A2 have been deduced from the numerical solution of the conventional Ginzburg-Landau expansion (Brandt 1997). Although this expansion has its own limit (basically it is valid close to the superconducting phase transition in the temperature-field phase diagram), a comparison between the results derived from the Ginzburg-Landau model and the commonly used Gaussian cutoff London model shows that the latter model strongly underestimates the effect of the field on the variance (Yaouanc *et al* 1997a). In fact, the Gaussian model does not have any theoretical support.

The motion of the vortices on a time scale shorter than a few microsecond may significantly effect the field distribution as probed by muons. Since the amplitude of such fluctuations is field dependent, the variance can exhibits a strong field dependence

as shown by Song 1995.

The Ginzburg-Landau model does not include the possibility of a Knight shift. Because this shift is expected to be different in the superconducting and in the normal regions, and since normal (vortex core) and superconducting regions coexist in the mixed state, the measured field distribution is a convolution of the distributions due to the Knight shift and the flux line lattice. This point was first raised by Feyerherm *et al* 1994.

Since a SANS experiment measures $|B_z(\mathbf{G})|$, one may estimate that SANS and μ SR experiments measure the same physical quantity. This idea seems to be supported by the fact that c_{10} and f_v have approximately the same field dependence (Yaouanc *et al* 1997a). But there is at least one important difference. In order to observe a Bragg peak by SANS, the correlation length of the vortex lattice must be sufficient. This is not required to observe a vortex field distribution by μ SR which is a local technique.

A “pure” field distribution is not observed because of broadening effects due to the finite lifetime of the muon, the defects of the vortex lattice, the demagnetization field and the nuclear dipolar broadening. We refer the reader to Riseman *et al* 1995 and Schneider *et al* 1995 for more information.

Up to now, we have only considered a three dimensional vortex lattice. But when the anisotropy of the penetration length is strong, it is more appropriate to describe the vortices as two dimensional “pancakes” vortices in individual coupled layers. Experimentally, $\text{Bi}_{2+x}\text{Sr}_{2-x}\text{CaCu}_2\text{O}_{8+\delta}$ corresponds to this case (see section 5.2). As first noticed by Brandt 1991, the misalignment between the layers leads to a variance smaller than for a standard three dimensional flux line lattice. A comparison between simulated field distributions for three and two dimensional vortex lattices has been made by Schneider *et al* 1995.

One of the most interesting parameters deduced from the investigation of a 3D field distribution is the penetration length λ ; indeed its determination is one way to probe the nature of the low energy excitations and therefore the pairing state of a superconductor. The relation between λ and these excitations is reviewed by Gross *et al* 1986 and Gross-Alltag *et al* 1991.

Acknowledgments

We would like first to take the opportunity to thank the accelerator crew and the instrument scientists at the ISIS and PSI facilities for enabling us to perform μ SR experiments. It is a pleasure to acknowledge helpful discussions with C M Aegerter, C Bernhard and Ch Niedermayer. Many thanks go to P Bonville, J P Boucher, I A Campbell, S F J Cox, P C M Gubbens, J A Hodges, M Lavagna and S W Lovesey who carefully read the whole or part of the manuscript. We are indebted to the following colleagues for providing us with data used to draw figures presented in this review : C M Aegerter, A Amato, S J Blundell, A Keren, K Kojima, G Solt and J E Sonier.

References

- Aegerter C M, Lee S L, Keller H, Forgan E M and Lloyd S H 1996 *Phys. Rev. B* **54** R15661–4
- Aegerter C M 1997, private communication
- Aeppli G, Yoshizawa H, Endoh Y, Bucher E, Hufnagl J, Onuki Y and Komatsubara T 1986 *Phys. Rev. Lett.* **57** 122–5
- Aeppli G, Bucher E, Broholm C, Kjems J K, Baumann J and Hufnagl J 1988 *Phys. Rev. Lett.* **60** 615–8
- Amato A, Baines C, Feyerherm R, Flouquet J, Gygax F N, Lejay P, Schenck A and Zimmermann U 1993 *Physica B* **186&188** 276–8
- Amato A, Feyerherm R, Gygax F N, Schenck A, Flouquet J and Lejay P 1994 *Phys. Rev. B* **50** 619–22
- Amato A, Feyerherm R, Gygax F N, Schenck A, Löhneysen H v and Schlager H G 1995 *Phys. Rev. B* **52** 54–6
- Amato A, Feyerherm R, Gygax F N and Schenck A, 1997, *Hyperfine Interact.* **104** 165–70
- Amato A, 1997 private communication
- Anderson P W 1954 *J. Phys. Soc. Japan* **9** 316–39
- Aristov D N and Maleyev S V 1994 *Z. Phys. B* **93** 181–7
- Attenborough M, Hall I, Nikolov O, Brown S R and Cox S F J 1996 *Phys. Rev. B* **54** 6448–56
- Barford W and Gunn J M F 1988 *Physica C* **156** 515–22
- Barsov S G, Gasnikova G P, Getalov A L, Koptev V P, Kotov S A, Kuz'min L A, Men'shikov A Z, Mikirtych'yants S M and Shcherbakov G V 1993 *JETP Lett.* **57** 672–5
- Barsov S G, Getalov A L, Koptev V P, Kotov S A, Kuz'min L A, Mikirtych'yants S M and Shcherbakov G V 1994 *JETP Lett.* **60** 796–9
- Basov D N, Liang R, Bonn D A, Hardy W N, Dabrowski B, Quijada M, Tanner D B, Rice J P, Ginsberg D M and Timusk T 1995 *Phys. Rev. Lett.* **74** 598–601
- Bernal O O, MacLaughlin D E, Amato A, Feyerherm R, Gygax FN, Schenck A, Heffner R H, Le L P, Nieuwenhuys G J, Andraka B, Löhneysen H v, Stockert O and Ott H R 1996 *Phys. Rev. B* **54** 13000–8
- Bernhard C, Wenger C, Niedermayer Ch, Pooke D M, Tallon J, Kotaka Y, Shimoyama J, Kishio K, Noakes D R, Stronach C E, Sembiring T and Ansaldo E J 1995a *Phys. Rev. B* **52** R7050–3
- Bernhard C, Niedermayer Ch, Binniger U, Hofer A, Wenger Ch, Tallon J L, Williams G V M, Ansaldo E J, Budnick J I, Stronach C E, Noakes D R and Blankson-Mills M A 1995b *Phys. Rev. B* **52** 10488–98
- Bernhard C, Tallon J L, Bucci C, De Renzi R, Guidi G, Williams G V M and Niedermayer Ch 1996 *Phys. Rev. Lett.* **77** 2304–7
- Berzin A A, Morozov A I and Sigov A S 1993 *Phys. Solid state* **35** 1463–5
- Blatter G, Feigel'man M V, Geshkenbein V B, Larkin A I and Vinokur V M 1994 *Rev. Mod. Phys.* **66** 1125–388
- Blundell S J, Pattenden P A, Valladares R M, Pratt F L, Sugano T and Hayes W 1994 *Solid State Com.* **92** 569–72
- Blundell S J, Pattenden P A, Pratt F L, Valladares R M, Sugano T and Hayes W 1995 *Europhys. Lett.* **31** 573–8
- Blundell S J, Sugano T, Pattenden P A, Pratt F L, Valladares R M, Chow K H, Uekusa H, Ohashi Y and Hayes W 1996 *J. Phys.: Condens. Matter* **8** L1–6
- Blundell S J, Pratt F L, Pattenden P A, Kurmoo M, Chow K H, Takagi S, Jestädt Th and Hayes W 1997a *J. Phys.: Condens. Matter* **9** L119–24
- Blundell S J, Pattenden P A, Pratt F L, Chow K H, Hayes W and Sugano T, 1997b, *Hyperfine Interact.* **104** 251–6
- Birrer P, Gygax F N, Hitti B, Lippelt E, Schenck A, Weber M, Cattani D, Cors J, Decroux M and Fischer Ø 1993 *Phys. Rev. B* **48** 16589–99
- Birrer P, Torikai E and Nishiyama K 1995 *J. Magn. Magn. Mater.* **140-144** 2177–8
- Bishop D 1996 *Nature* **382** 760–1 and *Science* **273** 1811–1
- Bonville P, Dalmas de Réotier P, Yaouanc A, Polatsek G, Gubbens P C M and Mulders A M 1996 *J. Phys.: Condens. Matter* **8** 7755–70
- Bonville P, LeBras G, Dalmas de Réotier P, Yaouanc A, Calemczuk R, Paulsen C, Kasaya M and Aliev F G 1997 *Physica B* **230&232** 266–8
- Borgs P, Kehr K W and Heitjans P 1995 *Phys. Rev. B* **52** 6668–83
- Borsa F, Carretta P, Cho J H, Chou F C, Hu Q, Johnston D C, Lascialfari A, Torgeson D R, Gooding R J, Salem N M and Vos K J E 1995 *Phys. Rev. B* **52** 7334–45
- Brandt E H 1991 *Phys. Rev. Lett.* **66** 3213–6

- 1995 *Rep. Prog. Phys.* **58** 1465–594
- 1997 *Phys. Rev. Lett.* **78** 2208–11
- Brandt E H, Dalmas de Réotier P and Yaouanc A 1997, private communication
- Brown S R, Attenborough M, Hall I, Nikolov O and Cox S F J 1996 *Phil. Mag. Lett.* **73** 195–9
- Cameron L M and Sholl C A 1994 *J. Phys.: Condens. Matter* **6** 3261–72
- Campbell I A, Amato A, Gygax F N, Herlach D, Schenck A, Cywinski R and Kilcoyne S H 1994 *Phys. Rev. Lett.* **72** 1291–4
- Caspary R, Hellmann, Keller M, Sparr G, Wassilew C, Köhler R, Geibel C, Schank C, Steglich F and Philips N E 1993 *Phys. Rev. Lett.* **71** 2146–9
- Celio M 1986 *Phys. Rev. Lett.* **56** 2720–3
- Chappert J and Grynszpan R I (ed) 1984 *Muon and Pions in Materials Research* (Amsterdam: North-Holland).
- Chappert J and Yaouanc A 1986 in *Topics in Current Physics* vol 40 ed Gonser U 297–316 (Berlin: Springer-Verlag)
- Chattopadhyay T, Scott C A and Löhneysen H v 1995 *J. Magn. Magn. Mater.* **140-144** 1259–60
- Chow K H, Pattenden P A, Blundell S J, Hayes W, Pratt F L, Jestädt Th, Green M A, Millburn J E, Rosseinsky M J, Hitti B, Dunsiger S R, Kiefl R F, Chen C and Chowdhury A J S 1996 *Phys. Rev. B* **53** R14725–8
- Cloots R, Ansaldo E J and Ausloos M 1994 *Physica C* **221** 104–8
- Condon J H 1966 *Phys. Rev.* **145** 526–35
- Condon J H and Walstedt R E 1968 *Phys. Rev. Lett.* **21** 612–4
- Cooke D W, Smith J L, Blundell S J, Chow K H, Pattenden P A, Pratt F L, Cox S F J, Brown S R, Morrobel-Sosa A, Lichti R L, Gupta L C, Nagarajan R, Hossain Z, Mazumdar C and Godart C 1995 *Phys. Rev. B* **52** R3864–7
- Cooke D W, Bennett B L, Lawson A C, Huber J G, Ootens J, Boekema C, Flint J A and Lichti R L 1996 *Phil. Mag. B* **74** 259–67
- Corti M, Rigamonti A, Tabak F, Carretta P, Licci F and Raffo L 1995 *Phys. Rev. B* **52** 4226–36
- Cox S F J 1987 *J. Phys. C: Solid State Phys.* **20** 3187–319
- Crabtree G W, and Nelson D R April 1997 *Physics Today* 38–44
- Cristofolini L, Lappas A, Vavakis K, Prassides K, DeRenzi R, Ricco M, Schenck A, Amato A, Gygax F N, Kosaka M and Tanigaki K 1995 *J. Phys.: Condens. Matter* **7** L567–73
- Crook M R and Cywinski R 1997 *J. Phys.: Condens. Matter* **9** 1149–58
- Cubitt R, Forgan E M, Yang G, Lee S L, Paul D McK, Mook H A, Yethiraj M, Kes P H, Li T W, Menovsky A A, Tarnawski Z and Mortensen K 1993 *Nature* **365** 407–11
- Cywinski R, Han Z P, Bewley R, Cubitt R, Wylie M T, Forgan E M, Lee S L, Warden M and Kilcoyne S H 1994 *Physica C* **233** 273–80
- Cywinski R, Coles B R, Kilcoyne S H and J-G Park 1995 *Physica B* **206&207** 412–4
- Dalmas de Réotier P, Yaouanc A, Gubbens P C M and L'Héritier P 1990, private communication
- Dalmas de Réotier 1990 PhD thesis, INPG, Grenoble, unpublished
- Dalmas de Réotier P and Yaouanc A 1992 *J. Phys.: Condens. Matter* **4** 4533–56
- 1994 *Phys. Rev. Lett.* **72** 290–3
- 1995 *Phys. Rev. B* **52** 9155–8
- Dalmas de Réotier P, Yaouanc A and Meshkov S V 1992 *Phys. Lett. A* **162** 206–12
- Dalmas de Réotier P, Yaouanc A and Frey E 1994 *Phys. Rev. B* **50** 3033–6
- Dalmas de Réotier P, Huxley A, Yaouanc A, Flouquet J, Bonville P, Imbert P, Pari P, Gubbens P C M and Mulders A M 1995 *Phys. Lett.* **205A** 239–43
- Dalmas de Réotier P, Yaouanc A and Bonville P 1996 *J. Phys.: Condens. Matter* **8** 5113–23
- Dalmas de Réotier P, Yaouanc A, Calemczuk R, Huxley A.D., Marcenat C, Bonville P, Lejay P, Gubbens P C M and Mulders A M 1997 *Phys. Rev. B* **55** 2737–40
- des Cloizeaux J and Pearson J J 1962 *Phys. Rev.* **128** 2131–5
- de Visser A, Keizer R J, van Harrevelt R, Menovsky A A, Franse J J M, Amato A, Gygax F N, Pinkpank M and Schenck A 1997 *Physica B* **230-232** 53–5
- Dunsiger S R, Kiefl R F, Chow K H, Gaulin B D, Gingras M J P, Greedan J E, Keren A, Kojima K, Luke G M, MacFarlane W A, Raju N P, Sonier J E, Uemura Y J and Wu W D 1996 *Phys. Rev. B* **54** 9019–22
- Duginov V N, Grebinnik V G, Horyń R, Kirillov B F, Klamut J, Krivosheev I A, Mamedov T N, Olshevsky V G, Pirogov A V, Pomjakushin V Yu, Ponomarev A N, Zaleski A J and Zhukov V A 1995 *J. Magn. Magn. Mater.* **140-144** 1577–8
- Duginov V N, Grebinnik V G, Gritsaj K I, Mamedov T N, Olshevsky V G, Pomjakushin V Yu, Zhukov V A, Krivosheev I A, Ponomarev A N, Nikiforov V N, Seropegin Yu D, Baran M and Szymczak H 1997 *Phys. Rev. B* **55** 12343–6

- Eccleston R S, Brown S R and S B Palmer 1995 *J. Magn. Magn. Mater.* **140-144** 745–6
- Feyerherm R, Amato A, Gygax F N, Schenck A, Geibel C, Steglich F, Sato N and Komatsubara T 1994 *Phys. Rev. Lett.* **73** 1849–52
- Feyerherm R, Amato A, Geibel C, Gygax F N, Hellmann P, Heffner R H, MacLaughlin D E, Müller-Reisener R, Nieuwenhuys G J, Schenck A and Steglich F 1995a *Physica B* **206&207** 596–9
- Feyerherm R, Amato A, Grayevsky A, Gygax F N, Kaplan N and Schenck A 1995b *Z. Phys. B* **99** 3–13
- Feyerherm R, Amato A, Gygax F N, Schenck A, Onuki Y and Sato N 1995c *J. Magn. Magn. Mater.* **140-144** 1175–6
- Fisher K H and Hertz J A 1991 *Spin Glasses* (Cambridge University press)
- Flaschin S J, Kratzer A, Burghart F J, Kalvius G M, Wäppling R, Noakes D R, Kadono R, Watanabe I, Takabatake T, Kobayashi K, Nakamoto G and Fujii H 1996 *J. Phys.: Condens. Matter* **8** 6967–83
- Frey E and Schwabl F 1988 *Z. Phys. B* **71** 355–68
- 1989 *Z. Phys. B* **76** 139–9
- 1994 *Adv. Phys.* **43** 577–683
- García-Muñoz J L, Lacorre P and Cywinski R 1995a *Phys. Rev. B* **51** 15197–202
- García-Muñoz J L, Suaaidi M and Martínez 1995b *Phys. Rev. B* **52** 4288–93
- Georges A and Kotliar G 1992 *Phys. Rev. B* **45** 6479–83
- Gingras M J P and Huse D A 1996 *Phys. Rev. B* **53** 15193–200
- Glazman L I and Koshelev A E 1991 *Phys. Rev. B* **43** 2835–43
- Glückler H, Niedermayer Ch, Bernhard C, Binninger U, Recknagel E, Tallon J L and Budnick J L 1995 *Physica C* **242** 39–45
- Grebinnik V G, Gritsai K I, Duginov V N, Zhukov V A, Kirillov B F, Koksharov Yu A, Krivosheev I A, Mamedov T N, Nikiforov V N, Nikolsky B A, Olshevsky V G, Pirogov A V, Pomyakushin V Yu, Ponomarev A N and Suetin V A 1996 *Phys. Atom. Nuclei* **59** 195–8
- Greer A J and Kossler W J 1995 *Low Magnetic Fields in Anisotropic Superconductors* Lecture Notes in Physics m30 (Berlin: Springer-Verlag)
- Gubbens P C M, Moolenaar A A, Dalmas de Réotier P, Yaouanc A, Menovsky A A, Prokes K and Snel C E 1995 *J. Magn. Magn. Mater.* **140-144** 1993–4
- Gubbens P C M, Mulders A M, Dalmas de Réotier P, Yaouanc A, Chevalier B and Menovsky AA 1996, private communication
- Goss Levi B October 1996 *Physics Today* 17–20
- Gross F, Chandrasekhar B S, Einzel D, Andres K, Hirschfeld P J, Ott H R, Beuers J, Fisk Z and Smith J L 1986 *Z. Phys. B* **64** 175–88
- Gross-Alltag F, Chandrasekhar B S, Einzel D, Hirschfeld P J and Andres K 1991 *Z. Phys. B* **82** 243–255
- Haldane F D M 1983a *Phys. Lett. A* **93** 464–8
- Haldane F D M 1983b *Phys. Rev. Lett.* **50** 1153–6
- Halperin B I and Hohenberg P C 1967 *Phys. Rev. Lett.* **19** 700–3
- Hardy W N, Bonn D A, Morgan D C, Liang R X and Zhang K 1993 *Phys. Rev. Lett.* **70** 3999–4002
- Harshman D R, Kleiman R N, Inui M, Espinosa G P, Mitzi D B, Kapitulnik A, Pfiz T and Williams D L 1991 *Phys. Rev. Lett.* **67** 3152–5
- Harshman D R, Brandt E H, Fiory A T, Inui M, Mitzi D B, Schneemeyer L F and Waszczak J V 1993 *Phys. Rev. B* **47** 2905–8
- Harshman D R and Fiory A T 1994 *Phys. Rev. Lett.* **72** 2501–1
- Harshman D R, Fiory A T, Haddon R C, Kaplan M L, Pfiz T, Koster E, Shinkoda I and Williams D L 1994 *Phys. Rev. B* **49** 12990–7
- Hayano R S, Uemura Y J, Imazato J, Nishida N, Yamazaki T and Kubo R 1979 *Phys. Rev. B* **20** 850–9
- Heffner R H, Cooke D W, Giordi A L, Hutson R L, Schillaci M E, Rempp H D, Smith J L, Willis J O, MacLaughlin D E, Boekema C, Lichti R L, Oostens J and Denison A B 1989 *Phys. Rev. B* **39** 11345–57
- Heffner R H, Le L P, Hundley M F, Neumeier J J, Luke G M, Kojima K, Nachumi B, Uemura Y J, MacLaughlin D E and Cheong S-W 1996 *Phys. Rev. Lett.* **77** 1869–72
- Heffner R H and Norman M R 1996 *Comm. Condens. Matter Phys.* **17** 361–408
- Heffner R H, Le L P, Nieuwenhuys G J, MacLaughlin D E, Amato A, Gygax F N, Schenck A, Kin J S, Stewart G and Ott H R 1997 *Physica B*, in press
- Hillberg M, de Melo M A C, Klauss H H, Wagener W, Litterst F J, Adelman P and Czjzek G, 1997 *Hyperfine Interact.* **104** 221–6
- Huxley A D, Dalmas de Réotier P, Yaouanc A., Caplan D, Couach M, Lejay P, Gubbens P C M and

- Mulders A M 1996 *Phys. Rev. B* **54** R9666–9
- Inui M and Harshman D R 1993 *Phys. Rev. B* **47** 12205–13
- Kadono R, Brewer J H, Chow K, Kreitzman S R, Niedermayer Ch, Riseman T M, Schneider J W and Yamazaki T 1993 *Phys. Rev. B* **48** 16803–6
- Kadono R, Okajima H, Yamashita A, Ishii K, Yokoo T, Akimitsu J, Kobayashi N, Hiroi Z, Takano M and Nagamine K 1996 *Phys. Rev. B* **54** R9628–30
- Kadono R 1997 *J. Phys. Soc. Japan* **66** 505–6
- Kalvius G M, Kratzer A, Wappling R, Takabatake T, Nakamoto G, Fujii H, Kiefl R F and Kreitzman S R 1995a *Physica B* **206&207** 807–9
- Kalvius G M, Noakes D R, Kratzer A, Munch K H, Wappling R, Tanaka H, Takabatake T and Kiefl R F 1995b *Physica B* **206&207** 205–8
- Kalvius G M, Kratzer A, Noakes D R, Munch K H, Wappling R, Tanaka H, Takabatake T and Kiefl R F 1995c *Europhys. Lett.* **29** 501–6
- Kambara H, Yoshizumi T, Mamiya T, Kimura N, Settai R, Yamamoto E, Haga Y and ˆOnuki Y 1996 *Europhys. Lett.* **36** 545–9
- Kambe S, Raymond S, Regnault L P, Flouquet J, Lejay P and Haen P 1996 *J. Phys. Soc. Japan* **65** 3294–300
- Karlsson E B 1995 *Solid State Phenomena as seen by Muons, Protons and Excited Nuclei* (Oxford: Clarendon)
- Kehr K W, Honig G and Richter D 1978 *Z. Phys. B* **32** 49–58
- Keren A, Le L P, Luke G M, Sternlieb B J, Wu W D, Uemura Y J, Tajima S and Uchida S 1993 *Phys. Rev. B* **48** 12926–35
- Keren A 1994 *Phys. Rev. B* **50** 10039–42
- Keren A, Kojima K, Le L P, Luke G M, Wu W D, Uemura Y J, Tajima S and Uchida S 1995 *J. Magn. Magn. Mater.* **140-144** 1641–2
- Keren A, Kojima K, Le L P, Luke G M, Nachumi B, Wu W D, Uemura Y J, Takano M, Dabkowska H and Gingas M J P 1996a *Phys. Rev. B* **53** 6451–4
- Keren A, Mendels Ph, Campbell I A and Lord J 1996b *Phys. Rev. Lett.* **77** 1386–9
- Kilcoyne S H and Telling M T F 1995 *J. Magn. Magn. Mater.* **140-144** 871–2
- Klauss H-H, de Melo M A C, Hillberg M, Litterst F J, Asch L, Kratzer A, Kalvius G M, Mattenberger K and Vogt O 1995 *J. Magn. Magn. Mater.* **140-144** 1163–4
- Kleiman R N, Broholm C, Aeppli G, Bucher E, Stucheli N, Bishop D J, Clausen K N, Mortensen K, Pedersen J S and Howard B 1992 *Phys. Rev. Lett.* **69** 3120–3
- Kogan V G 1981 *Phys. Lett. A* **85** 298–300
- Kojima K, Keren A, Luke G M, Nachumi B, Wu W D, Uemura Y J, Azuma M and Takano M 1995a *Phys. Rev. Lett.* **74** 2812–5
- Kojima K, Keren A, Le L P, Luke G M, Nachumi B, Wu W D, Uemura Y J, Kiyono K, Miyasaka S, Takagi H and Uchida S 1995b *Phys. Rev. Lett.* **74** 3471–4
- Kojima K, Fudamoto Y., Larkin M., Luke G M, Merrin J, Nachumi B, Uemura Y J, Motoyama N, Eisaki H., Uchida S, Yamada Y., Endoh Y., Hosoya S, Sternlieb B.J. and Shirane G. 1997 *Phys. Rev. Lett.* **78** 1787–90
- Kondo S, Johnston D C, Swenson C A, Borsa F, Mahajan A V, Miller L L, Gu T, Goldman A I, Maple M B, Gajewski D A, Freeman N R, Dilley N R, Dickey R P, Merrin J, Kojima K, Luke G M, Uemura Y J, Chmaissem O and Jorgensen J D 1997 *Phys. Rev. Lett.* **78** 3729–32
- Kornilov E I and Pomjakushin V Yu 1991 *Phys. Lett. A* **153** 364–7
- Kotzler J 1986 *J. Magn. Magn. Mater.* **54-57** 649–54
- Krivosheev I A, Nezhivoi A A, Nikol’skii B A, Ponomarev A N, Duginov V N, Ol’shevskii V G and Pomjakushin V Yu 1997 *JETP Lett.* **65** 81–5
- Kuramoto Y and Miyake K 1990 *J. Phys. Soc. Japan* **59** 2831–40
- Kubo R 1981 *Hyperfine Interact.* **8** 731–8
- Kyogaku M, Kitaoka Y, Asayama K, Geibel C, Schank C and Steglich F 1993 *J. Phys. Soc. Japan* **62** 4016–30
- Lappas A, Prassides K, Amato A, Feyerherm R, Gygax F N and A Schenck 1994 *Z. Phys. B* **96** 223–6
- Lappas A, Prassides K, Amato A, Feyerherm R, Gygax F N and A Schenck 1995 *J. Magn. Magn. Mater.* **140-144** 1291–2
- Latroche M, Figiel H, Wiesinger G, Kapusta Cz, Mietniowski P, Paul-Boncour V, Percheron-Guegan A and Cywinski R 1996 *J. Phys.: Condens. Matter* **8** 4603–15
- Le L P, Keren A, Luke G M, Sternlieb B J, Wu W D, Uemura Y J, Brewer J H, Riseman T M, Upasani R V, Chiang L Y, Kang W, Chaikin P M, Csiba T and Gruner 1993a *Phys. Rev. B* **48** 7284–96

- Le L P, Keren A, Luke G M, Wu W D, Uemura Y J, Tamura M, Ishikawa M and Kinoshita M 1993b *Chem. Phys. Lett* **206** 405–8
- Le L P, Heffner R.H., Nieuwenhuys G, Canfield P C and Cho B K, Amato A, Feyerherm R, Gygax F N, MacLaughlin D E and Schenck A 1995 *Physica B* **206&207** 552–4
- Le L P, Heffner R.H., Thompson J.D., MacLaughlin D E, Nieuwenhuys G J, Amato A, Feyerherm R, Gygax F N, Schenck A, Canfield P C and Cho B K 1996a *Phys. Rev. B* **53** R510–3
- Le L P, Heffner R H, MacLaughlin D E, Kojima K, Luke G M, Nachumi B, Uemura Y J, Sarrao J L and Fisk Z 1996b *Phys. Rev. B* **54** 9538–41
- Lee S L, Zimmermann P, Keller H, Warden M, Savić I M, Schauwecker R, Zech D, Cubitt R, Forgan E M, Kes P H, Li T W, Menovsky A A and Tarnawski Z 1993 *Phys. Rev. Lett.* **71** 3862–5
- Lee S L, Warden M, Keller H, Schneider J W, Zech D, Zimmermann P, Cubitt R, Forgan E M, Wylie M T, Kes P H, Li T W, Menovsky A A and Tarnawski Z 1995 *Phys. Rev. Lett.* **75** 922–5
- Lee S L, Aegerter C M, Keller H, Willemin M, Stäubli-Pümping B, Forgan E M, Lloyd S H, Blatter G, Cubitt R, Li T W and Kes P H 1997 *Phys. Rev. B* **55** 5666–9
- Lidström E, Wäppling R, Hartmann O, Ekström M and Kalvius G M 1996a *J. Phys.: Condens. Matter* **8** 6281–96
- Lidström E, Wäppling R and Hartmann O 1996b *Physica Scripta* **54** 210–5
- Luke G M, Le L P, Sternlieb B J, Wu W D, Uemura Y J, Brewer J H, Kadono R, Kiefl R F, Kreitzman S R, Riseman T M, Dalichaouch Y, Lee B W, Maple M B, Seaman C L, Armstrong P E, Ellis R W, Fisk Z and Smith J L 1991 *Phys. Lett. A* **157** 173–7
- Luke G M, Keren A, Kojima K, Le L P, Sternlieb B J, Wu W D and Uemura Y J 1994 *Phys. Rev. Lett.* **73** 1853–6
- Luke G M, Keren A, Kojima K, Le L P, Wu W D and Uemura Y J, Kalvius G M, Kratzer A, Nakamoto G, T. Takabatake and M. Ishikawa 1995 *Physica B* **206&207** 222–4
- Lussier B, Taillefer L, Buyers W J L, Mason T E and Petersen 1996 *Phys. Rev. B* **54** R6873–6
- Lovesey S W, Karlsson E B and Trohidou K N 1992 *J. Phys.: Condens. Matter* **4** 2043–60
- Lovesey S W and Engdahl E 1995 *J. Phys.: Condens. Matter* **7** 769–76
- Lovesey S W, Balcar E and Cuccoli A 1995 *J. Phys.: Condens. Matter* **7** 2615–31
- MacFarlane W A, Kiefl R F, Dunsiger S, J E Sonier and Fischer J E 1995 *Phys. Rev. B* **52** R6995–7
- MacLaughlin D E, Gupta L C, Cooke D W, Heffner R H, Leon M and Schillaci M E 1983 *Phys. Rev. Lett.* **51** 927–30
- MacLaughlin D E, Bernal O O and Lukefahr H G 1996 *J. Phys.: Condens. Matter* **8** 9855–70
- Merrin H D and Wagner H 1966 *Phys. Rev. Lett.* **17** 1133–6
- Matsuda M, Katsumata, K, Kojima K M, Larkin M, Luke G M, Merrin J, Nachumi B, Uemura Y J, Eisaki H, Motoyama N, Uchida S and Shirane G, 1997 *Phys. Rev. B* **55** 11953–6
- McMullen T and Zaremba E 1978 *Phys. Rev. B* **18** 3026–40
- Mendels P, Alloul H, Brewer J H, Morris G D, Duty T L, Johnston S, Ansaldo E J, Collin G, Marucco J F, Niedermayer Ch, Noakes D R and Stronach C E 1994 *Phys. Rev. B* **49** R10035–8
- Mekata M, Asano T, Sugino T, Nakamura H, Asai N, Shiga M, Keren A, Kojima K, Luke G M, Wu W D, Uemura Y J, Dunsinger S and Gingas M 1995 *J. Magn. Magn. Mater.* **140-144** 2177–8
- Mezei F and Murani A P 1979 *J. Magn. Magn. Mater.* **14** 211–4
- Moussa F, Hennion M, Rodriguez-Carvajal J, Moudouen H, Pinsard L, and Revcolevschi A 1996 *Phys. Rev. B* **54** 15149–55
- Murani A P and Eccleston R S 1996 *Phys. Rev. B* **53** 48–51
- Muzikar P 1997 *J. Phys.: Condens. Matter* **9** 1159–79
- Nachumi B, Keren A, Kojima K, Larkin M, Luke G M, Merrin J, Tchernyshöv O, Uemura Y J, Ichikawa N, Goto M and Uchida S 1996 *Phys. Rev. Lett.* **77** 5421–4
- Nelson D R 1997 *Nature* **385** 675–6
- Noakes D R, Ismail A, Ansaldo E J, Brewer J H, Luke G M, Mendels P and Poon S J 1995 *Phys. Lett. A* **199** 107–112
- Niedermayer Ch, Bernhard C, Binniger U, Glückler H, Tallon J L, Ansaldo E J and Budnick J I 1993 *Phys. Rev. Lett.* **71** 1764–7
- Nieuwenhuys G J, Mentink S A M, Menovsky A A, Amato A, Feyerherm R, Gygax F N, Heffner R H, Le L P, MacLaughlin D E and Schenck A 1995 *Physica B* **206&207** 470–2
- Park J-G, Coles B R, Scott C and Cywinski R 1996 *Physica B* **223&224** 189–191
- Pattenden P A, Valladares R M, Pratt F L, Blundell S J, Fisher A J, Hayes W and Sugano T 1995 *Synthetic Metals* **71** 1823–4
- Pépin C and Lavagna M 1997, submitted for publication
- Perring T G, Aeppli G, Hayden S M, Carter S A, Remeika J P and Cheong S-W 1996 *Phys. Rev. Lett.* **77** 711–4
- Pomjakushin V Yu, Zakharov A A, Amato A, Duginov V N, Gygax F N, Herlach D, Ponomarev A

- N and Schenck A 1996 *Physica C* **272** 250–6
- Prassides K, Lappas A, Buchgeister M and Verges P 1995 *Europhys. Lett.* **29** 641–6
- Pratt F L, Sasaki T, Toyota N and Nagamine 1995 *Phys. Rev. Lett.* **74** 3892–5
- Prokes K, Svoboda P, Sechovsky V, Brück E, Amato A, Feyerherm R, Gygax F N, Schenck A, Maletta H and de Boer F R 1995 *J. Magn. Magn. Mater.* **140-144** 1381–2
- Rainford B D, Cywinski R and Dakin S J 1995a *J. Magn. Magn. Mater.* **140-144** 805–6
- Rainford B D, Adroja D T, Wäppling R, Kalvius G M and Kratzer A 1995b *Physica B* **206&207** 202–4
- Regnault L P, Erkelens W A, Rossat-Mignod J, Lejay P and Flouquet J 1988 *Phys. Rev. B* **38** 4481–7
- Rice T M, Gopalan S and Sigrist M 1993 *Europhys. Lett.* **23** 445–9
- Riseman T M, Brewer J H, Chow K h, Hardy W N, Kiefl R F, Kreitzman S R, Liang R, MacFarlane W A, Mendels P, Morris G D, Rammer J and Schneider J W 1995 *Phys. Rev. B* **52** 10569–80
- Ryu S, Kapitulnik A and Doniach S 1996 *Phys. Rev. Lett.* **77** 2300–3
- Ryu S and Stroud D 1996 *Phys. Rev. B* **54** 1320–33
- Sauls J A 1994 *Adv. Phys.* **43** 113–41
- Schatz G and Weidinger A 1995 *Nuclear Condensed Matter Physics* (Chichester: John Wiley & Sons)
- Schenck A 1985 *Muon Spin Rotation Spectroscopy* (Bristol: Adam Hilger)
- Schenck A, Birrer P, Gygax F N, Hitti B, Lippelt E, Weber M, Böni P, Fischer P, Ott H R and Fisk Z 1990 *Phys. Rev. Lett.* **65** 2454–7
- Schenck A and Gygax F N 1995 in *Handbook of Magnetic Materials* vol 9 ed Bushow K H J 57–302 (Amsterdam: Elsevier)
- Schneider J W, Schafroth S and Meier P F 1995 *Phys. Rev. B* **52** 3790–3
- Seeger A 1978 in *Topics in Current Physics* vol 28 ed Alefeld G and Völkl J 349–97 (Berlin: Springer-Verlag)
- Shibata F and Shimoo Y 1995 *Physica A* **215** 87–103
- Shoenberg D 1984 *Magnetic Oscillations in Metals* (Cambridge University press)
- Sohma A, Okajima H, Yokoo T, Yamashita A, Akimitsu J, Nishiyama K and Nagamine K 1995 *J. Phys. Soc. Japan* **64** 3060–5
- Song Y -Q 1995 *Physica C* **241** 186–90
- Sonier J E, Kiefl R F, Brewer J H, Bonn D A, Carolan J F, Chow K H, Dosanjh P, Hardy W N, Ruixing L, MacFarlane W A, Mendels P, Morris G D, Riseman T M and Schneider J W 1994 *Phys. Rev. Lett.* **72** 744–7
- Sonier J E, Kiefl R F, Brewer J H, Bonn D A, Dunsiger S R, Hardy W N, Ruixing L, MacFarlane and Riseman T M 1997 *Phys. Rev. B* **55** 11789–92
- Solt G 1994 *Phys. Lett. A* **189** 390–4
- 1995 *Hyperfine Interact.* **96** 167–75
- Solt G, Baines C, Egorov V S, Herlach D, Krasnoperov E and Zimmermann U 1996a *Phys. Rev. Lett.* **76** 2575–8
- 1996b in *From Quantum Mechanics to Technology*, Lecture Notes in Physics Vol. 477, eds. Petru Z, Przystawa J, Rapcewicz K (Berlin: Springer-Verlag)
- Stammler Th, Grund Th, Hampele M, Major J, Nötter M, Scheuermann R, Schimmele L and Seeger A 1995 *Phil. Mag. B* **72** 285–94
- Storchak V, Kirillov B F, Pirogov A V, Duginov V N, Grebinnik V G, Ol'shevsky V G, Pomyakushin V Yu, Lazarev A B, Shilov S N and Zhulov V A 1994 *Phys. Lett. A* **185** 338–42
- Strong S P February 1997 *Physics Today* 13–3
- Sulaiman Shukri B, Srinivas Sudha, Sahoo N, Hagelberg F, Das T P, Torikai E and Nagamine K 1994 *Phys. Rev. B* **49** 9879–84
- Süllow S, Hendrix R W A, Gortemulder T J, Nieuwenhuys G J, Menovsky A A, Schenck A and Mydosh J A 1994 *Physica C* **233** 138–42
- Szeto K Y 1987 *Phys. Rev. B* **35** 5209–18
- Tallon J L, Bernhard C, Binniger U, Hofer A, Williams G V M, Ansaldo E J, Budnick J I and Niedermayer ch 1995 *Phys. Rev. Lett.* **74** 1008–11
- Tallon J L, Williams G V M, Bernhard C, Pooke D M, Staines M P, Johnson J D and Meinhold R H 1996 *Phys. Rev. B* **53** R11972–5
- Tamura M, Nakazawa Y, Shiomi D, Nozawa K, Hosokoshi Y, Ishikawa M, Takahashi M and Kinoshita M 1991 *Chem. Phys. Lett.* **186** 401–4
- Tchernyshyov O, Blaer A S, Keren A, Kojima K, Luke G M, Wu W D, Uemura Y J, Hase M, Uchinokura K, Ajiro Y, Asano T and Mekata M 1995 *J. Magn. Magn. Mater.* **140-144** 1687–8
- Telling M T F and Cywinski R 1995 *J. Magn. Magn. Mater.* **140-144** 45–6
- Tsuei C C, Kirtley J P, Chi C C, Yu-Jahnes Lock See, Gupta A, Shaw T, Sun J Z, Ketchen M B 1994 *Phys. Rev. Lett.* **73** 593–6

- Uemura Y J, Le L P, Luke G M, Sternlieb B J, Wu W D, Brewer J H, Riseman T M, Seaman C L, Maple M B, Ishikawa M, Hinks D G, Jorgensen J D, Saito G and Yamochi H 1991 *Phys. Rev. Lett.* **66** 2665–8
- Uemura Y J, Keren A, Le L P, Luke G M, Wu W D, Kubo Y, Manako T, Shimakawa Y, Subramanian M, Cobb J L and Markert J T 1993 *Nature* **364** 605–7
- Uemura Y J, Keren A, Kojima K, Le L P, Luke G M, Wu W D, Ajiro Y, Asano T, Kuriyama Y, Mekata M, Kikuchi H and Kakurai K 1994 *Phys. Rev. Lett.* **73** 3306–9
- Uemura Y J, Kojima K, Luke G M, Wu W D, Oszlanyi G, Chauvet O and Forro L 1995 *Phys. Rev. B* **52** R6991–3
- Vinokur V M, Kes P H and Koshelev A E 1990 *Physica C* **168** 29–39
- Walstedt R E and Walker L P 1974 *Phys. Rev. B* **9** 4857–67
- Weber M, Amato A, Gygax F N, Schenck A, Maletta H, Duginov V N, Grebinnik V G, Lazarev A B, Olshevsky V G, Pomjakushin V Yu, Shilov S N, Zhukov V A, Kirillov B F, Pirogov A V, Ponomarev A N, Storchak V G, Kapusta S and Bock J 1993 *Phys. Rev. B* **48** 13022–36
- Wiesinger G, Bauer E, Häufler Th, Amato A, Gygax F N and Schenck A 1995 *Physica B* **206&207** 261–3
- Wu W D, Keren A, Le L P, Sternlieb B J, Luke G M, Uemura Y J, Dosanjh P and Riseman T M 1993 *Phys. Rev. B* **47** 8172–86 L
- Wu W D, Keren A, Le L P, Luke G M, Sternlieb B J, Uemura Y J, Seaman C L, Dalichaouch Y and Maple M B 1994 *Phys. Rev. Lett.* **72** 3722–5
- Yang S-H, Kumigashira H, Yokoya T, Chainani A, Takahashi T, Takeya H and Kadowaki K 1996 *Phys. Rev. B* **53** R11946–8
- Yaouanc A and Dalmas de Réotier P 1991 *J. Phys.: Condens. Matter* **3** 6195–201
- Yaouanc A, Dalmas de Réotier P and Frey E 1993a *Europhys. Lett.* **21** 93–8
- 1993b *Phys. Rev. B* **47** 796–809
- Yaouanc A and Dalmas de Réotier P 1994 *Hyperfine Interact.* **87** 1147–51
- 1995 *Phys. Rev. B* **51** 12011–2
- Yaouanc A, Dalmas de Réotier P, Gubbens P C M, Mulders A M, Kayzel F E and Franse J J M 1996a *Phys. Rev. B* **53** 350–3
- Yaouanc A, Dalmas de Réotier P, Gubbens P C M, Mulders A M, Kayzel F E and Franse J J M 1996b, private communication
- Yaouanc A, Dalmas de Réotier P and Brandt E H 1997a *Phys. Rev. B* **55**, 11107–10
- Yaouanc A, Dalmas de Réotier P, Huxley A, Flouquet J, Bonville P, Gubbens P C M and Mulders A M, 1997b private communication
- Yaouanc A, Dalmas de Réotier P, Gubbens P C M, Kaiser C T, Amato A, Baines C, Gygax F N, Schenck A, Huxley A and Flouquet J 1997c, private communication
- Zheludev A, Ressouche E, Schweizer J, Turek P, Wan Meixiang and Wang Hailiang 1994 *Sol. Stat. Comm.* **90** 233–5
- Zimmermann P, Keller H, Lee S L, Savić I M, Warden M, Zech D, Cubitt R, Forgan E M, Kaldis E, Karpinski J and Krüger C 1995 *Phys. Rev. B* **52** 541–52